

**A THEORETICAL STUDY OF STELLAR PULSATIONS IN
YOUNG BROWN DWARFS**



A thesis submitted for examination in partial fulfillment of the requirements for the degree of Magister Scientiae in the department of Physics University of the Western cape

By

OKENG'O GEOFFREY ONCHONG'A

Supervisor: Dr E. A. Olivier

February 2011

A THEORETICAL STUDY OF STELLAR PULSATIONS IN YOUNG BROWN DWARFS

By

Okeng'o Geoffrey Onchong'a

Keywords

Brown dwarfs
Very low mass stars
Pulsation equations
Perturbation equations
Work integrals
Frozen-in approximation
Pulsation constants
Period ratios
Time-dependent treatment
Turbulent viscosity
Turbulent pressure
Free parameters



Disclaimer

I declare that *A theoretical study of stellar pulsations in young brown dwarfs* is my own work, that it has not been submitted for any degree or examination in any other university, and that all the sources I have used or quoted have been indicated and acknowledged by complete references.

Full name

Date

Signed



Abstract

A theoretical study of stellar pulsations in young brown dwarfs

G O Okeng'o

A thesis submitted in partial fulfilment of the requirements for the degree of Magister Scientiae in the Department of Physics, University of the Western Cape.

UNIVERSITY of the
WESTERN CAPE

This thesis reports the results of a twofold study on the recently proposed phenomenon of '*stellar pulsations*' in young brown dwarfs by the seminal study of Palla and Baraffe (2005) (PB05, thereafter). The PB05 study presents results of a non-adiabatic linear stability analysis showing that young brown dwarfs should become pulsationally unstable during the deuterium burning phase of their evolution.

The PB05 calculations on which this prediction is based have already been applied in a number of ground and space-based observational campaigns aimed at searching for this newly proposed putative class of potential pulsators. However, despite their significance and implications, the theoretical calculations by PB05 have not yet, to date, been subjected to independent verification in a different computational framework. To achieve this, we have generated equilibrium brown dwarf models and performed non-adiabatic linear stability calculations similar to PB05 assuming their 'frozen-in convection' approximation and the relevant input physics. The calculations performed in this thesis show, in overall, that there is a good agreement between the results from our study and those in PB05. However, there seem to be significant differences for very low mass objects as pointed out in

our comparative results. We attribute this difference to our different boundary conditions. Our outer boundary condition is equivalent to the Eddington approximation in the 3-D case (e.g see Unno and Spiegel (1966)), while PB05 use a combination of different atmospheric profiles as discussed in Chabriel and Baraffe (2000).

The validity of the frozen-in assumption used by PB05, which is based on the argument that the convective time scales calculated for these objects are much less than the pulsation time scales, has not been investigated. In this thesis, we have invoked a time-dependent theory of convection similar to Kuhfuss (1986) and Stellingwerf (1982) which includes turbulent pressure, turbulent diffusion and turbulent viscosity to study the pulsations. We have also investigated the effects of varying a number of free parameters in the above theoretical models. Our results show that turbulent pressure dominates in driving the pulsations in young brown dwarfs yielding growth rates much higher than in the frozen-in scenario. This is a new result that requires further analysis. The perturbation in the convective flux is found to have a damping effect on the acoustic modes. Turbulent viscosity is found to lead to damping which increases with increase in the value of the turbulent viscosity parameter and is found to have very little effect on the fundamental mode pulsation periods. Variation in the turbulent diffusion parameter has a very small effect on the fundamental mode periods and e-folding times.

As a side lobe, we have determined theoretical pulsation constants for the fundamental mode and calculated the period ratios for the fundamental mode to those of the first and second harmonics. We find values of pulsation constants falling within the theoretical values calculated for variable stars shown in Cox (1980). This is explained in relation to the terms that go into the theoretical formula discussed later in this thesis. We find a correlation between the period ratios and the BDs mass and argue that such plots of the period ratios vs mass of the BDs could be useful in constraining the masses, given known periods from observations.

Acknowledgement

This thesis is a product of many people whose support, encouragement, ideas and guidance made this research possible. In this regard, I would like to acknowledge the following in no particular order:

My **parents and family** for their unwavering love, prayers and for believing in me all the way.

My supervisor **Dr. E A. Olivier**; firstly for introducing me to the exciting field of pulsations in brown dwarfs, secondly for his *General Astrophysics 2* lectures that sparked my interest in stellar astrophysics, thirdly for being available to answer my endless questions about modeling, bearing with me when it took a little longer to get things done and helping me develop a scientific approach to solving real research problems, fourthly for organizing partial funding for two trips during my research period and fifthly, and more importantly, for sticking it through with me for the entire period of my research. The scholarly line of thought presented in this thesis, is therefore, his inspiration.

Prof. Isabelle Baraffe of Ecole Normale Supérieure centre de Recherche (France) for providing us with two of her models for comparison and the brown dwarfs equation of state that made this research a success.

The NASSP steering committee, in particular **Prof P. A. Whitelock** and **Prof P.K.S Dunsby** for the initial offer of a NASSP scholarship.

The South Africa SKA program for the prestigious **Youth into Science SKA Postgraduate Scholarship** and travel grants, that made this MSc research possible. In particular, very special thanks to Kim (SKA), Daphne (formerly SKA), Rose (NRF office) and Mabrey (UWC) for their wonderful support.

The **SAAO** for providing me with **office space** during my research. In this regard, thanks to **Prof Patricia, Linda Tobin, Glenda Snowball, Dalene Fischer** and the **IT crowd** for their support.

Prof C. M. Cress (UWC), for the kind words of advice, encouragement and support.

Dr Andreas Faltenbacher for going through my thesis draft and giving a number of useful suggestions that improved this work greatly.

My many friends at the **SAAO** and **Observatory** for the good times, company and inspiring discussions; I cannot be able to put all your names in caption, but to name just a few: I would like to thank **Ms Thembela Mantungwa, Ms Nomgcobo Ntsham, Ms Pakama Ngceni, Pumuza, Nimrod, Marissa, Christian Hetlage and Sivuyile.**

A very special thanks to my office mates **François , Zara and Bro** (Oyigamba) for providing a vibrant company during my stay at the SAAO.

My two flatmates **Solohery** and **Toky** for making my stay in Observatory much more easier.

My wonderful and generous **Uncle Joel** and **In-law Ken** for their moral and financial support and being willing to sacrifice for me whenever I sought their help. It's difficult to thank you enough for what you did to me, but, God bless you so much! My little sister Lynnette and little brother Eric, my beloved sisters Everline, Jane and Gladys; I love you very much.

And finally, glory be to **God** for the gift of life!!!

Dedication

This thesis is dedicated to my son



AMOS MBAKA ONCHONG'A

-for celebrating his second birthday this year-

UNIVERSITY of the
WESTERN CAPE

This thesis is also dedicated to my grand parents: JOHNSON MBAKA ONCHONG'A and SIBIA NYANDUKO who passed away before seeing me reach this far, I loved you so much and miss you dearly....

- Nyasae asesenie intwe oroiboro rw'enda yaino-

(God bless us, your generation)

*“.... A fact is a simple statement that everyone believes. It is innocent, unless found guilty.
A hypothesis is a novel suggestion that no one wants to believe. It is guilty, until found
effective.”*

- Edward Teller¹(1991)

UNIVERSITY *of the*
WESTERN CAPE

¹former American Nuclear Physicist and Nobel Prize winner

Contents

Disclaimer	iii
Abstract	iv
Acknowledgement	vi
Dedication	viii
	ix
1 Introduction	1
1.1 Background	1
1.2 Brief introduction to stellar pulsations	7
1.3 Stellar Pulsations in young brown dwarfs	12
1.4 Aims and thesis outline	17
2 Equations, theory and physical input	21
2.1 The pulsation and convection equations	21
2.1.1 The partial differential equations	22
2.1.2 The Linearized Equations	25
2.2 The Work integrals	31
2.3 The physical input	39
3 Results I: static models and the ‘frozen-in approximation’	40



3.1	Comparison of hydrostatic equilibrium structures for our models and PB05 models	40
3.2	Linear stability analysis	48
3.2.1	Comparison of Our Linear stability analysis with PB05 results for five models	48
3.2.2	Extended results and other models	52
3.2.2.1	Eigen-frequencies, periods and e-folding times for 1st and 2nd harmonics	52
3.2.2.2	Pulsation constants and the period ratios	52
3.2.2.3	The radial eigen functions and the work integrals	55
4	Results II: A Time-Dependent Model of Convection	66
4.1	Effect of perturbation in convective flux	66
4.1.1	The pulsation periods, growth rates and e-folding times	66
4.1.2	The Work integrals	68
4.2	Effect of turbulent pressure	78
4.3	Effect of turbulent viscosity	83
4.4	Effect of the turbulent diffusion parameter	83
5	Discussions, conclusions and call for further work	86
A	Numerical modelling	90
A.1	The Difference Equations	90
A.2	The boundary conditions	94
A.3	Solution of the difference equations	96
A.4	Linear stability Analysis	103
	Bibliography	108

List of Tables

3.1	The various model parameters used in the $0.04M_{\odot}$ and $0.08M_{\odot}$ models used in the comparison. R_{start} and $\log(L/L_{\odot})_{start}$ are the starting values of the Radius and the log of the luminosity (in solar units) while D/D_0 is the ratio of the central deuterium abundance (D) to the initial value (D_0). Here α'_{λ} , α'_s and α'_d are the scaled values of modeling parameters described in section (2.1) given by equations (3.1), (3.2) and (3.3) respectively, defined so as to satisfy the MLT values proposed by Kuhfuß (1986).	49
3.2	Comparison of the fundamental mode periods, P_0 and the e-folding times, τ_e , the effective temperature in Kelvin and the log of the luminosity in solar units from our study and the PB05 linear stability analysis results for the $0.04 M_{\odot}$ Model. Here, D is the value of the initial central deuterium abundance adopted in the linear stability analysis.	50
3.3	Effective temperatures and the log of surface luminosities from our calculations shown with those from PB05.	52
3.4	The real and the imaginary parts of the pulsation frequencies for the fundamental mode.	53
3.5	A Summary of the results for the First Harmonic in the frozen-in case. . . .	54
3.6	A summary of the results for the Second Harmonic mode in the frozen-in approximation case.	54
3.7	Pulsation constants for the fundamental mode and the first two harmonics from our study. The ratio of the first harmonic to the fundamental mode periods is also shown.	55

4.1	Some properties of five BD models with the turbulent treatment of convection ignoring turbulent pressure and turbulent viscosity for the fundamental mode. The pulsation frequencies have been scaled by the factors, ω_{scale} , same as in chapter (3).	67
4.2	Some properties of five BD models with the turbulent treatment of convection ignoring turbulent pressure and turbulent viscosity for the first harmonic.	67
4.3	Some properties of five BD models with the turbulent treatment of convection ignoring turbulent pressure and turbulent viscosity for the second harmonic.	68



List of Figures

1.1	Theoretical H-R diagram for various LMS and SSO's from Chabriel and Baraffe, 2000. The dotted lines, from left to right represent 10^6 , 10^7 , 10^8 , and 10^9 years isochrones. A mixing length $l = 1.9H_p$ is used in calculation of these models. (Figure from Chabriel and Baraffe, 2000 pg 360).	3
1.2	log of surface gravity, g (in cgs) plotted against effective temperature, T_{eff} (in K) for LMSs (solid curves) and SSO's (dashed lines) from $1M_{\odot} - 0.001M_{\odot}$ from Chabriel and Baraffe, 2000. Dotted lines, from top to bottom, represent 10^6 , 10^7 , 10^8 , and $5 \cdot 10^9$ years isochrones. (Figure from Chabriel and Baraffe, 2000 pg. 361).	4
1.3	Examples of different spherical harmonics for various values of l and m . Credit: Figure from " <i>Lecture Notes on Stellar Oscillations</i> " by Jørgen Christensen-Dalsgaard, page 6, Figure 2.1. The cases illustrated are: a) $l = 1, m = 0$; b) $l = 1, m = 1$; c) $l = 2, m = 0$; d) $l = 2, m = 1$; e) $l = 2, m = 2$; f) $l = 3, m = 0$; g) $l = 3, m = 1$; h) $l = 3, m = 2$; i) $l = 3, m = 3$; j) $l = 5, m = 5$; k) $l = 10, m = 5$; l) $l = 10, m = 10$	9
1.4	P-V diagram for a driving layer of an RR Lyrae star model (Credit: Figure from Carrol and Ostlie (1996), page 552, figure 14.9).	10
1.5	P-V diagram for a damping layer of an RR Lyrae star model (Credit: Figure from Carrol and Ostlie (1996), page 552, figure 14.9).	10
1.6	The evolution of the D-abundance, fundamental period p_0 (in h) and growth time scale τ_{growth} (in Myr) as a function of time during the D-burning phase of a $0.1M$ star (dashed line), and $0.06 M$ (dash-dotted line) and $0.03 M$ (solid line) BD [From Palla & Baraffe 2005]	14

1.7	Location of the D-instability strip (shaded area) in the HR diagram. Tracks of different masses and isochrones are indicated as labelled. The isoperiod curves (in h) are shown by the thick lines within the strip [From Palla & Baraffe 2005].	14
1.8	A summary of the properties of VLMSs and BDs during D-burning phase for different masses (From PB05)	15
1.9	The differential work integral dW/dm (in arbitrary units, the solid line) as a function of interior mass (in units of total mass), the pulsation amplitude $\delta r/r$ (dotted line), arbitrary normalized to 1 at the surface, and the nuclear energy generation rate ϵ_{nuc} (in erg/g/s, dashed line) for a $0.03 M_{\odot}$ BD [From Palla & Baraffe 2005]	16
1.10	From left, <i>panel 1</i> : Full and empty dots show the Asiago data for CFHT BD3 and for the artificial comparison star, respectively; the solid line is a fit to the data; <i>panel 2</i> : DFT for BD3; <i>panels 3 & 4</i> : as <i>panels 1 & 2</i> , but for star number 24 [From Marconi et al. 2007].	17
1.11	A Plot of the possible candidates for pulsational variability among known BD candidates in five young star clusters plotted with the PB05 D-instability strip from Cody (2009).	18
1.12	The periodogram for a brown dwarf in the AC09 sample together with a light curve phased to possible signal [From Cody 2009]	19
3.1	Various dynamical variables plotted for the $0.04 M_{\odot}$ static model. Results from our study (continuous red lines) and those from PB05 (dashed blue lines) are shown for comparison.	41
3.2	A Similar plot as in figure 3.1 but for the $0.08 M_{\odot}$ static model. Both the PB05 results and our results are shown for comparison.	42
3.3	Plots of the temperature and density in zone functions of the radial coordinate for the $0.07 M_{\odot}$ static model. The log of the temperature in zone and mass density in zone as functions of the log of total pressure are also plotted.	43
3.4	Plots same as figure 3.3 but for the $0.06 M_{\odot}$ static model.	44
3.5	Plots same as figure 3.3 but for the $0.05 M_{\odot}$ static model.	45

3.6	Plots same as figures 3.3 but for the $0.03M_{\odot}$ static model.	46
3.7	Plots same as figure 3.3 but for the $0.02M_{\odot}$ model.	47
3.8	Plots of the fundamental mode periods (in hours) and e-folding times (in Myrs) from our calculations (GOB10) and the PB05 calculations as functions of mass in solar units.	51
3.9	An H-R diagram showing the position of the BDs from our study. Data from the PB05 study is also plotted.	53
3.10	A plot of the pulsation constants for the first three modes as functions of the mass to radius ratio (in solar units).	56
3.11	Plot of the theoretical pulsation constants of the fundamental mode and the first two overtones as a function of mass from our study.	56
3.12	Plots of the ratio of the fundamental mode periods to the first harmonic periods (top plot) and the second harmonic periods (bottom plot) from our study.	57
3.13	The radial eigen functions and the total integrated work integrals plotted as functions of the mass coordinate in the frozen-in approximation case for the $0.08M_{\odot}$ model.	58
3.14	A similar plot as 3.13 for the $0.04M_{\odot}$ model.	59
3.15	The total partial work integrals and the radial eigenfunction for the $0.02M_{\odot}$	61
3.16	The total partial work integrals and the radial eigenfunction for the $0.03M_{\odot}$	62
3.17	The total partial work integrals and the radial eigenfunction for the $0.05M_{\odot}$	63
3.18	The total partial work integrals and the radial eigenfunction for the $0.06M_{\odot}$	64
3.19	The total partial work integrals and the radial eigenfunction for the $0.07M_{\odot}$	65
4.1	Plots of the real and imaginary parts of the convective luminosity eigenfunctions as a function of the radial mass coordinate M_r for the $0.04M_{\odot}$ model.	69

4.2	Plots of the analytical expressions for contributions from the perturbation in the convective flux (top plot) and the perturbation in nuclear energy generation rate (bottom plot), as functions of mass for the $0.04M_{\odot}$. Here, turbulent viscosity and turbulent pressure are ignored. Contribution from the convective flux can be seen to dominate that from the nuclear energy generation rate which is what leads to net overall damping displayed in work integral plots for this case.	70
4.3	Plots of the total partial work integrals (top plot) and the radial eigenfunctions (bottom plot) when the perturbations in the convective flux are included and turbulent pressure and turbulent viscosity ignored for the $0.04M_{\odot}$ model.	71
4.4	Plots same as figure 4.3 but for the $0.05M_{\odot}$ model.	72
4.5	Plots for the $0.06M_{\odot}$ model. Same as figure 4.3.	73
4.6	Plots for the $0.07M_{\odot}$ model. Same as figure 4.3.	74
4.7	Plots for the $0.08M_{\odot}$ model. Same as figure 4.3.	75
4.8	Plots for the $0.03M_{\odot}$ model. Same as figure 4.3.	76
4.9	Plots for the $0.02M_{\odot}$ model. Same as figure 4.3.	77
4.10	Plots of the work integrals and the radial eigenfunction vs mass coordinate for the $0.08M_{\odot}$ model.	79
4.11	Same as figure 4.10 but for the $0.04M_{\odot}$ model.	80
4.12	Plots of the phase difference between turbulent pressure and the density as a function of radius for three masses from our study.	81
4.13	Plots of the absolute ratios of the perturbations in turbulent velocity to the perturbations in turbulent pressure, σ , for the $0.04 M_{\odot}$ model and $0.08 M_{\odot}$ and the ratio of the absolute value of perturbations in specific volume to the absolute value of perturbations in turbulent pressure, β	82
4.14	Plots of the fundamental mode periods vs the turbulent viscosity parameter α_{μ} for masses $0.08M_{\odot}$, $0.06M_{\odot}$ and $0.04M_{\odot}$ (top graph) and the growth rate, η , per cycle vs α_{μ} (bottom graph).	84

4.15	Plots of the fundamental mode periods vs the turbulent diffusion parameter, α_t , for three objects(top graph) and the pulsation amplitude decay rate (per cycle) for the fundamental mode, η_0 , for the same objects(bottom graph).	85
A.1	Stellar envelope mesh.	91
A.2	Structure of the Jacobian matrix J for a 6 zone stellar model. Here x denotes a possible non-zero matrix element and a blank entry denotes a zero value matrix element.	99



Chapter 1

Introduction

This introductory chapter is arranged as follows: section (1.1) provides a brief background to the nature, the discovery, some of the interesting properties of BDs and an overview of the fast growing field of stellar astrophysics research in brown dwarfs. Section (1.2) gives a brief discussion of the theory of pulsating stars with a specific focus on brown dwarfs. Deuterium burning as a cause for pulsational instability in young brown dwarfs is considered in section (1.3) while the recently proposed phenomenon of stellar pulsations in young BDs and a brief review of the most recent literature on this subject is also presented in (1.3). Finally, the aims of this thesis are outlined in section (1.4).

1.1 Background

‘Brown dwarfs’¹(BDs), esoterically referred to in common literature as ‘stellar misfits’, ‘cosmic misfits’, ‘failed stars’, ‘shit stars’, ‘substars’ and even ‘planeters’ (due to their inability to evolve into ‘true’ stars), are a putative class of sub-stellar objects unable to sustain stable fusion of Hydrogen into Helium-4 in their centers. They are characterized by masses in the range $\sim 0.013 M_{\odot}$ (the deuterium-burning minimum mass, DBMM²) to $\sim 0.08 M_{\odot}$ (the hydrogen-burning minimum mass, HBMM³) (i.e 13.6-83.8 M_J) (Chabriel

¹The term brown dwarf was invented by Jill Tarter in the 1975 to refer to objects below the hydrogen burning limit ($\lesssim 0.1$ sun masses).

²The mass below which deuterium burning does not occur.

³The mass below which stable hydrogen burning does not occur.

and Baraffe, 2000), where M_{\odot} is the mass of the Sun ($\sim 1.989 \times 10^{33}$ g) and M_J is the mass of Jupiter ($\sim 1.90 \times 10^{30}$ g).

In evolutionary terms, BDs are thought to begin their pre-main sequence (PMS) phase of evolution with the full amount of core deuterium, equal to the interstellar value, since during the preceding phase of evolution (the protostellar phase; Palla and Baraffe 2005) their centers do not become hot enough to start nuclear burning. BDs and Very Low Mass Stars (VLMSs) are therefore thought to contract during the PMS phase before the ignition of D-burning can take place. Once the critical temperature is reached ($\sim 10^6$ K), the D-burning phase occurs on time scales of the order ~ 2.5 Myrs for a $0.1 M_{\odot}$ low mass star and ~ 20 Myrs for a $0.02 M_{\odot}$ brown dwarf (1 Myr = 1 Mega year = 10^6 years). According to Chabriel and Baraffe (2000), an interest in the physics of objects at the bottom of and below the main sequence developed following an early demonstration by Kumar (1963) that there exists a minimum mass below which H-burning does not occur. Kumar also showed that below this minimum mass, the balance between the outward pressure and the inward pull of gravity on these objects (hydrostatic equilibrium) is provided by electron degeneracy pressure.

For objects with masses $\gtrsim 0.013$ sun masses, initial deuterium burning occurs quickly, lasting for only $\sim 10^6 - 10^8$ years, while for masses $\gtrsim 0.07M_{\odot}$ (for metallicity: $\log[Z/Z_{\odot}] = 0$) to $0.08M_{\odot}$ (for $\log[Z/Z_{\odot}] = -2.0$), the internal energy from nuclear reactions quickly balances the energy provided by gravitational contraction making these lowest-mass objects to reach a state of equilibrium for both metallicities (Chabriel and Baraffe, 2000). Figure 1.1 displays the evolutionary properties for low mass stars and substellar objects for several masses and isochrones from 1 Myr to 5 Gyrs from Chabriel and Baraffe (2000). The evolutionary tracks for these objects from the same study are shown in figure 1.2. These figures can be used in the determination of the mass and age of an object from its surface gravity and effective temperatures calculated from its inferred spectrum (Chabriel and Baraffe, 2000).

During the last decade, BDs have been of much interest to astronomers (see e.g. Bailer-Jones and Mundt, 1999; Morales et al., 2005; Basri, 2000), with much efforts devoted to determining their characteristic properties (mass, age, effective temperature, luminosities) (Basri, 2000; Chabriel and Baraffe, 2000). With masses intermediate between massive

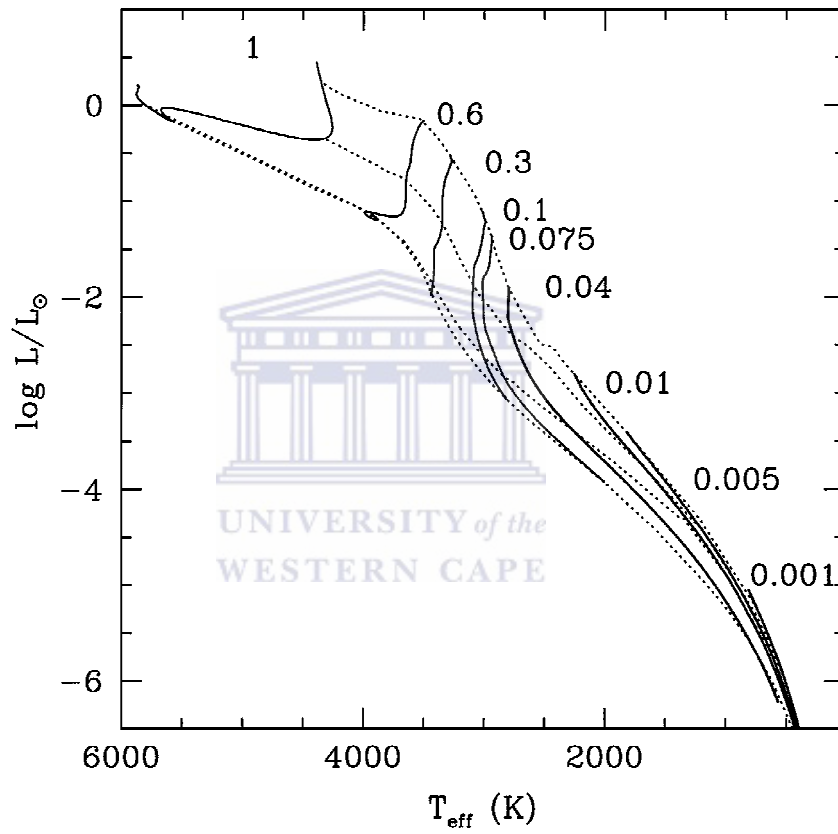


Figure 1.1: Theoretical H-R diagram for various LMS and SSO's from Chabriel and Baraffe, 2000. The dotted lines, from left to right represent 10^6 , 10^7 , 10^8 , and 10^9 years isochrones. A mixing length $l = 1.9H_p$ is used in calculation of these models. (Figure from Chabriel and Baraffe, 2000 pg 360).

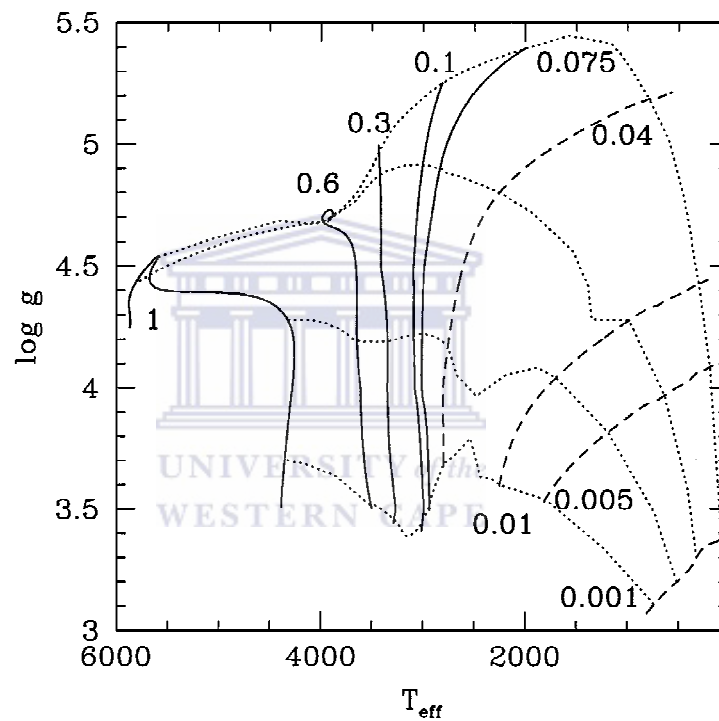


Figure 1.2: log of surface gravity, g (in cgs) plotted against effective temperature, T_{eff} (in K) for LMSs (solid curves) and SSO's (dashed lines) from $1M_{\odot} - 0.001M_{\odot}$ from Chabriel and Baraffe, 2000. Dotted lines, from top to bottom, represent 10^6 , 10^7 , 10^8 , and 5×10^9 years isochrones. (Figure from Chabriel and Baraffe, 2000 pg. 361).

planets and low mass stars, BDs are understood to be the ‘missing link’ between the intertwined processes of star and giant planet formation. Proper understanding of the physical properties of these objects is thought to bear major consequences for a range of domains of physics and astrophysics, including: the physics of dense matter, the formation of stars and planets and their evolution, atmospheric chemistry, galactic evolution and the missing mass problem (Chabriel and Baraffe, 2000). Other aspects that make these objects feasible targets for current studies in stellar astrophysics include: their less centrally condensed interiors (with $\rho_c/\bar{\rho} \sim 4.5 - 6$, due to their low mass and the high sensitivity of nuclear reactions on temperature, where ρ_c is the central density and $\bar{\rho}$ is the mean density) (Palla and Baraffe, 2005), their low effective temperatures ($\sim 1300 - 2,000$ K for L class; $\sim 700 - 1,300$ K for T class and < 600 K for the proposed Y class; Wikipedia), cloudy and cool atmospheres (depending on age and spectral types), associated magnetic fields, rotation and accretion events, X-ray variability, flaring and eclipsing events.

The discovery of the first bonafide browns dwarfs in 1995 (Rebolo et al., 1995; Nakajima et al., 1995; Oppenheimer et al., 1995) and the subsequent blooming of the search for faint (sub)stellar objects (Chabriel and Baraffe, 2000), saw them cited by the American National Academy of Science’s (NAS) “*Astronomy and Astrophysics in the New Millennium*” Astro2010 Decadal Review White Paper, as “one of the highlights of this era and a critical development for future studies of star formation”. Since then, the numbers of newly discovered BDs has risen steeply with a number of past and ongoing surveys such as COROT⁴, UKIDSS⁵, WISE⁶ and NIRSPEC BDSS⁷ (Rice et al., 2010), generating large amounts of data for Very Low Mass Stars (VLMSs; $\lesssim 0.1 M_{\odot}$; Palla and Baraffe 2005; Chabriel and Baraffe 2000) and BDs spanning ages between $\sim 1-10$ Myr. These data are not only crucial for future discoveries but also are important in studies aimed at providing essential insights into low mass star and giant planet formation processes (see e.g. Baraffe et al., 2002; Comerón et al., 2000; Baraffe et al., 1998).

Variability studies of young brown dwarfs (BDs) and very low mass stars (VLMS) is an active area of ongoing research in both observational and theoretical modeling (Palla

⁴Convection ROTation and planetary Transits

⁵United Kingdom Infra-Red Telescope(UKIRT), Infrared Deep Sky Survey

⁶Wide-field Infrared Survey Explorer

⁷Near Infra-Red SPECTroscopic Brown Dwarfs Sky Survey

and Baraffe, 2005; Morales et al., 2005; Cody, 2007, 2009). In particular, current research suggests that there can be various possible causes of variability in these objects: (Palla and Baraffe, 2005; Cody, 2007; Morales et al., 2005);

- (i) Rotational modulation from co-rotating, asymmetrically distributed, cool or hot, magnetically induced surface deformations and star spots that leads to periodic photometric variability revealed through the analysis of periodic time series light curves (see e.g. Scholz et al., 2009).
- (ii) Inhomogeneities in edges (e.g. inner edge; (Scholz et al., 2009)) of accretion disks and, or angular momentum instabilities and even surface flaring.
- (iii) BDs and VLMSs, (just as their massive counterparts) are thought to pass through a phase similar to the T Tauri phase at which variability may be induced through accretion of matter from circumstellar discs, a very common observed feature in (sub)stellar objects (see e.g. Morales et al., 2005; y Navascués and Martín, 2003; Muzerolle et al., 2003; Scholz and Eislöffel, 2004b,a; Zapatero-Osorio et al., 2003; Scholz et al., 2009), during their evolution and mass outflow events.
- (iv) Atmospheric events such as magnetic activity and atmospheric weather in their atmospheres (see e.g. Chabriel et al., 2005; Cody, 2009) and even holes in the atmospheric cloud deck (see e.g. Goldman et al., 2008).
- (v) Eclipsing events as a result of unseen companions or disks leading to periodic light variations (see e.g. Zapatero-Osorio et al., 2003).

Currently, it is generally believed that the kinds of variability observed in the very low mass objects and BDs is mainly caused by the above listed causes (i-v). However, periodic variability observed on time scales of a few hours has been hard to explain in terms of rotation since the inferred rotational velocities could exceed 100 km s^{-1} , the break-up velocities for these objects. A recently proposed interpretation in terms of stellar pulsations offers a new explanation based on their sub-stellar properties (see e.g. Palla and Baraffe, 2005, and references therein). This new proposed cause of variability in BDs and VLMSs is discussed further in section 1.3.

1.2 Brief introduction to stellar pulsations

Stellar Pulsations in stars

Pulsations in stars are analogous to vibrations of the strings in any stringed instrument such as *obokano*⁸ when plucked. The strings vibrate with different oscillatory patterns called modes where each mode is characterized by distinct features such as wavelength, number of nodes, and a frequency. In a three dimensional system such as a star, a rich variety of oscillations have been predicted by theory and these have already been observed in a large number of systems across the HR diagram. Stellar oscillations have been reported in the sun and solar type stars, giants and dwarfs, high metallicity and metal poor stars as well as stellar remnants such as white dwarfs(WDs) and neutron stars (NSs). One significance of stellar pulsations is that they strongly depend on the structure of the star, hence, by studying the oscillation frequencies one gets information about the interior structure of the star.

The pulsation period-mass (or density) relation is well established, and for a spherically symmetric star of radius R and mass M , the pulsation period P can be written as (see eg. Cox, 1976);

$$P \sim 2 \left(\frac{3}{\Gamma_1} \right)^{1/2} (MR^2)^{1/2} (-U)^{-1/2} \sim \left(\frac{I}{-U} \right)^{1/2} \quad (1.1)$$

where, $U = -\frac{\xi GM^2}{R}$ is the gravitational potential energy, $I = \int r^2 dm$ is the moment of inertia of the star about it's center of mass, Γ_1 is an ionization parameter and ξ is a constant. Equation ((1.1)) shows that for specific values of M and R , the pulsation period P will be shorter for a less centrally condensed star than for highly centrally condensed counterpart, provided other things are kept equal (Cox 1976). From the models used by Cox 1976, the mean densities of known kinds of stars fall approximately in the range $10^6 \gtrsim \frac{\bar{\rho}}{\rho_0} \gtrsim 10^{-9}$ leading to pulsation periods in the range $3seconds \lesssim P \lesssim 1000days$, which indeed spans the range of periods observed for most types of variable stars. Furthermore, this result provides a good general support for the pulsation theory of variable stars.

⁸A twelve stringed instrument famous among the Kisii community in Kenya usually held shoulder high by the player while dancing in cycles.

Types of Stellar Pulsations

The pulsations occurring in stars can be classified into two main classes; radial and non-radial pulsations. *Radial pulsations* are those in which the spherical symmetry of the stellar envelope is maintained throughout the pulsation cycle, while in *non-radial pulsations* the star no longer remains spherically symmetric through any pulsation cycle. In such pulsating systems the individual pulsation modes with nodes along the stellar surface can be characterized by two quantum numbers l and m where $l \geq |m|$. Radial oscillations are characterized by $l = 0$ and are spherically symmetric. An illustration of spherical harmonics for different values of l and m is displayed in figure 1.3.

The Driving mechanism of stellar Pulsations

The physical mechanism leading to pulsation instabilities in stars such as cepheids and cepheid-like stars is well understood, a simplified picture being that the radiation travelling from the interior of the star interacts with and gets modulated by the stellar matter in the outer opaque layers. Under favorable conditions the temperature and density dependence on the radiative absorption coefficients and the specific heats in these layers can lead to an oscillatory instability. However, if most of the energy is transported by convection as is the case in very cool stars, the stability will be dependent on the interaction between convection and pulsation. Since this thesis mentions two main effects encountered in stellar oscillations i.e *driving* and *damping* of the oscillations, a general description of these two effects is illustrated in figures 1.4 and 1.5 respectively. For driving to occur (see figure 1.4), heat needs to enter the system during the high temperature part of the cycle (i.e during maximum compression) and leave during the lower temperature part (i.e maximum expansion). This implies that maximum pressure will occur *after* maximum compression leading to amplification of the oscillations. This is what is shown in figure 1.4. On the other hand, when heat leaves the system during maximum compression (higher temperature part) and enters during maximum expansion (lower temperature part), maximum pressure will occur *before* maximum compression leading to damping. This is illustrated in figure 1.5. Here below, we discuss two mechanisms important in driving pulsations in stars.

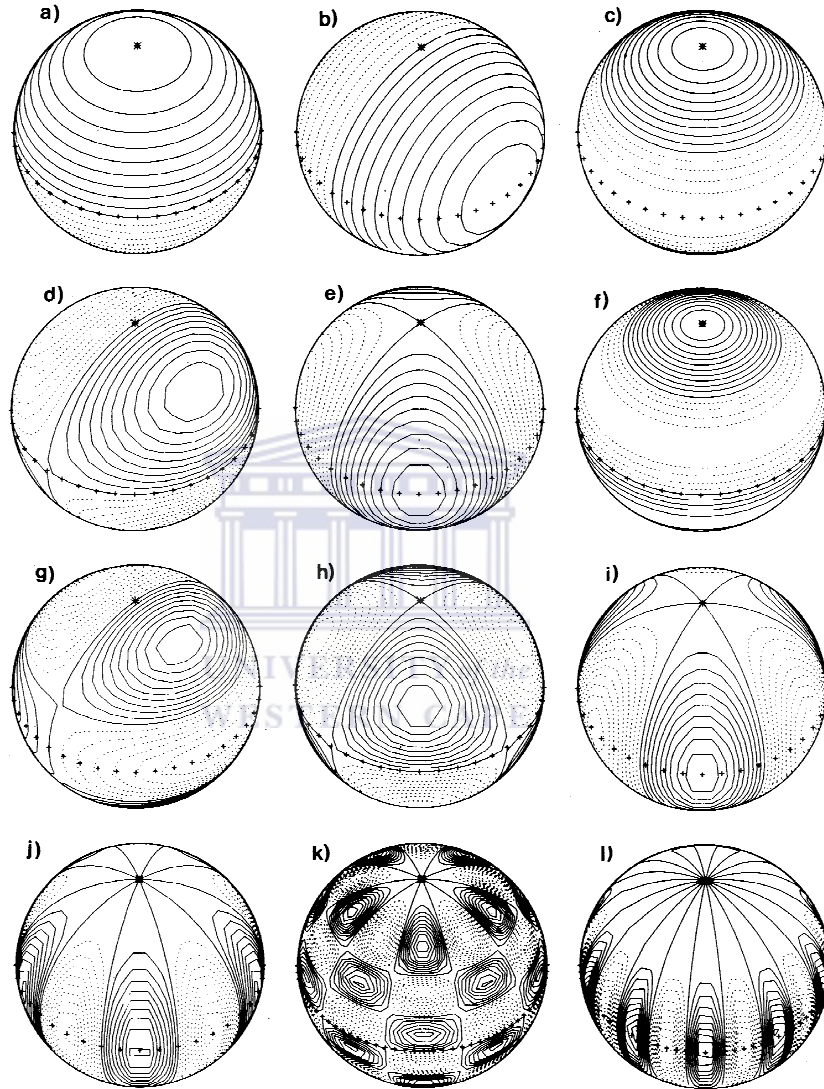


Figure 1.3: Examples of different spherical harmonics for various values of l and m . Credit: Figure from “*Lecture Notes on Stellar Oscillations*” by Jørgen Christensen-Dalsgaard, page 6, Figure 2.1. The cases illustrated are: a) $l = 1, m = 0$; b) $l = 1, m = 1$; c) $l = 2, m = 0$; d) $l = 2, m = 1$; e) $l = 2, m = 2$; f) $l = 3, m = 0$; g) $l = 3, m = 1$; h) $l = 3, m = 2$; i) $l = 3, m = 3$; j) $l = 5, m = 5$; k) $l = 10, m = 5$; l) $l = 10, m = 10$.

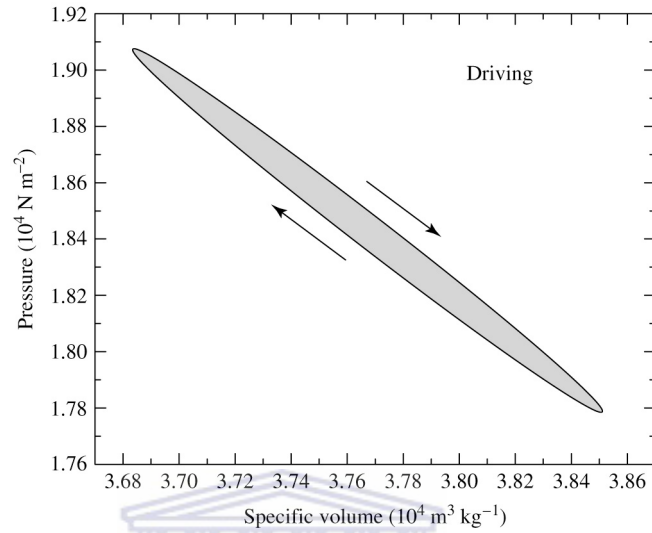


Figure 1.4: P-V diagram for a driving layer of an RR Lyrae star model (Credit: Figure from Carrol and Ostlie (1996), page 552, figure 14.9).

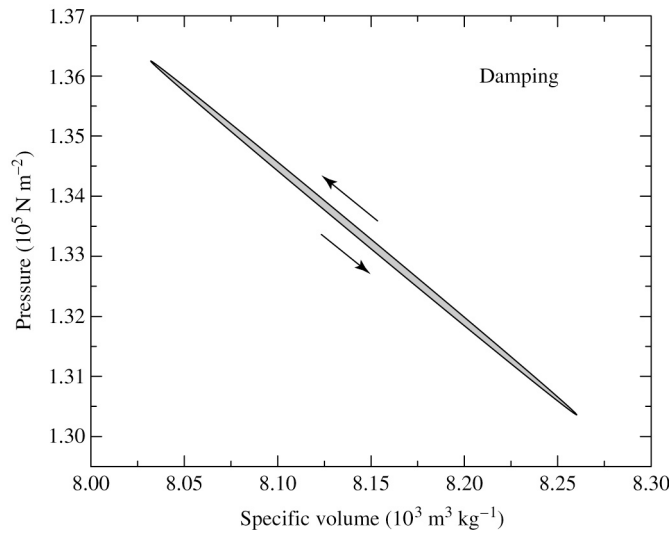


Figure 1.5: P-V diagram for a damping layer of an RR Lyrae star model (Credit: Figure from Carrol and Ostlie (1996), page 552, figure 14.9).

The kappa mechanism

The opacity of the stellar gas inside a star usually decreases with temperature, causing the damping of any oscillations that may be present. However, in the ionization zones of H and He, the opacity is found to increase with temperature. These ionization zones, therefore, become important in driving the pulsations as is the case in the classical pulsating variable stars.

This mechanism can be understood by studying what happens when the gas inside an ionization zone is compressed. Such a compression will cause the zone to heat up increasing its temperature leading to an increased ionization of (for example) HeI into HeII. This in turn causes the opacity to increase. The high opacity makes the zones more efficient in trapping of energy escaping from the stellar interior. This then leads to a build up of heat within the zone which leads to the zone storing more energy than needed to maintain a state of equilibrium with the weight of upper layers. The zone then pushes outwards, leading to an expansion of the gas inside the stellar zone. Meanwhile the expansion of the gas causes a decrease in opacity within the zone allowing an outward transport of energy. The result is a decrease in energy within the zone and a resultant weaker outward force unable to maintain a state of equilibrium with the upper layers. The upper layers then push inwards and the cycle is repeated. This process is called the '*kappa mechanism*' and is now known to be the underlying driving mechanism driving pulsations in stars located in the well known cepheid instability strip.

The epsilon mechanism

Driving due to the epsilon mechanism can be understood by following Eddington's proposal that a star is a form of thermodynamic heat engine in which, like any heat engine, the work done by a given layer inside the star is equal to the difference between the heat gained by the layer and the heat leaving the layer. It is related to the strong dependence of nuclear reactions on temperature and can be explained by studying what happens in the central nuclear burning region of a star during compression and expansion phases. When a star is compressed, the following happens: the volume decreases and the density increases.

The central temperature increases as the layer gains thermal energy as a result of the compression, which leads to an increase in the rate of nuclear reactions. This in turn increases the central temperature even further. It then happens that at maximum compression the density becomes maximum but since matter is still gaining heat from nuclear reactions, maximum pressure lags behind the maximum density. The central pressure then becomes higher than the inward pull of gravity and pushes the layer outwards. During the expansion phase, an increase in volume leads to a decrease in density and temperature. Due to the decrease in temperature, the rate of nuclear reactions decreases and the layer loses heat decreasing the temperature even further. At maximum expansion, the density and temperature becomes minimum and rate of the nuclear reactions becomes less than the equilibrium value as matter continues to lose heat. The result is that the central pressure becomes less than the equilibrium value so that the inward pull of gravity pushes the layers back towards the center. The cycle is repeated again. This driving is exactly the same as the heat engine proposed by Eddington since the system gains heat at maximum compression and loses heat during minimum compression (maximum expansion).

However, in many stars the effect due to this mechanism is found to be generally small when compared to the term of energy transfer which is responsible for damping the pulsations in these layers (see e.g. Lenain et al., 2006). It is therefore too weak to excite pulsations in most stars except very massive ones ($\gtrsim 100M_{\odot}$) (Saio, 1993), and the now proposed new class of BD and VLMSs. The possibility of this mechanism in driving stellar oscillations in VLMSs and BDs is discussed in section (1.3).

1.3 Stellar Pulsations in young brown dwarfs

There are a number of driving mechanisms behind the different classes of pulsating stars that we observe today, one of these, the ε -mechanism (defined in section (1.2)) is related to nuclear burning in the central regions of a star. Normally, we do not expect this mechanism to contribute significantly to the driving of the pulsations seen in stars. This is because the amplitudes of the oscillations that develop near the central nuclear burning regions of stars are predicted to be very small and the amount of driving due to this mechanism should, therefore, be negligible. However, stars with less centrally condensed interiors

(low mass stars and substellar objects) are thought to be potential sites for the ϵ -mechanism since the relative amplitudes of the radial eigenfunctions in the central regions appear to be significantly larger than those in massive stars. This phenomenon, in low mass main sequence stars, was first put forth by Gabriel (1964) and later by Toma (1972), in pre-main-sequence stars, in the mass range $0.2 - 2.0M_{\odot}$, although there has been no observational evidence to date for some of the reasons stated in PB05.

BDs have too little mass to start the combustion of light hydrogen into Helium-4 ($4^1H \rightarrow {}^4_2He$) in their centers, the nuclear reaction that powers all main sequence stars. However, BDs do still shine, though mainly by converting gravitational potential energy into thermal energy. When young they also generate energy from Deuterium-Helium3 conversion. Deuterium is a heavier form and a much rarer isotope of hydrogen (hydrogen-2).

It is due to the low temperature requirement of deuterium burning that even BDs (with low central temperatures) are able to ignite it. Moreover, since deuterium burning is exquisitely sensitive to the star's temperature (energy generation rate is proportional to the *twelfth* power of temperature), small fluctuations in temperature can lead to large increases in heat generation , and thus possibly trigger stellar oscillations.

PB05 propose that brown dwarfs (BDs) should pulsate when young during the deuterium burning phase in their centers, with periods in the range 1 – 5 hours for masses $0.02 - 0.1M_{\odot}$ and ages 1 – 15 Myrs. They predict growth rate time scales for the pulsation amplitudes well below the deuterium burning time scales for such objects, indicating that the perturbations may have time to grow to attain possibly observable amplitudes. Figure (1.6) from PB05 shows that in the early stages of the D-burning phase τ_e , the e-folding time characterizing the time scale for the growth of pulsation amplitudes (called τ_{growth} in PB05), is shorter than the D-burning time scale, τ_D , and remains small during a significantly larger part of the D-burning phase in lowest mass BDs (Palla and Baraffe, 2005). They also propose possible candidates for pulsational variability amongst known BDs in two of the nearest star-forming regions of Taurus and Auriga. A plot of their proposed D-instability strip is shown in figure (1.7).

Figure (1.8) shows the various properties of BDs and VLMSs from the PB05 study. Analysis of the differential work integral dW/dm within the structure of the D-burning objects reveals zones of both positive (driving) and negative (damping) work integrals with

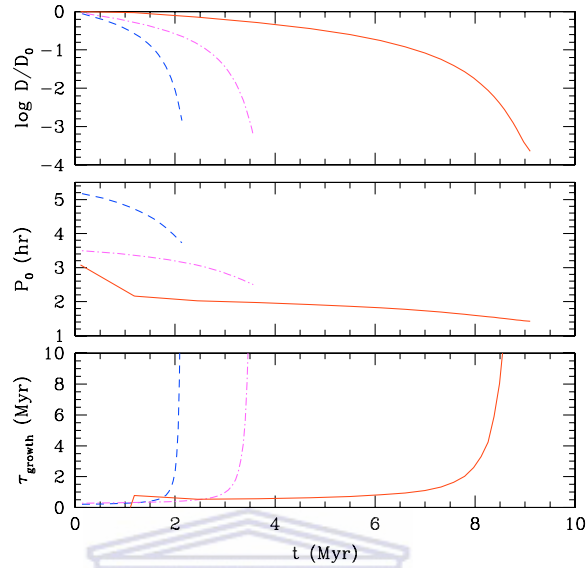


Figure 1.6: The evolution of the D-abundance, fundamental period p_0 (in h) and growth time scale τ_{growth} (in Myr) as a function of time during the D-burning phase of a $0.1M_\odot$ star (dashed line), and $0.06 M_\odot$ (dash-dotted line) and $0.03 M_\odot$ (solid line) BD [From Palla & Baraffe 2005]

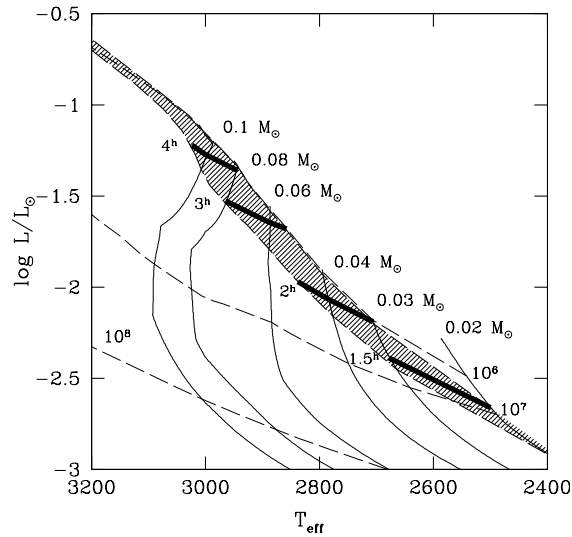


Figure 1.7: Location of the D-instability strip (shaded area) in the HR diagram. Tracks of different masses and isochrones are indicated as labelled. The isoperiod curves (in h) are shown by the thick lines within the strip [From Palla & Baraffe 2005].

M (M_{\odot})	age (Myr)	D/D_0	T_{eff} (K)	$\log L$ (L_{\odot})	P_0 (h)	τ_{growth} (Myr)
0.02	2.22	0.982	2540	-2.516	1.67	3.03
	15.9	0.054	2450	-2.801	1.18	2.49
	18.9	0.002	2390	-2.927	1.04	25.1
0.03	1.18	0.936	2710	-2.138	2.16	0.78
	6.60	0.121	2690	-2.271	1.77	0.94
	8.49	0.004	2680	-2.380	1.52	8.02
0.04	1.23	0.66	2790	-1.915	2.52	0.41
	3.71	0.148	2790	-1.985	2.26	0.65
	5.16	0.004	2780	-2.092	1.92	5.92
0.06	0.86	0.644	2890	-1.567	3.41	0.31
	2.16	0.218	2890	-1.616	3.15	0.43
	3.36	0.005	2890	-1.728	2.63	4.10
0.08	0.65	0.642	2950	-1.322	4.25	0.26
	1.39	0.315	2940	-1.356	4.02	0.32
	2.54	0.006	2940	-1.475	3.27	3.32
0.1	0.56	0.618	3010	-1.125	5.04	0.23
	1.11	0.307	3000	-1.162	4.77	0.29
	2.00	0.008	3000	-1.281	3.92	2.40

Figure 1.8: A summary of the properties of VLMSs and BDs during D-burning phase for different masses (From PB05)

the positive work in the central regions originating from the perturbation of the nuclear energy generation rate, a characteristic of the ε – mechanism as shown in figure (1.9).

A summary of other current articles making a follow-up to the PB05 proposal and relevant to this thesis are discussed briefly here below:

Barrado et al. (2005)

This paper presents the first results of variability studies of BDs and VLMSs found in the Lambda Orionis cluster. Twelve members of the cluster have been monitored in the J band during one night observation. One candidate, LOri167 with mass close to the limiting mass of planets is argued to show variability that can be associated with deuterium burning with a possibility of other causes not being ruled out.

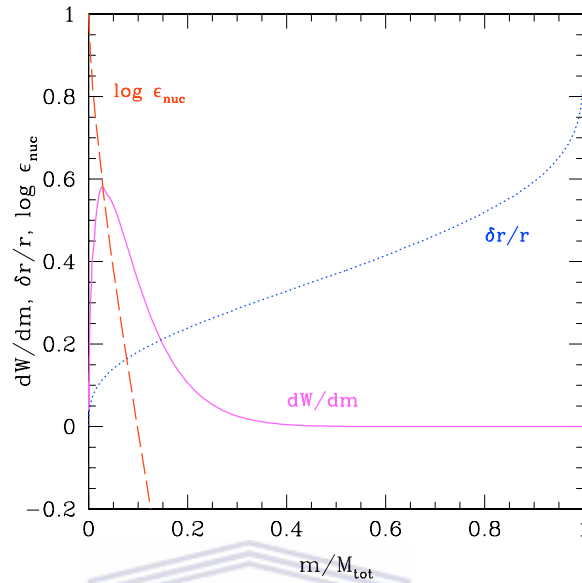


Figure 1.9: The differential work integral dW/dm (in arbitrary units, the solid line) as a function of interior mass (in units of total mass), the pulsation amplitude $\delta r/r$ (dotted line), arbitrary normalized to 1 at the surface, and the nuclear energy generation rate ϵ_{nuc} (in erg/g/s , dashed line) for a $0.03 M_{\odot}$ BD [From Palla & Baraffe 2005]

Marconi et al. (2007)

This study reports the launch of a program dedicated to test the results of PB07. Two particularly promising brown dwarf candidates: CFHT BD2 and CFHT BD3, which fall within the PB05 instability strip were selected and observed during winter 2005 with the 1.8m and 1.5m Asiago and Loiano telescopes respectively. The light curve and frequency analysis from preliminary results indicate that CFHT BD3 may be a periodic variable. The results displaying the observed variability are shown in figure (1.10).

Cody (2009)

A photometric campaign to search for low-amplitude pulsations among young star-clusters using various telescopes is presented, the aim is to independently test the models of PB05 using independent observations, and hence, better constrain- using fundamental physics- the basic parameters of BDs and eventually confirm the pulsational signatures in young

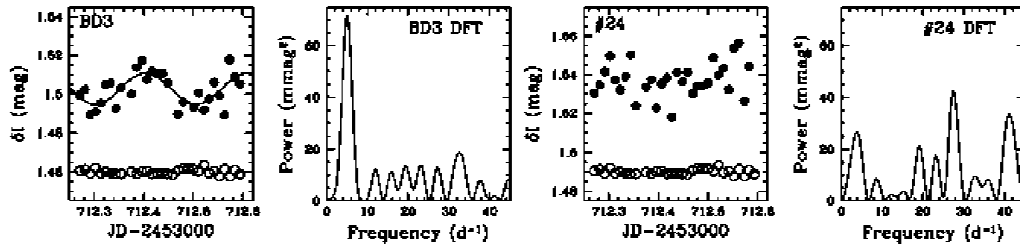


Figure 1.10: From left, *panel 1*: Full and empty dots show the Asiago data for CFHT BD3 and for the artificial comparison star, respectively; the solid line is a fit to the data; *panel 2*: DFT for BD3; *panels 3 & 4*: as *panels 1 & 2*, but for star number 24 [From Marconi et al. 2007].

BDs. A plot of the PB05 D-instability strip is plotted together with the possible candidates of pulsational variability from five young clusters as shown in figure (1.11).

Their preliminary results show a lack of variability on most of the BD targets on any timescale, with the only observed periods not shorter than 15 hours. Only a handful of cases show a possibility of periodicities in the periodogram at 1-5 hours, which in actual sense are barely above the detection limit at $S/N \gtrsim 4.0$, hence their evidence is not definitive. Conclusively, therefore, only upcoming space-based observations may provide the final word on the predicted variability. The periodogram for the most promising young brown dwarf candidate and a phased light curve in the Cody (2009) sample are shown in figure (1.12).

1.4 Aims and thesis outline

The main aims of this thesis are to:

- Generate equilibrium brown dwarf models with masses in the range $\sim 0.02M_{\odot} - 0.08M_{\odot}$ spanning the BD regime.
- Perform a non-adiabatic linear stability analysis with the ‘frozen-in convection approximation and test the prediction by PB05.

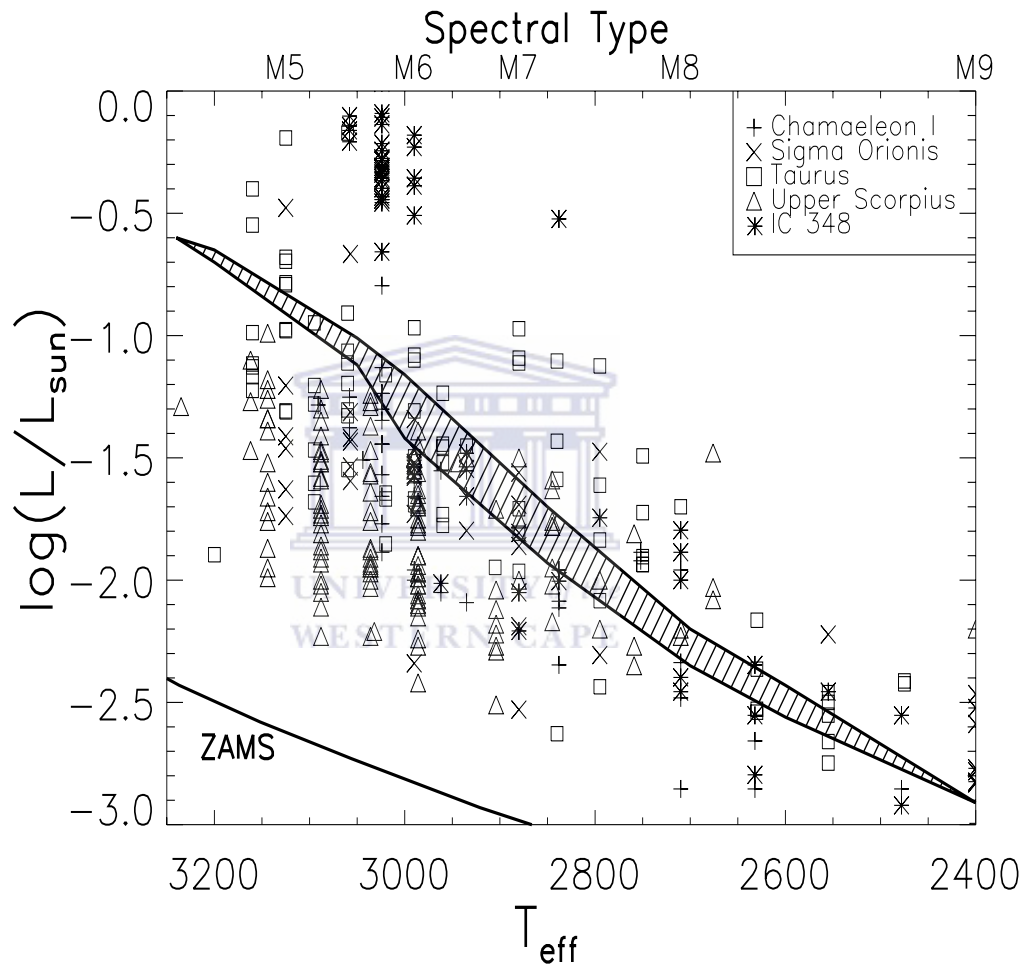


Figure 1.11: A Plot of the possible candidates for pulsational variability among known BD candidates in five young star clusters plotted with the PB05 D-instability strip from Cody (2009).

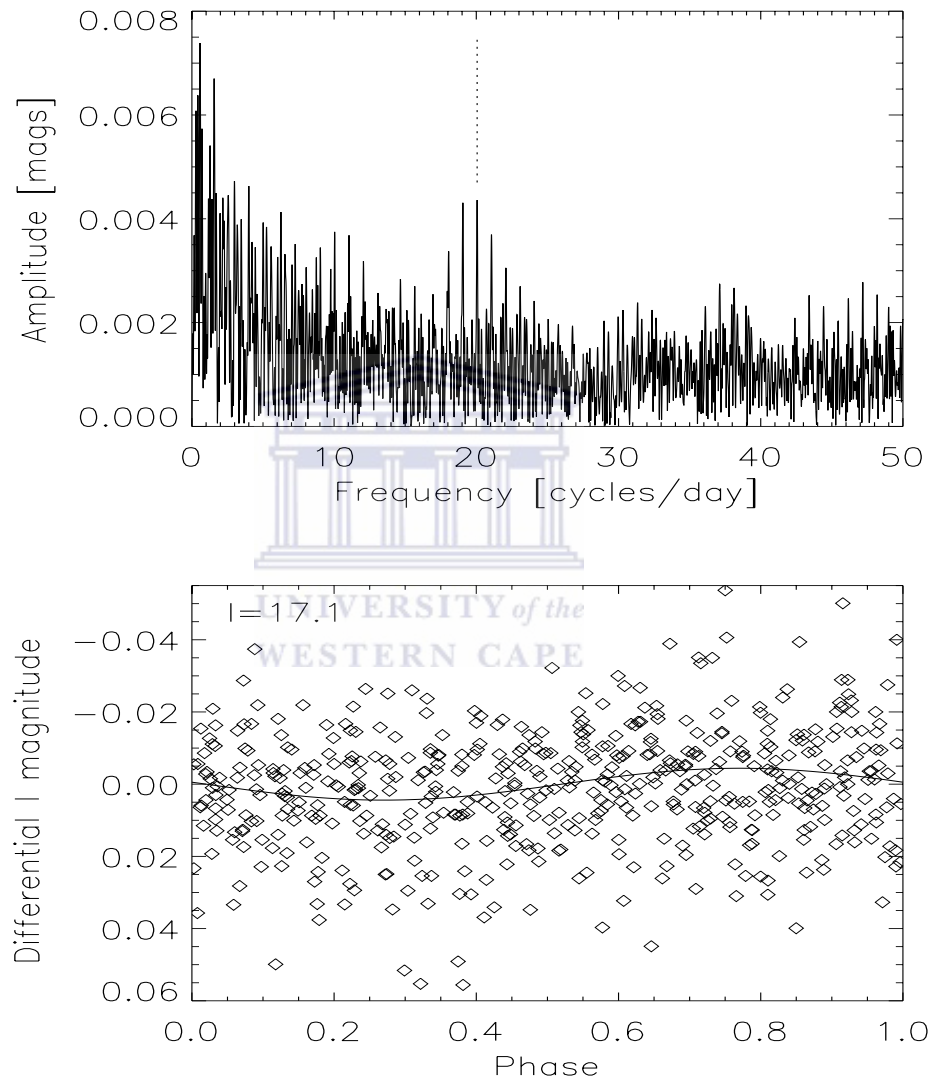


Figure 1.12: The periodogram for a brown dwarf in the AC09 sample together with a light curve phased to possible signal [From Cody 2009]

- Study the effects a time-dependent treatment of convection (including turbulent pressure, turbulent viscosity and turbulent diffusion) has on the pulsation properties of young brown dwarfs.
- Estimate pulsation constants and period ratios from the linear calculations that will be useful in direct comparisons with future observations.
- Study the effects of variations in the main ‘free parameters’ associated with current non local theories of time-dependent turbulent convection such as Kuhfuß (1986) and Stellingwerf (1984).

This thesis is arranged as follows:

Chapter 1 presents the background of the growing field of research in BDs and sub-stellar objects, a brief introduction to stellar oscillations in stars and a discussion of the recently predicted phenomenon of stellar pulsations in young BDs including a review of the most recent articles featuring this area.

Chapter 2 deals with the partial differential fluid and convection equations, a derivation of the corresponding perturbation and linear pulsation equations, a derivation of formulae for the pulsation work integrals and a description of the relevant physical input and numerical methods used in this thesis.

Chapter 3 presents results of detailed calculations to verify the predictions by PB05 using their assumptions and calculations of theoretical pulsation constants and period ratios for various objects falling within the BD mass regime.

Chapter 4 introduces a time-dependent model of convection, studies the effects of turbulent pressure, turbulent viscosity and turbulent diffusion on the stability properties of various BD models.

Chapter 5 provides our discussions, conclusions and a call for further work.

Chapter 2

Equations, theory and physical input

This chapter presents a summary of the basic pulsation and convection equations used in this study. Only purely radial, spherically symmetric fluid flow is assumed. Magnetic stresses and rotational effects are ignored. It is assumed that the only forces acting are those due to gravity and pressure gradients. Turbulent pressure and turbulent viscosity are included. A Lagrangian description is adopted in which the interior mass, M_r (total mass within a sphere of radius r) and time, t , are treated as independent variables. The basic fluid and convection equations (in partial differential form) are presented in §2.1.1. Their linearized forms are derived in §2.1.2. The main equations presented here include; the mass conservation equation, the momentum equation, the total energy equation, the radiative energy equation and the turbulent energy equation. The numerical solutions employed are discussed in appendix A. Expressions for the total (integrated) work integrals (WIs) are derived in §2.2. Finally, a discussion of the relevant physical input is given in § 2.3.

2.1 The pulsation and convection equations

The equations presented here are based on the original fluid and convection equations given in Olivier and Wood (2005) (OW05, hereafter). A time-dependent equation for radiative transfer from Castor (1972) is included (see equations 2.6 and 2.9) and the radiation and gas contributions to the total pressure and internal energy respectively are explicitly separated. The nuclear energy generation rate is included in the total energy equation. There

are two types of descriptions available for spherically symmetric fluid flow: *Eulerian* and *Lagrangian*. In the Eulerian formalism, the various physical properties of the moving fluid such as the mass density ρ , the temperature T , the total pressure P and the mean radial velocity v_r , are treated as *field* quantities (i.e as functions of the position r and time t). The Eulerian variable r does not give the position of any particular moving fluid element but denotes the position of ‘*the point of observation*’ and is an independent variable. In the Lagrangian description, the motion of a particular fluid element is followed. In this case, the Lagrangian variable r denotes the position of a particular fluid element and is a dependent variable. In general, a Eulerian description is found to be more suitable in problems involving many degrees of freedom (multi-space dimension) while the Lagrangian description is preferable in problems of only one degree of freedom. Because this thesis deals with the one-dimensional problem of radial stellar pulsations only, a Lagrangian description is adopted throughout.

2.1.1 The partial differential equations

The equations in terms of a time variable t and the Lagrangian variable M_r , governing the motion and thermodynamics of a stellar envelope are:

$$\frac{\partial r^3}{\partial M_r} - \frac{3}{4\pi\rho} = 0 \quad (2.1)$$

$$\frac{dr}{dt} - v_r = 0 \quad (2.2)$$

$$\frac{dv_r}{dt} + 4\pi r^2 \frac{\partial}{\partial M_r} [P_g + P_r + P_t + P_{tv}] + \frac{GM_r}{r^2} = 0 \quad (2.3)$$

$$\frac{d}{dt} \left(e_g + \frac{J}{\rho} + \varpi^2 \right) - \frac{[P_g + P_r + P_t + P_{tv}]}{\rho^2} \frac{\partial \rho}{\partial t} + \frac{\partial L}{\partial M_r} - \varepsilon_{nuc} = 0 \quad (2.4)$$

$$\frac{d\varpi^2}{dt} - \frac{P_t + P_{tv}}{\rho^2} \frac{d\rho}{dt} + \frac{\partial L_t}{\partial M_r} - C_\varpi = 0 \quad (2.5)$$

$$\frac{d}{dt} \left(\frac{J}{\rho} \right) - \frac{P_r}{\rho^2} \frac{d\rho}{dt} + \frac{\partial L_r}{\partial M_r} - C_r = 0 \quad (2.6)$$

with

$$L = L_r + L_c + L_t \quad (2.7)$$

and

$$\frac{d}{dt} \equiv \frac{\partial}{\partial t} + v_r \frac{\partial}{\partial r} \quad (2.8)$$

being the total luminosity and the Stokes (or substantial or material) derivative respectively. Here ρ is the mass density, e_g is the internal gas energy per unit mass, and v_r is the radial velocity. These quantities represent their mean values over a spherical surface of radius r . G is the gravitational constant, P_g is the local gas pressure, M_r is the total mass within a sphere of radius r and L_r is the radiative luminosity given by:

$$L_{rad} = -\frac{16\pi^2 c}{\kappa} \frac{\partial J}{\partial M_r} \quad (2.9)$$

where J is the radiation energy density (energy per unit volume, V), κ is the mean Rosseland opacity and c is the speed of light. The radiation pressure is $P_r = \frac{1}{3}J$. The term C_r in equation (2.6) is given by;

$$C_r = c\kappa (aT^4 - J) \quad (2.10)$$

where T is the temperature and a is the radiation energy constant. The remaining independent variables in equations (2.3) to (2.5) characterize the turbulent convective flow. The mean specific turbulent energy is ϖ^2 and it is a measure of the strength of the turbulence. The turbulent pressure is given by:

$$P_t = \alpha_p \rho \varpi^2 \quad (2.11)$$

It is given by the trace of the so called Reynolds stress tensor, from which it follows immediately that $\alpha_p = \frac{2}{3}$ by definition (see Kuhfuß 1986). The traceless part of the Reynolds stress tensor is responsible for the dissipation of the kinetic energy of pulsation, and needs to be modeled. Kuhfuß (1986) models this using a tensor similar to the usual stress tensor, by defining a turbulent viscosity $\mu = \alpha_\mu \varpi \Lambda$, where Λ is some scale length and α_μ is a free

parameter. Here we prefer to model it as a small scale pressure term similar to Stellingwerf (1984). Our only requirement is that it behave as a purely dissipative term and is close in form (dimensionally) to the original terms in the momentum and energy relations derived by Kuhfuß (1986). We adopt the following for this turbulent viscous “pressure” term:

$$P_{tv} = -\frac{4}{3}\mu\rho\frac{1}{r^2}\frac{\partial r^2}{\partial r}v_r = -\frac{16}{3}\pi\mu\rho^2\frac{\partial r^2}{\partial M_r}v_r \quad (2.12)$$

Although in general P_t can be both positive and negative, we show in section 2.2 that it is purely dissipative in nature.

The turbulent luminosity L_t (turbulent energy transported per unit time) is modelled using a diffusion approximation:

$$L_t = -4\pi\alpha_t\Lambda\varpi r^2\rho^2\frac{\partial\varpi^2}{\partial M_r} \quad (2.13)$$

where α_t is a free parameter of order unity. The term C_ϖ in equation (2.5) can be written as $C_\varpi = S - D_t$ where:

$$D_t = \frac{\alpha_d}{\Lambda}(\varpi^3 - \varpi_F^3) \quad (2.14)$$

and

$$S = \frac{\nabla_{ad}}{H_p}\Pi \quad (2.15)$$

the equation for C_ϖ becomes;

$$C_\varpi = \frac{\nabla_{ad}}{H_p}\Pi - \frac{\alpha_d}{\Lambda}(\varpi^3 - \varpi_F^3) \quad (2.16)$$

where α_d is a free parameter and ϖ_F is a small positive velocity (see Olivier & Wood 2005 for details). D_t represents the (slightly modified) dissipation of specific turbulent energy due to molecular viscosity. S is the source (or sink) of specific turbulent energy due to buoyancy forces, $H_p = -\left(\frac{\partial \ln P}{\partial r}\right)^{-1}$ is the pressure scale height, $\nabla_{ad} = \left(\frac{\partial \ln T}{\partial \ln P}\right)_{ad}$ is the adiabatic temperature gradient and $\Pi = \frac{\langle T \rangle \langle [\rho v' s] \rangle}{\langle \rho \rangle}$ is the velocity-entropy correlation function. The angular brackets denotes the mean over a spherical surface and v' is the

fluctuating velocity. All quantities inside the brackets refer to local (as opposed to mean) values (see Kuhfuß 1986 for details) . Π is modelled in the same way as Kuhfuß (1986) using a diffusion approximation:

$$\Pi = -\alpha_s \varpi \Lambda T \frac{\partial s}{\partial r} \quad (2.17)$$

With this result, it can easily be shown that:

$$\Pi = \alpha_s \varpi \frac{\Lambda}{H_p} c_p T (\nabla - \nabla_{ad}) \quad (2.18)$$

where $\nabla = \frac{d \ln T}{d \ln P}$ and c_p is the specific heat at constant pressure. Kuhfuß (1986) compared the above convection model, in the local and static limit (ignoring P_t), to the usual mixing-length treatment and found that:

$$\alpha_s = \sqrt{\frac{2}{3}} \alpha_\Lambda \quad (2.19)$$

$$\alpha_d = \frac{128}{9} \frac{1}{\alpha_s} \quad (2.20)$$

Here, the scale length Λ is identified with the usual mixing-length and is taken to be proportional to the local hydrostatic pressure scale height:

$$\Lambda = \alpha_\Lambda H_p = \alpha_\Lambda \frac{r^2 P}{GM_r \rho} \quad (2.21)$$

The convective luminosity is given by:

$$L_c = 4\pi r^2 \rho \Pi \quad (2.22)$$

The model presented above, therefore, contains only three free parameters α_t , α_Λ and α_μ .

2.1.2 The Linearized Equations

The general equations presented in §(2.1.1) are nonlinear, partial differential equations (PDE's) whose exact solutions are, generally, not known in analytic form. Consider a

particular solution at a time $t = t_0$ (the ‘unperturbed’ solution) and a second ‘perturbed’ solution (at say, $t = t_1$) which differs only slightly from the former. If the two solutions differ from each other only slightly, then the dynamical variables such as ρ , P , T e.t.c corresponding to the perturbed solution can be expressed as the sum of their corresponding values for the unperturbed solution and a small Lagrangian perturbation, as shown below for example:

$$\begin{aligned}
 r &= r_o \left(1 + \frac{\delta r}{r_o} \right) \\
 \rho &= \rho_0 \left(1 + \frac{\delta \rho}{\rho_0} \right) \\
 P &= P_0 \left(1 + \frac{\delta P}{P_0} \right) \\
 L_r &= L_{r,0} \left(1 + \frac{\delta L}{L_{r,0}} \right) \\
 \varpi &= \varpi_0 \left(1 + \frac{\delta \varpi}{\varpi_0} \right)
 \end{aligned} \tag{2.23}$$

In this thesis, we take the static model as our ‘unperturbed’ solution while the solution to the dynamical equations to constitute the ‘perturbed’ solution. To obtain the linearized equations from the original PDEs, the following steps are followed: (1) The perturbations of the form (2.23) are inserted in the PDEs. (2) Taylor expansions are performed and higher order terms (more than first order) ignored. (3) The equations for the static model are then subtracted from the resulting equations to give the linearized equations.

The mass equation:

Substituting the expressions for r and ρ from equation (2.23) into equation (2.1) and performing the steps just outlined above, we get:

$$\frac{\partial}{\partial M_r} \left[r_o \left(1 + \frac{\delta r}{r_o} \right) \right]^3 - \frac{3}{4\pi \left[\rho_0 \left(1 + \frac{\delta \rho}{\rho_0} \right) \right]} = 0 \tag{2.24}$$

where the mass conservation equation for the static case is:

$$\frac{\partial r_0^3}{\partial M_r} - \frac{3}{4\pi\rho_0} = 0 \quad (2.25)$$

Using Taylor expansion and neglecting higher than first order terms: $r_0^3 \left(1 + \frac{\delta r}{r_0}\right)^3 \approx r_0^3 + 3r_0^2\delta r$ and $\frac{1}{1+\frac{\delta\rho}{\rho}} \approx 1 - \frac{\delta\rho}{\rho}$, and, (2.24) becomes;

$$\frac{\partial r_0^3}{\partial M_r} - \frac{3}{4\pi\rho_0} + 3\frac{\partial}{\partial M_r}(r_0^2\delta r) + \frac{3}{4\pi\rho_0^2}\delta\rho = 0 \quad (2.26)$$

Subtracting equation (2.25) from equation (2.26) leads to:

$$\frac{\partial}{\partial M_r}(r_0^2\delta r) + \frac{1}{4\pi\rho_0^2}\delta\rho = 0 \quad (2.27)$$

which is the *linearized mass conservation equation*.

The velocity equation:

From the definition of the radial velocity (2.2), substituting the expressions $r = r_0 + \delta r$ and $v_r = v_{r,0} + \delta v_r$ for the perturbed position and radial velocity respectively, we obtain:

$$\frac{d}{dt}(r_0 + \delta r) - (v_{r,0} + \delta v_r) = 0 \quad (2.28)$$

but, in the static case $\frac{dr_0}{dt} = 0$ and $v_{r,0} = 0$. This gives:

$$\frac{d}{dt}(\delta r) - \delta v_r = 0 \quad (2.29)$$

which is the *linearized radial velocity equation*.

The momentum equation:

Substituting expressions of the form (2.23) into equation (2.3) and noting that the Taylor expansions of $(r_0 + \delta r)^2$ and $(r_0 + \delta r)^{-2}$ are: $r_0^2 + 2r_0\delta r + (\delta r)^2$ and $r_0^{-2} - 2r_0^{-3}\delta r + 3(\delta r)^2 r_0^{-4} \equiv r_0^{-2}(1 - 2\frac{\delta r}{r_0} + (\frac{\delta r}{r_0})^2)$ respectively, we get:

$$\frac{d}{dt}(v_{r,0} + \delta v_r) + 4\pi(r_0^2 + 2r_0\delta r + \delta r^2) \frac{\partial}{\partial M_r} (P_{tot} + \delta P_{tot}) + \frac{GM_r}{r_0^2 \left(1 + 2\frac{\delta r}{r_0} + \left(\frac{\delta r}{r_0}\right)^2\right)} = 0 \quad (2.30)$$

Ignoring higher than first order terms and rearranging, leads to:

$$\frac{d\delta v_r}{dt} + 4\pi r_0^2 \frac{\partial P_{tot,0}}{\partial M_r} + 4\pi r_0^2 \frac{\partial \delta P_{tot}}{\partial M_r} - 8\pi r_0 \delta r \frac{\partial P_{tot}}{\partial M_r} + \frac{GM_r}{r_0^2} - \frac{2GM_r}{r_0^2} \left(\frac{\delta r}{r_0}\right) = 0 \quad (2.31)$$

Subtracting the equilibrium equation for the static case:

$$4\pi r_0^2 \frac{\partial P_{tot,0}}{\partial M_r} + \frac{GM_r}{r_0^2} = 0 \quad (2.32)$$

and noting that;

$$8\pi r_0 \delta r \frac{\partial P_{tot}}{\partial M_r} = 2 \left(4\pi r_0^2 \frac{\partial P_{tot,0}}{\partial M_r}\right) \frac{\delta r}{r_0} = \frac{2GM_r}{r_0^2} \left(\frac{\delta r}{r_0}\right) \quad (2.33)$$

yields:

$$\frac{d\delta v_r}{dt} + 4\pi r_0^2 \frac{\partial \delta P_{tot}}{\partial M_r} - \frac{4GM_r}{r_0^2} \left(\frac{\delta r}{r_0}\right) = 0 \quad (2.34)$$

where $P_{tot} = P_g + P_r + P_t + P_{tv}$ is the total pressure and $\delta P_{tot} = \delta p_g + \delta P_r + \delta P_t + \delta P_{tv}$ is the sum of the perturbations of the different pressure terms. Equation (2.34) is the *linearized momentum equation*.

The total energy equation:

The internal gas energy per unit mass e_g , the radiation energy density J and the turbulent energy density ϖ^2 can also be written in the form (2.23). Putting these expressions into the total energy equation leads to:

$$\frac{d}{dt} \left(e_{g,0} + \delta e_g + \frac{J_0 + \delta J}{\rho_0 + \delta \rho} + (\varpi_0 + \delta \varpi)^2 \right) - \frac{P_{tot,0} + \delta P_{tot}}{(\rho_0 + \delta \rho)^2} \frac{\partial(\rho_0 + \delta \rho)}{\partial t} \quad (2.35)$$

$$+ \frac{\partial(L_{tot,0} + \delta L_{tot})}{\partial M_r} - (\varepsilon_{nuc,0} + \delta \varepsilon_{nuc}) = 0 \quad (2.36)$$

noting that;

$$\frac{J_0 + \delta J}{\rho_0 + \delta \rho} = (J_0 + \delta J) \left[\frac{1}{\rho_0 \left(1 + \frac{\delta \rho}{\rho_0}\right)} \right] \simeq \frac{J_0}{\rho_0} - J_0 \frac{\delta \rho}{\rho_0^2} + \frac{\delta J}{\rho_0} \quad (2.37)$$

and

$$(\varpi_0 + \delta \varpi)^2 \simeq \varpi_0^2 + 2\varpi_0 \delta \varpi \quad (2.38)$$

where we have ignored the higher order terms $\left(\frac{\delta J \delta \rho}{\rho_0^2}\right)$ and $\delta \varpi^2$

equation (2.35) becomes:

$$\frac{d\delta e_g}{dt} + \frac{1}{\rho_0} \frac{d\delta J}{dt} - \frac{d}{dt} \left(J_0 \frac{\delta \rho}{\rho_0^2} \right) + 2\varpi_0 \frac{d\delta \varpi}{dt} + \frac{P_{tot,0}}{\rho_0^2} \frac{d\delta \rho}{dt} + \frac{dL_{tot,0}}{dM_r} + \frac{d\delta L_{tot}}{dM_r} - \varepsilon_{nuc,0} - \delta \varepsilon_{nuc} = 0 \quad (2.39)$$

where $\frac{d\rho_0}{dt} = 0$ and $\frac{d}{dt} \left(e_{g,0} + \frac{J_0}{\rho_0} + \varpi_0^2 \right) = 0$ in the static case.

Subtracting the equation for the static equilibrium:

$$\frac{dL_{tot,0}}{dM_r} - \varepsilon_{nuc,0} = 0 \quad (2.40)$$

we get:

$$\frac{d\delta e_g}{dt} + \frac{d\delta J}{dt} - \frac{d}{dt} \left(J_0 \frac{\delta \rho}{\rho_0^2} \right) + 2\varpi_0 \frac{d\delta \varpi}{dt} + \frac{P_{tot,0}}{\rho_0^2} \frac{d\delta \rho}{dt} + \frac{d\delta L}{dM_r} - \delta \varepsilon_{nuc} = 0 \quad (2.41)$$

which is the *linearized total energy equation*.

The radiative energy equation:

Equation (2.6) for radiative energy becomes (substituting $J = J_0 + \delta J$, $P_r = P_{r,0} + \delta P_r$, $\rho = \rho_0 + \delta \rho$, $L_r = L_{r,0} + \delta L_r$ and $C_r = C_{r,0} + \delta C_r$):

$$\frac{d}{dt} \left(\frac{J_0 + \delta J}{\rho_0 + \delta \rho} \right) - \frac{P_{r,0} + \delta P_r}{(\rho_0 + \delta \rho)^2} \frac{d(\rho_0 + \delta \rho)}{dt} + \frac{\partial(L_{r,0} + \delta L_r)}{\partial M_r} - (C_{r,0} + \delta C_r) = 0 \quad (2.42)$$

Applying Taylor expansion and separating terms, we get:

$$\begin{aligned} & \frac{d}{dt} \left[(J_0 + \delta J) \left(\frac{1}{\rho_0} - \frac{\delta \rho}{\rho_0^2} \right) \right] - \left[(P_{r,0} + \delta P_r) \left(\frac{1}{\rho_0^2} - 2 \frac{\delta \rho}{\rho_0^3} \right) \left(\frac{d\rho_0}{dt} + \frac{d\delta \rho}{dt} \right) \right] \\ & \quad + \frac{dL_{r,0}}{dM_r} + \frac{d\delta L_r}{dt} - C_{r,0} - \delta C_r = 0 \\ \implies & \left[\frac{d}{dt} \left(\frac{J_0}{\rho_0} \right) - \frac{P_{r,0}}{\rho_0^2} \frac{d\rho_0}{dt} + \frac{dL_{r,0}}{dM_r} - C_{r,0} \right] + \frac{d}{dt} \left(\frac{\delta J}{\rho_0} \right) - \frac{d}{dt} \left(J_0 \frac{\delta \rho}{\rho^2} \right) \\ & \quad + 2P_{r,0} \frac{\delta \rho}{\rho_0^3} \frac{d\rho_0}{dt} + 2P_{r,0} \frac{\delta \rho}{\rho_0^3} \frac{d\delta \rho}{dt} - \frac{P_{r,0}}{\rho_0^2} \frac{d\delta \rho}{dt} + \frac{\delta P_r}{\rho_0^2} \frac{d\rho_0}{dt} + \frac{d\delta L_r}{dM_r} - \delta C_r = 0 \end{aligned}$$

subtracting the equation for static equilibrium and applying the static case condition ($\frac{d\rho_0}{dt} = 0$), we get:

$$\frac{d}{dt} \left(\frac{\delta J}{\rho_0} - J_0 \frac{\delta \rho}{\rho_0^2} \right) + 2P_{r,0} \frac{\delta \rho}{\rho_0^3} \frac{d\delta \rho}{dt} - \frac{P_{r,0}}{\rho_0^2} \frac{d\delta \rho}{dt} + \frac{d\delta L_r}{dM_r} - \delta C_r = 0 \quad (2.43)$$

which is the required *linearized radiative energy equation*.

The turbulent energy equation:

Similar to the above derivations, introducing Lagrangian perturbations of ϖ , P_t , P_{tv} , ρ , L_t and C_ϖ , equation (2.5) becomes:

$$\begin{aligned}
\frac{d}{dt} (\varpi_0^2 + 2\varpi_0 \delta\varpi_0) + \frac{P_{t,0} + \delta P_t + P_{tv,0} + \delta P_{tv}}{(\rho_0^2 + \delta\rho)^2} \frac{d}{dt} (\rho_0 + \delta\rho) + \frac{d}{dM_r} (L_{t,0} + \delta L_t) - C_{\varpi,0} - \delta C_{\varpi} &= 0 \\
\frac{d\varpi_0}{dt} + 2\varpi_0 \frac{d\delta\varpi}{dt} + \frac{P_{t,0} + \delta P_t + \delta P_{tv}}{\rho_0^2 \left(1 + \frac{\delta\rho}{\rho_0}\right)} \left(\frac{d\delta\rho}{dt}\right) + \frac{dL_{t,0}}{dM_r} + \frac{d\delta L_t}{dM_r} - C_{\varpi,0} - \delta C_{\varpi} &= 0 \\
\implies 2\varpi_0 \frac{d\delta\varpi}{dt} + \frac{P_{t,0}}{\rho_0^2} \frac{d\delta\rho}{dt} + \frac{d\delta L_t}{dM_r} - \delta C_{\varpi} &= 0
\end{aligned}$$

is the *linearized turbulent energy equation*.

2.2 The Work intergrals

Using the result $\delta v_r = \frac{d}{dt}(\delta r)$ (equation 2.29), we can write the linearized momentum equation (2.34) as:

$$\frac{d^2(\delta r)}{dt^2} + 4\pi r^2 \frac{\partial}{\partial M_r} (\delta P_{tot}) - \frac{4GM_r}{r_0^2} \left(\frac{\delta r}{r_0}\right) = 0 \quad (2.44)$$

Assuming a time-dependence of the form $\delta x = \delta x_{sp} e^{\omega t} = |\delta x| e^{(\omega t + \phi_x)}$ where ϕ_x is the phase difference, for perturbations such as $\delta r, \delta \rho$ etc, where $\omega = \omega_R + \omega_I$ is the complex eigen frequency, we can write equation (2.44) as:

$$\omega^2 \delta r + 4\pi r^2 \frac{\partial}{\partial M_r} (\delta P_{tot}) - \frac{4GM_r}{r_0^2} \left(\frac{\delta r}{r_0}\right) = 0 \quad (2.45)$$

substituting for ω and making it the subject of the formula gives:

$$(\omega_R^2 + 2i\omega_r \omega_i - \omega_I^2) \delta r = -4\pi r^2 \frac{\partial (\delta P_{tot})}{\partial M_r} + \frac{4GM_r}{r_0^2} \left(\frac{\delta r}{r}\right) \quad (2.46)$$

Multiply both sides of equation (2.46) by $\pi(\delta r^*) dM_r$ (where δr^* is the complex conjugate) and integrate from the center (where $M_r = 0$) to the surface (where $M_r = M$). Noting that the relative pulsation amplitude at the center is zero and the perturbation in pressure

becomes zero at the surface (boundary conditions), integrating and separating the real and imaginary parts gives:

$$2\pi\omega_I^2 \frac{\omega_R}{\omega_I} \int_0^M \delta r \delta r^* dM_r = -4\pi^2 \int_0^M I_m \left[r^2 \frac{\partial}{\partial m_r} (\delta P_{tot}) \delta r^* \right] dM'_r \quad (2.47)$$

$$= -4\pi^2 \int_0^M I_m \left[(\delta P_{tot}) \left(\frac{1}{4\pi} \frac{\delta \rho^*}{\rho} \right) \right] dM'_r \quad (2.48)$$

$$= -\pi \int_0^M I_m \left[(\delta P_{tot}) \frac{\delta \rho^*}{\rho} \right] dM'_r \quad (2.49)$$

where in the second step, we have used the linearized form of the continuity equation which gives; $r^2 \frac{\partial \delta r^*}{\partial M_r} = \frac{1}{4\pi} \frac{\delta \rho^*}{\rho}$.

Noting that $2\pi \frac{\omega_R}{\omega_I}$ is the pulsation amplitude growth rate for a cycle, η , we can write;

$$\eta = 2\pi \frac{\omega_R}{\omega_I} = \frac{\pi}{E_k} \int I_m \left[(\delta P_{tot}) \frac{\delta \rho^*}{\rho} \right] dM'_r \quad (2.50)$$

with $E_k = \omega_I^2 \int \delta r \delta r^* dM_r$.

The total integrated work per cycle is then defined as:

$$W = -\pi \int_0^M I_m \left[\delta P_{tot} \delta \rho^* / \rho^2 \right] dM'_r \quad (2.51)$$

which is the general expression for the pulsation IWs (where the initials IWs stand for Integrated Work integrals). The partial work integral defined by $W_r = -\pi \int_0^M I_m \left[\delta P_{tot} \delta \rho^* / \rho^2 \right] dM'_r$ is used in identifying the ‘driving’ regions ($\frac{dW_r}{dr} > 0$) and ‘damping’ regions ($\frac{dW_r}{dr} < 0$) inside a given stellar model.

The Work integrals in alternative forms

Formulae for the IWs from gas pressure W_{gp} , radiation pressure W_{rp} , turbulent pressure, W_{tp} and the turbulent viscous pressure, W_{tvp} , are derived in this section. The total work integral is then defined to be the sum $W = W_{gp} + W_{rp} + W_{tp} + W_{tvp}$. The total energy equation (2.4) can be split into three independent equations corresponding to each of the three components (gas, radiation and turbulent stresses). These can be written as:

$$\frac{dE_g}{dt} - \frac{P_g}{\rho^2} \frac{d\rho}{dt} = \epsilon_{nuc} - \frac{\partial L_c}{\partial M_r} - C_r - C_{\varpi} \quad (2.52)$$

$$\frac{dE_r}{dt} - \frac{P_r}{\rho^2} \frac{d\rho}{dt} = -\frac{\partial L_r}{\partial M_r} + C_r \quad (2.53)$$

$$\frac{dE_t}{dt} - \frac{P_t}{\rho^2} \frac{d\rho}{dt} = -\frac{\partial L_t}{\partial M_r} + C_{\varpi} \quad (2.54)$$

with E_r and E_t defined as; $E_r = \frac{I}{\rho}$ and $E_t = \varpi^2$.

Using,

$\frac{d}{dt} \left(\frac{1}{\rho} \right) = -\frac{1}{\rho^2} \frac{d\rho}{dt}$ and $\frac{1}{\rho} = V$ where V is the specific volume, the equations (2.52), (2.53) and (2.54) become:

$$\frac{dE_g}{dt} + P_g \frac{dV}{dt} = \epsilon_{nuc} - \frac{dL_c}{dM_r} - C_r - C_{\varpi} \quad (2.55)$$

$$\frac{dE_r}{dt} + P_r \frac{dV}{dt} = -\frac{dL_r}{dM_r} + C_r \quad (2.56)$$

$$\frac{dE_t}{dt} + (P_t + P_{tv}) \frac{dV}{dt} = -\frac{dL_t}{dM_r} + C_{\varpi} \quad (2.57)$$

The linearized forms of these equations are:

$$\frac{d(\delta E_g)}{dt} + P_g \frac{d(\delta V)}{dt} = \delta Q_g \quad (2.58)$$

$$\frac{d(\delta E_r)}{dt} + P_r \frac{d(\delta V)}{dt} = \delta Q_r \quad (2.59)$$

$$\frac{d(\delta E_t)}{dt} + (P_t + P_{tv}) \frac{d(\delta V)}{dt} = \delta Q_t \quad (2.60)$$

where $\delta Q_g = \delta \epsilon_{nuc} - \delta \left(\frac{dL_c}{dM_r} \right) - \delta C_r - \delta C_{\varpi}$, $\delta Q_r = \delta C_r - \delta \left(\frac{dL_r}{dM_r} \right)$ and $\delta Q_t = \delta C_{\varpi} - \delta \left(\frac{dL_t}{dM_r} \right)$.

From equation (2.51), it can be noted that to derive an expression for the total IWs, an equation for the perturbation δP (with δP defined as stated earlier i.e $\delta P = \delta P_g + \delta P_r + \delta P_t + \delta P_{tv}$) is needed. In this derivation, the definition, $\delta Q = \delta Q_g + \delta Q_r + \delta Q_t$, is also

used. The individual perturbations δP_g , δP_r , δP_t and δP_{tv} are first calculated individually and then summed to give the required perturbation in the total pressure, δP .

(i) Expression for δP_g :

Putting $\delta V = -\frac{\delta \rho}{\rho^2}$, equation (2.58) becomes;

$$\frac{d(\delta E_g)}{dt} - \frac{P_g}{\rho^2} \frac{d(\delta \rho)}{dt} = \delta Q_g \quad (2.61)$$

$$\omega \delta E_g - \omega \frac{P_g}{\rho^2} \delta \rho = \delta Q_g \quad (2.62)$$

$$\Rightarrow \delta E_g - \frac{P_g}{\rho^2} \delta \rho = \frac{\delta Q_g}{\omega} \quad (2.63)$$

Noting that; $E_g = E_g(V, T)$ and $P_g = P_g(V, T)$ and using basic calculus, leads to:

$$\delta E_g = \left(\frac{\partial E_g}{\partial T} \right)_V \delta T + \left(\frac{\partial E_g}{\partial V} \right)_T \delta V \quad (2.64)$$

and

$$\delta P_g = \left(\frac{\partial P_g}{\partial T} \right)_V \delta T + \left(\frac{\partial P_g}{\partial V} \right)_T \delta V \quad (2.65)$$

$$\Rightarrow \delta T = \left[\delta P_g - \left(\frac{\partial P_g}{\partial V} \right)_T \delta V \right] / \left(\frac{\partial P_g}{\partial T} \right)_V \quad (2.66)$$

Substituting (2.66) into (2.64) gives:

$$\delta E_g = \left[\left(\frac{\partial E_g}{\partial T} \right)_V / \left(\frac{\partial P_g}{\partial T} \right)_V \right] \delta P_g + \left[\left(\frac{\partial E_g}{\partial V} \right)_T - \left(\frac{\partial E_g}{\partial T} \right)_V \left(\frac{\partial P_g}{\partial V} \right)_T / \left(\frac{\partial P_g}{\partial T} \right)_V \right] \delta V \quad (2.67)$$

Defining: $E_p = \left(\frac{\partial E_g}{\partial T} \right)_V / \left(\frac{\partial P_g}{\partial T} \right)_V$ and $E_V = \left(\frac{\partial E_g}{\partial V} \right)_T - \left(\frac{\partial E_g}{\partial T} \right)_V \left(\frac{\partial P_g}{\partial V} \right)_T / \left(\frac{\partial P_g}{\partial T} \right)_V$ equation (2.67) becomes;

$$\delta E_g = E_p \delta P_g + E_V \delta V \quad (2.68)$$

or

$$\delta E_g = E_p \delta P_g - E_V \frac{\delta \rho}{\rho^2} \quad (2.69)$$

where:

$$E_p = \left(\frac{\partial E_g}{\partial P_g} \right)_V \equiv \frac{V}{\Gamma_3 - 1} \quad (2.70)$$

and

$$E_V = \left(\frac{\partial E_g}{\partial V} \right)_P \quad (2.71)$$

where $\Gamma_3 = \left(\frac{d \ln T}{d \ln \rho} \right)_{ad} - 1$ is one of the adiabatic exponents. Substituting equation (2.69) into equation (2.63) then gives:

$$(E_V + P_g) \delta V + E_p \delta P_g = \frac{\delta Q_g}{\omega} \quad (2.72)$$

From which it can be seen that;

$$\delta P_g = \frac{1}{E_p} \frac{\delta Q_g}{\omega} - \frac{(E_V + P_g)}{E_p} \delta V \quad (2.73)$$

Substituting for E_p and E_V and simplifying then leads to:

$$\delta P_g = \frac{\Gamma_3 - 1}{V} \frac{\delta Q_g}{\omega} - \frac{\Gamma_3}{V} P_g \delta V \quad (2.74)$$

(ii) Expression for δP_r :

The linearized radiative energy equation (2.59) leads to:

$$\delta E_r + P_r \delta V = \frac{\delta Q_r}{\omega} \quad (2.75)$$

following a similar argument as (i) above, we can write:

$$\delta E_r = E_{p'} \delta P_r + E_{V'} \delta V \quad (2.76)$$

with

$E_{p'} = \left(\frac{\partial E_r}{\partial P_r} \right)_V \equiv 3V$ and $E_{V'} = \left(\frac{\partial E_r}{\partial V} \right)_{P_r} \equiv 3P_r$ (where $E_r = VJ$ and $P_r = \frac{1}{3}J \implies E_r = 3P_r V$). Therefore equation (2.76) can be written as:

$$3V \delta P_r + 3P_r \delta V \quad (2.77)$$

Hence, (2.75) becomes:

$$3V \delta P_r + 4P_r \delta V = \frac{\delta Q_r}{\omega} \quad (2.78)$$

from which it follows that:

$$\delta P_r = \frac{\delta Q_r}{3\omega V} - \frac{4P_r \delta V}{3V} \quad (2.79)$$

(iii) Expression for δP_t :

Starting from the linearized form of the turbulent energy equation (2.54) one also gets an equation similar to equations (2.63) and (2.75) which can be written as:

$$\delta E_t + P_t \delta V = \frac{\delta Q_r}{\omega} \quad (2.80)$$

Defining, $E_t = \varpi^2$ and $P_t = \alpha_p \rho \varpi^2 \implies E_t = \alpha_p P_t V$ and invoking the differentiation rules used in (i) and (ii) above and following a similar argument we get:

$$\delta P_t = \frac{\delta Q_t}{\alpha_p \omega V} - \frac{(\alpha_p P_t + P_t)}{\alpha_p V} \delta V \quad (2.81)$$

(iv) Expression for δP_{tv} :

Using the Lagrangian perturbations, equation (2.12) becomes:

$$\begin{aligned}
(P_{tv,0} + \delta P_{tv}) &= -\frac{16}{3}\pi\mu(\rho_0 + \delta\rho)^2 \frac{\partial}{\partial M_r} (r_0 + \delta r)^2 (v_{r,0} + \delta v_r) \\
&= -\frac{16}{3}\pi\mu(\rho_0^2 + 2\rho_0\delta\rho + \delta\rho^2) \frac{\partial}{\partial M_r} (r_0^2 + 2r_0\delta r + \delta r^2) (v_{r,0} + \delta v_r) \\
&= -\frac{16}{3}\pi\mu(\rho_0^2 + 2\rho_0\delta\rho) \frac{\partial}{\partial M_r} (r_0^2 + 2r_0\delta r) (v_{r,0} + \delta v_r) \\
\implies \delta P_{tv} &= -\frac{16}{3}\pi\mu \left[\frac{dr^2}{dM_r} \delta v_r \right] = -\frac{16}{3}\pi\mu\omega\delta V
\end{aligned} \tag{2.83}$$

where in the last equation, we have used the perturbed form of the continuity equation (2.27), ignored higher order terms and noted that $v_{r,0} = 0$ in the static case. Here δV is the perturbation in the specific volume.

Multiplying both sides of equation (2.83) by δV^* and taking the imaginary part, we obtain the quantity:

$$I_m(\delta P_{tv}\delta V^*) = -\frac{16}{3}\pi\mu I_m(\omega|\delta V|^2) = -\frac{16}{3}\pi\mu|\delta V|^2 I_m(\omega) \tag{2.84}$$

from which it can be clearly seen that this quantity *will always* have a negative contribution to the total work integral defined by equation (2.51). It will therefore be always dissipative as stated in section (2.1.1).

Expression for the total work integral

Taking the sum of equations (2.74), (2.79) and (2.81), multiplying both sides by $\delta V^* \frac{\omega^*}{\omega}$ ($\delta V^* \frac{\omega^*}{\omega}$ (where ‘*’ denotes the complex conjugate) and taking the imaginary part of both sides yields:

$$I_m(\delta P_{tot}\delta V^*) = \frac{1}{|\omega|^2} I_m \left\{ [(\Gamma_3 - 1)\delta Q_g + \frac{1}{3}\delta Q_r + \frac{1}{\alpha_p}\delta Q_t] \frac{\delta V^*}{V} \omega^* \right\} \tag{2.85}$$

Letting $Y = \frac{\delta V^*}{V} \delta Q_g$ and $X^* = \omega^*$, where X and Y are complex quantities, and defining:

$$X = X_R + iX_I$$

$$Y = Y_R + iY_I$$

it follows straightforwardly that:

$$I_m(YX^*) = X_R Y_I - X_I Y_R \quad (2.86)$$

Applying this rule in equation (2.85) gives:

$$\begin{aligned} I_m(\delta P \delta V^*) &= \frac{(\Gamma_3 - 1)}{|\omega|} \left[\frac{\omega_R}{|\omega|} I_m \left(\frac{\delta V^*}{V} \delta Q_g \right) - \frac{\omega_I}{|\omega|} \text{Re} \left(\frac{\delta V^*}{V} \delta Q_g \right) \right] \\ &+ \frac{1}{3|\omega|} \left[\frac{\omega_R}{|\omega|} I_m \left(\frac{\delta V^*}{V} \delta Q_r \right) - \frac{\omega_I}{|\omega|} \text{Re} \left(\frac{\delta V^*}{V} \delta Q_r \right) \right] \\ &+ \frac{1}{\alpha_p |\omega|} \left[\frac{\omega_R}{|\omega|} I_m \left(\frac{\delta V^*}{V} \delta Q_t \right) - \frac{\omega_I}{|\omega|} \text{Re} \left(\frac{\delta V^*}{V} \delta Q_t \right) \right] \end{aligned}$$

For $\frac{\omega_R}{|\omega|} \ll 1$, the terms with the expression $\frac{\omega_R}{|\omega|}$ can be ignored yielding:

$$\begin{aligned} I_m(\delta P \delta V^*) &= -\frac{(\Gamma_3 - 1)}{|\omega|} \left[\frac{\omega_I}{|\omega|} \text{Re} \left(\frac{\delta V^*}{V} \delta Q_g \right) \right] \\ &- \frac{1}{3|\omega|} \left[\frac{\omega_I}{|\omega|} \text{Re} \left(\frac{\delta V^*}{V} \delta Q_r \right) \right] \\ &- \frac{1}{\alpha_p |\omega|} \left[\frac{\omega_I}{|\omega|} \text{Re} \left(\frac{\delta V^*}{V} \delta Q_t \right) \right] \end{aligned}$$

In this thesis, it is found that $10^{-10} \lesssim \frac{\omega_R}{|\omega|} \lesssim 10^{-6}$ hence the approximation above is reasonably valid for this study. The total work integral can then be written as (including the result for P_{tv} from equation (2.84)):

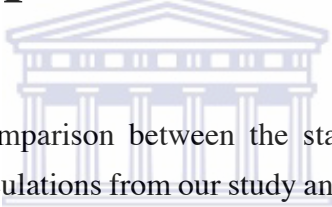
$$\begin{aligned}
W_{tot} &= -\pi \int_0^M \{I_m(\delta P_{tot} \delta V^*)\} dM_r \\
&= W_{gp} + W_{rp} + W_{tp} + W_{tv} \\
&= -\pi \int_0^M [I_m(\delta P_g \delta V^*) + I_m(\delta P_r \delta V^*) + I_m(\delta P_t \delta V^*) + I_m(\delta P_{tv} \delta V^*)] dM_r \\
&= + \frac{\pi(\Gamma_3 - 1)}{|\omega|} \int_0^M \left\{ \left[\frac{\omega_I}{|\omega|} \text{Re} \left(\frac{\delta V^*}{V} (\epsilon_{nuc} - \frac{dL_c}{dM_r} - C_r - C_\varpi) \right) \right] \right\} dM_r \\
&+ \frac{\pi}{3|\omega|} \int_0^M \left\{ \left[\frac{\omega_I}{|\omega|} \text{Re} \left(\frac{\delta V^*}{V} \delta \left(-\frac{dL_r}{dM_r} + C_r \right) \right) \right] \right\} dM_r \\
&+ \frac{\pi}{\alpha_p |\omega|} \int_0^M \left\{ \left[\frac{\omega_I}{|\omega|} \text{Re} \left(\frac{\delta V^*}{V} \delta \left(-\frac{dL_t}{dM_r} + C_\varpi \right) \right) \right] \right\} dM_r \\
&- \int_0^M \left\{ \frac{16}{3} \pi \mu |\delta V|^2 I_m(\omega) \right\} dM_r
\end{aligned}$$

2.3 The physical input

In the calculations presented in this thesis, we use the Saumon-Chabriel EOS (Saumon and Chabriel, 1991, 1992; Saumon et al., 1995), specially devoted to the description of low-mass stars and brown dwarfs (see Chabriel & Baraffe 2000 for a detailed discussion). A analytic expression for the nuclear energy generation for deuterium burning in the total energy equation (Caughlin and Fowler, 1988) is used and calculations are done assuming an initial deuterium abundance of 2×10^{-5} by mass fraction characteristic of the local interstellar medium (Linsky and Jeffrey, 1998) and, a mixing length parameter equal to the pressure scale height as assumed by PB05 unless otherwise stated. An electron screening routine used by PB05 was kindly supplied by Baraffe and used to calculate the electron screening factors. The opacity was calculated by a bi-cubic spline interpolation in the OPAL opacity tables of Grevesse and Noels (1993), supplemented by the Alexander and Ferguson (1994) tables at low temperatures, extended to $\log R = -7.5$ and -8 by linear extrapolation in $\log R$ at constant $\log T$ ($R = \rho/T_6^3$, with $T_6 = T/10^6$). The relevant boundary conditions and the difference equations are described in appendix A.

Chapter 3

Results I: static models and the ‘frozen-in approximation’



This chapter presents a comparison between the static model structures and the non-adiabatic linear stability calculations from our study and those from PB05. Results from an additional analysis not reported by PB05 are also presented. The static model structures are compared in §3.1. Linear stability analysis results (e.g. periods, e-folding times, effective temperatures and luminosities) are compared and discussed in §3.2.1. Eigen-frequencies, scaling factors, periods and e-folding times for the first and second harmonics are presented in §3.2.2.1. Exploratory calculations of theoretical pulsation constants for young brown dwarfs (for the three unstable eigen modes) are presented and discussed in §3.2.2.2. Finally, the radial-eigenfunctions and the work integrals are presented in §3.2.2.3.

3.1 Comparison of hydrostatic equilibrium structures for our models and PB05 models

In this thesis, the term ‘hydrostatic equilibrium’ is used to refer to a state in which all the internal pressure gradients inside a star are exactly in balance with the force of gravity. Such a state is described by the equations of static stellar structure (where all the accelerations are ignored) and is very important in the *linear stability theory* presented in section 2.1.1.

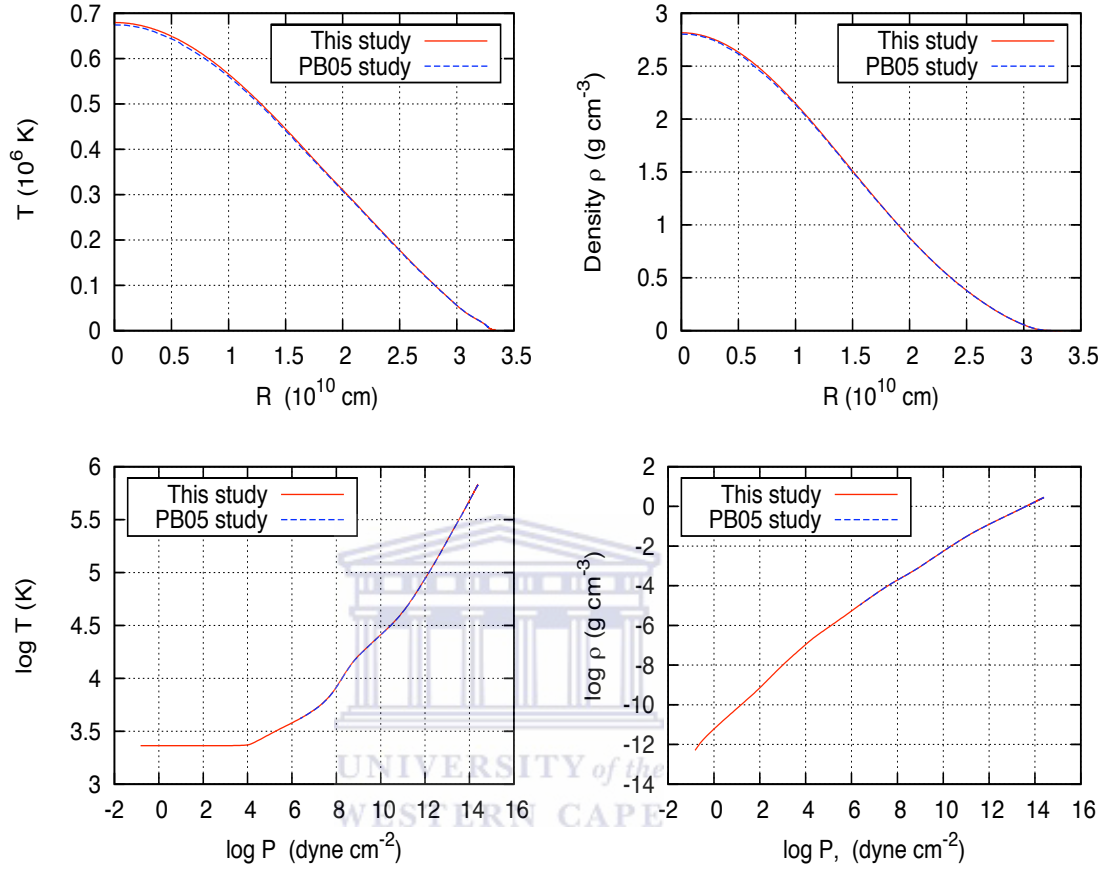


Figure 3.1: Various dynamical variables plotted for the $0.04 M_{\odot}$ static model. Results from our study (continuous red lines) and those from PB05 (dashed blue lines) are shown for comparison.

To explicitly compare our linear stability results with those from the PB05 study (presented in section 3.2), we first compared the static structures of two objects with masses $0.04 M_{\odot}$ and $0.08 M_{\odot}$ to static models of the same masses kindly supplied by I. Baraffe. Our models, just as PB05 models (and as stated earlier) use the most current equation of state (EOS) and energy generation rates.

Figure 3.1 shows plots of the density, temperature and pressure for the $0.04 M_{\odot}$ BD model. Similar plots for the $0.08 M_{\odot}$ BD model are shown in figure 3.2. The plotted variables are: the temperature as a function of the radial coordinate (top left), the mass density as function of the radial coordinate (top right), the log of the temperature as a

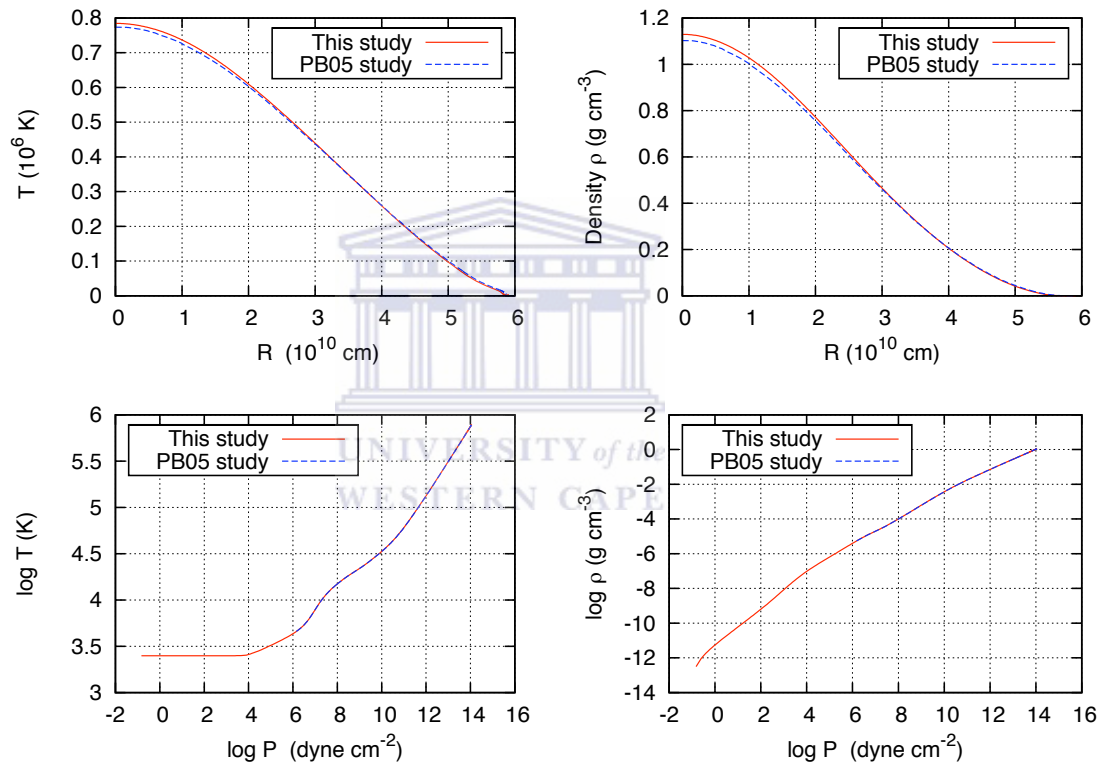


Figure 3.2: A Similar plot as in figure 3.1 but for the $0.08 M_{\odot}$ static model. Both the PB05 results and our results are shown for comparison.

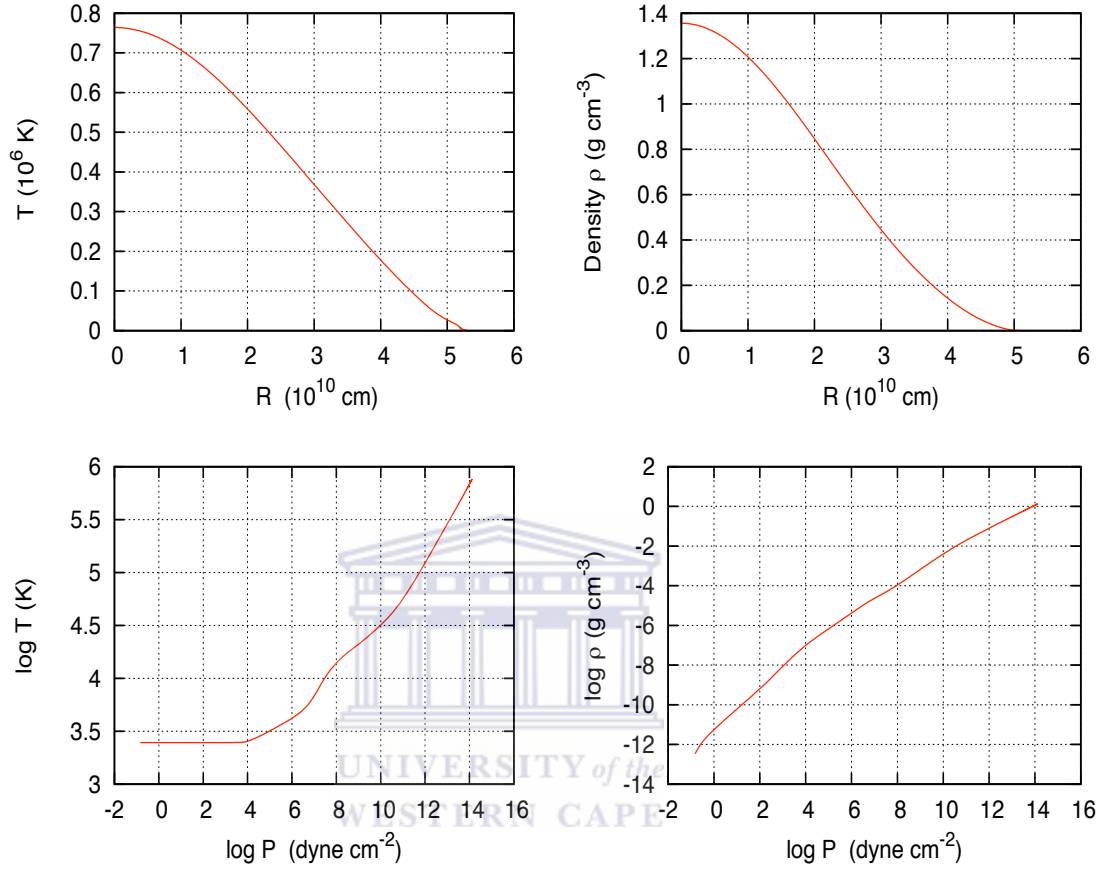


Figure 3.3: Plots of the temperature and density in zone functions of the radial coordinate for the $0.07M_{\odot}$ static model. The log of the temperature in zone and mass density in zone as functions of the log of total pressure are also plotted.

function of the log of the total pressure (bottom left) and the log of the mass density (ρ) as a function of the log of the total pressure (bottom right). Plots using the PB05 $0.04M_{\odot}$ and $0.08M_{\odot}$ static models are also shown for comparison (kindly supplied by I. Baraffe). A good agreement in the static model structures can be seen from this comparison. The only slight differences in the central temperatures and hence densities for the $0.08M_{\odot}$ are due to our different outer boundary conditions which seem to have a stronger effect for the heavier mass BDs.

We also generated other static BD models with masses $0.07M_{\odot}$, $0.06M_{\odot}$, $0.05M_{\odot}$, $0.03M_{\odot}$ and $0.02M_{\odot}$ whose static structures are shown in figures 3.3-3.7.

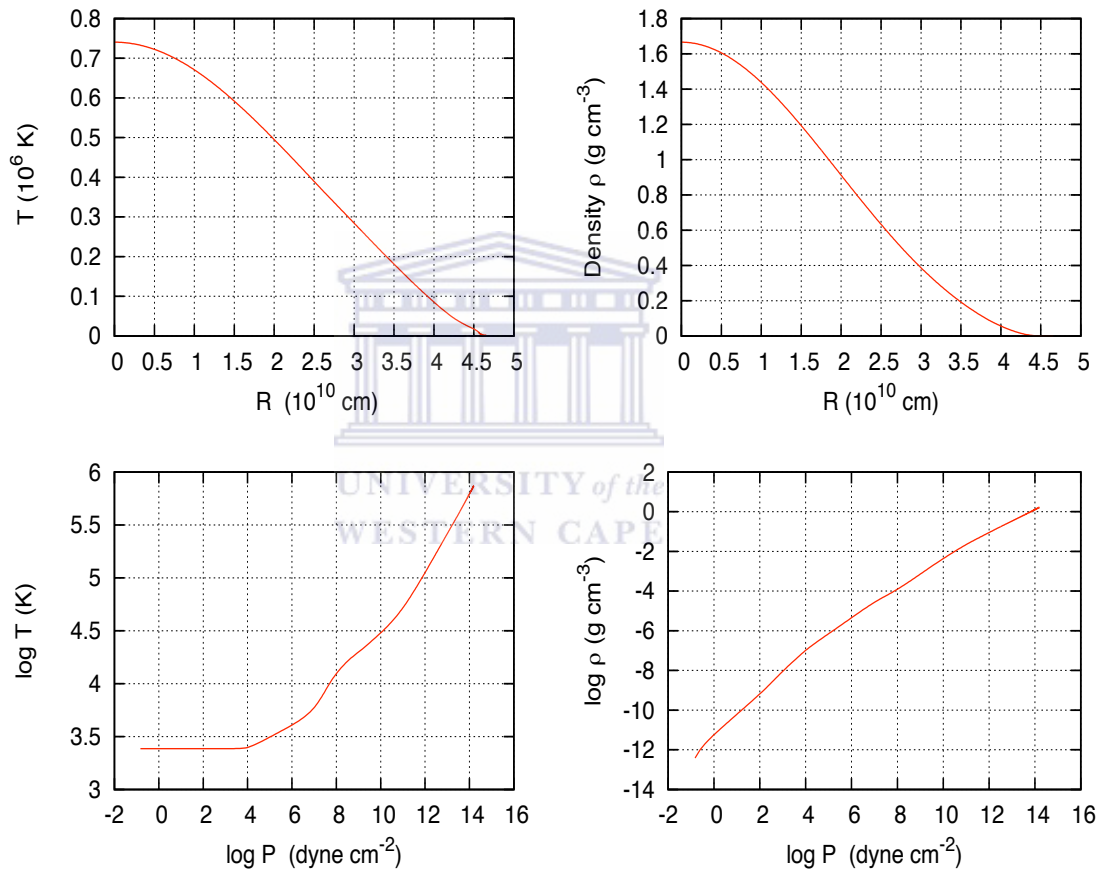


Figure 3.4: Plots same as figure 3.3 but for the $0.06M_{\odot}$ static model.

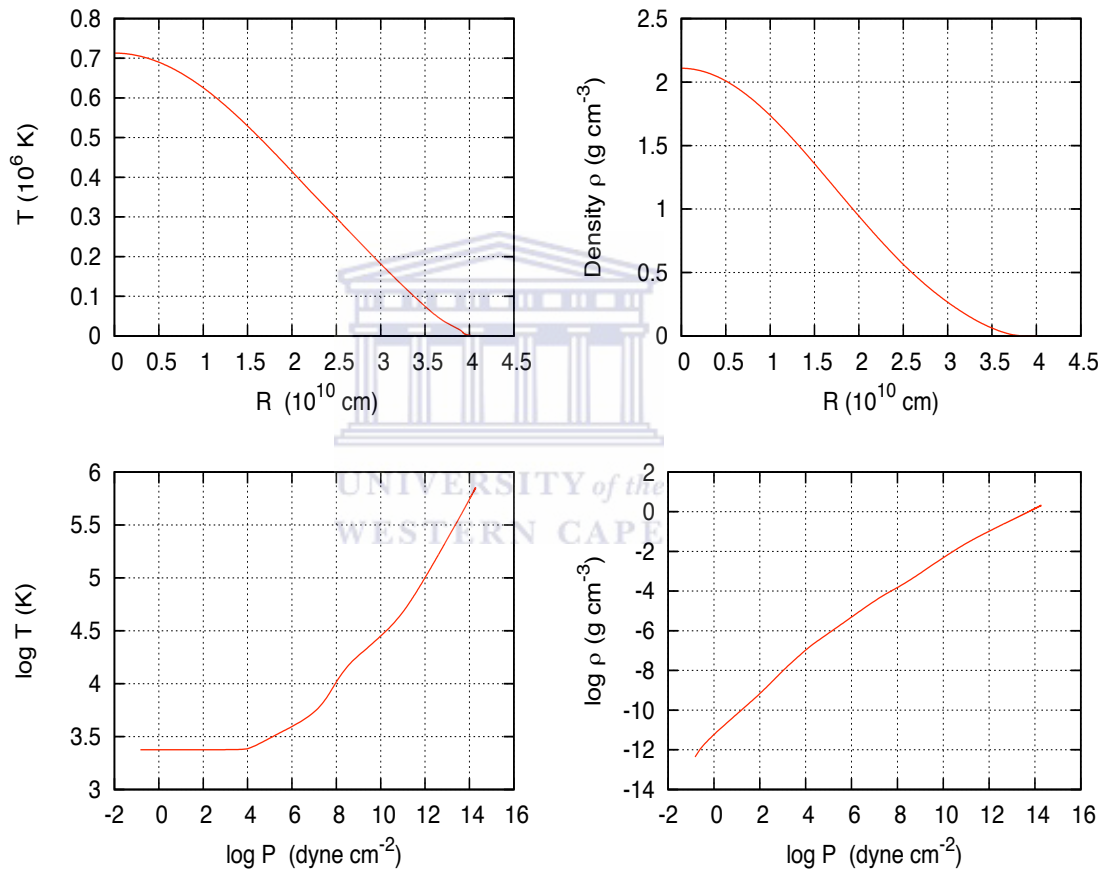


Figure 3.5: Plots same as figure 3.3 but for the $0.05M_{\odot}$ static model.

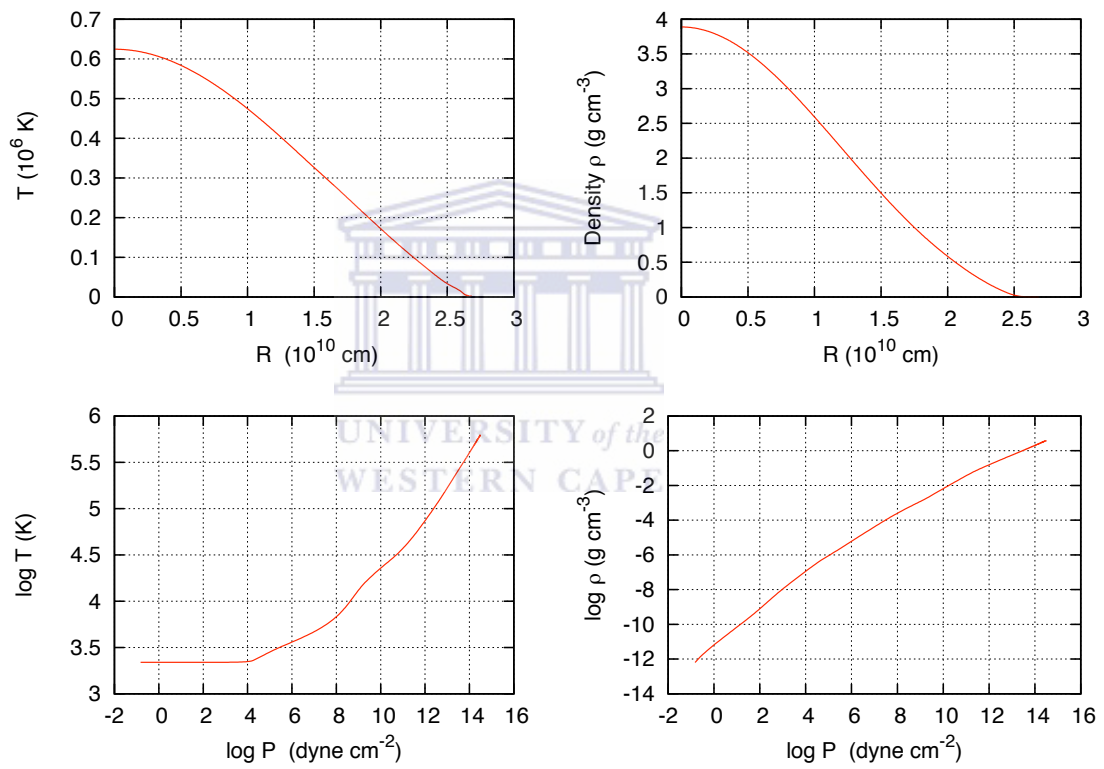


Figure 3.6: Plots same as figures 3.3 but for the $0.03M_{\odot}$ static model.

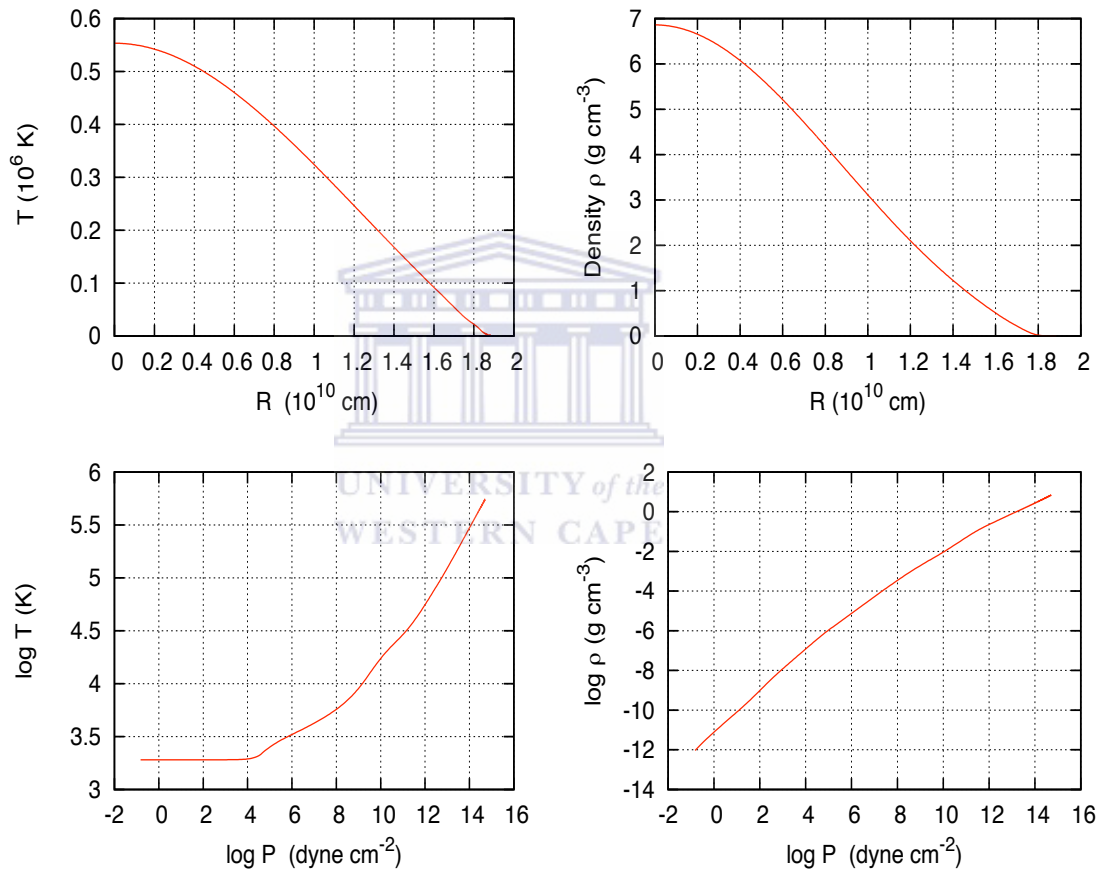


Figure 3.7: Plots same as figure 3.3 but for the $0.02M_{\odot}$ model.

Figures 3.3-3.7 show an exactly similar behaviour for $\log T$ vs $\log P$ and $\log \rho$ vs $\log P$ relations to the $0.04M_{\odot}$ and $0.08M_{\odot}$ models. The central temperatures and central densities are found to decrease with mass as can be seen from the respective profiles. No comparison was done for the former static models since no similar models were provided by I. Baraffe.

3.2 Linear stability analysis

Linear stability theory is concerned with identifying whether the equilibrium model structures (called static structures in this thesis) will be stable or unstable when subjected to small perturbations about the hydrostatic equilibrium configuration. In the case of stellar pulsations, a linear stability analysis involves a search for unstable radial eigen models along the perturbed modal structures. Apart from periods and e-folding times, the linear theory of pulsation cannot be used to estimate the amplitudes of the pulsations. It is however, still powerful enough to predict the pulsation periods and the pulsation amplitude growth rates and is therefore useful in predicting the existence of stellar pulsations in stars. Such a theory has only been applied to young BDs and VLMSs by PB05 in their groundbreaking prediction of pulsations in these objects. A detailed verification of the PB05 linear stability results and their prediction is discussed in the next section.

3.2.1 Comparison of Our Linear stability analysis with PB05 results for five models

In this section, we present the results of a comparison between the linear stability analysis results of five models from our work and similar models from the PB05 study kindly supplied by I. Baraffe. The models compared here are the same models whose static structures have been presented in section 3.1. Results of other models from our study are presented subsection 3.2.2.

The various model parameters and the starting values for the luminosity and radius used in modeling are given in table (3.1). The α 's (with primes) are related to the free parameters (alpha's) introduced in subsection 2.1.1. They are defined by the following scaling relations:

M/M_{\odot}	R_{start}	$\log(L/L_{\odot})_{start}$	α'_{Λ}	α'_s	α'_d
$0.08 M_{\odot}$	0.474	-1.911	1.0	1.0	1.0
$0.06 M_{\odot}$	0.845	-1.322	1.0	1.0	1.0
$0.04 M_{\odot}$	0.474	-1.911	1.0	1.0	1.0
$0.03 M_{\odot}$	0.372	-2.138	1.0	1.0	1.0
$0.02 M_{\odot}$	0.261	-2.761	1.0	1.0	1.0

Table 3.1: The various model parameters used in the $0.04M_{\odot}$ and $0.08M_{\odot}$ models used in the comparison. R_{start} and $\log(L/L_{\odot})_{start}$ are the starting values of the Radius and the log of the luminosity (in solar units) while D/D_0 is the ratio of the central deuterium abundance (D) to the initial value (D_0). Here α'_{Λ} , α'_s and α'_d are the scaled values of modeling parameters described in section (2.1) given by equations (3.1), (3.2) and (3.3) respectively, defined so as to satisfy the MLT values proposed by Kuhfuß (1986).

$$\alpha'_s = \left(\frac{3}{2}\right)^{1/2} \frac{\alpha_s}{\alpha_{\Lambda}} \quad (3.1)$$

$$\alpha'_d = \frac{9}{128} \alpha_d \alpha_s \quad (3.2)$$

$$\alpha'_{\Lambda} = \alpha_{\Lambda} \quad (3.3)$$

Table 3.2 shows the periods and e-folding times from our study and those from PB05 for five objects. Comparison of the results shows a good agreement in the fundamental mode periods to within less than 0.1% for the higher masses ($0.08M_{\odot}$, $0.06M_{\odot}$, $0.04M_{\odot}$ and $0.03M_{\odot}$) and $\sim 10\%$ for the lowest mass ($0.02M_{\odot}$). For the e-folding times, our results agree to within less than $\sim 8\%$ for the higher masses ($0.08M_{\odot}$, $0.06M_{\odot}$ and $0.04M_{\odot}$) and $\sim 25\%$ for the $0.03M_{\odot}$ and $0.02M_{\odot}$. To help visualize the differences in the periods and e-folding times between the two studies, in figure 3.8, we show plots of the fundamental mode periods and the e-folding times as functions of mass. The pulsation periods range between $\sim 1 - 5$ hours and increase with increasing mass in a more-or-less linear relation.

M (M_{\odot})	D	P_0 (GOB10) (h)	P_0 (PB05) (h)	$\% \Delta P$	τ_e (GOB10) (Myr)	τ_e (PB05) (Myr)	$\% \Delta \tau_e$
0.08	1.284e-05	4.214	4.25	0.08	0.248	0.26	3.8
0.06	1.288e-05	3.397	3.41	0.04	0.308	0.31	0.1
0.04	1.325e-05	2.523	2.52	0.01	0.441	0.41	7.6
0.03	1.872e-05	2.090	2.16	0.03	0.582	0.78	25.0
0.02	1.964e-05	1.515	1.67	9.00	2.228	3.03	26.0

Table 3.2: Comparison of the fundamental mode periods, P_0 and the e-folding times, τ_e , the effective temperature in Kelvin and the log of the luminosity in solar units from our study and the PB05 linear stability analysis results for the $0.04 M_{\odot}$ Model. Here, D is the value of the initial central deuterium abundance adopted in the linear stability analysis.

On the other hand, the e-folding times show an opposite behavior i.e decrease, but do so non-linearly, first decreasing sharply for the lower masses and then decrease monotonically for the higher masses.

The effective temperatures and the log of the luminosities (in solar units) are presented in table 3.3. The values from PB05 are also shown for comparison. For the objects with higher masses ($0.08M_{\odot}$, $0.06M_{\odot}$ and $0.04M_{\odot}$), we find that the effective temperatures agree to within $\sim 1\%$, while the luminosities agree to within one decimal place in magnitude, with the PB05 values. However, for two lowest mass objects ($0.03M_{\odot}$ and $0.02M_{\odot}$), we note a significant disagreement in both the effective temperatures and the luminosities. The differences could be due to the different outer boundary conditions used in our calculations as opposed to those of PB05. To establish the location of our objects on the H-R diagram, we show in Figure 3.9 an HR diagram displaying five BDs from our study together with those from PB05. We find that only massive BDs from our study are located close to those from PB05, the lowest masses show a significant deviation in location from similar masses from PB05. This results may be indicative of differences in structures for

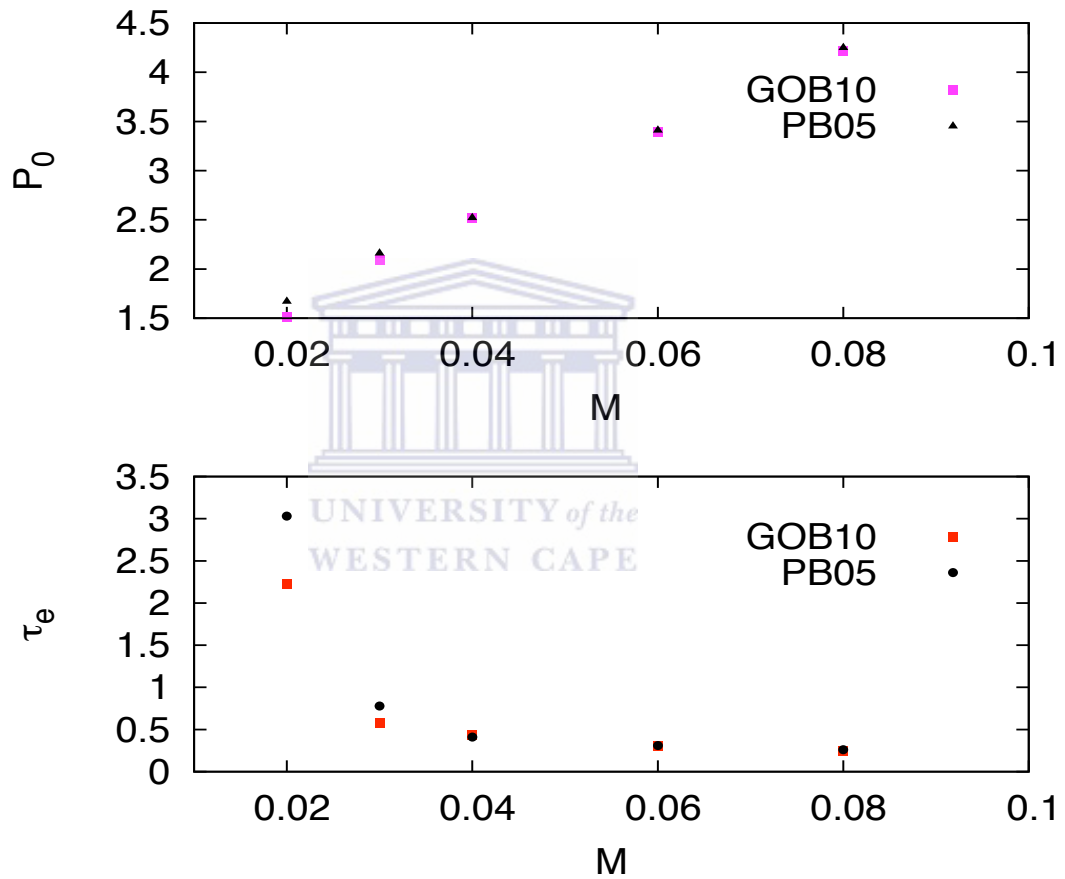


Figure 3.8: Plots of the fundamental mode periods (in hours) and e-folding times (in Myrs) from our calculations (GOB10) and the PB05 calculations as functions of mass in solar units.

M (M_{\odot})	T_{eff} (Our study)	T_{eff} (PB05 study)	$\log L/L_{\odot}$ (Our study)	$\log L/L_{\odot}$ (PB05 study)
0.08	2989	2950	-1.296	-1.322
0.06	2910	2890	-1.551	-1.567
0.04	2766	2790	-1.926	-1.915
0.03	2620	2710	-2.211	-2.138
0.02	2283	2540	-2.756	-2.516

Table 3.3: Effective temperatures and the log of surface luminosities from our calculations shown with those from PB05.

the lowest masses and needs to be investigated further. Due to this, in the next analysis we focus only on the higher mass models and exclude the $0.02M_{\odot}$ and $0.03M_{\odot}$ models.

3.2.2 Extended results and other models

3.2.2.1 Eigen-frequencies, periods and e-folding times for 1st and 2nd harmonics

In this section we present extended results from our linear stability calculations not discussed in the previous section. Included here are: the general results for the fundamental mode and the first two harmonics, the theoretical pulsation constants and period ratios, the radial-eigenfunctions and the partial work integrals. Tables 3.4-3.6 show a summary of the results for the fundamental mode and the first two harmonics. ω_R and ω_I are the real and imaginary parts of the pulsation frequency given in radians per unit time. The pulsation periods are then given by, $\frac{2\pi}{\omega_I}$, while the e-folding times are approximated by ω_R^{-1} .

3.2.2.2 Pulsation constants and the period ratios

The ‘pulsation constant’, usually denoted by ‘Q’ in standard literature, relates the pulsation period of a star to the the mass-radius cubed ratio (M/R^3). It is given by the standard formular

$$Q = \Pi (MR_{\odot}^3/M_{\odot}R^3)^{1/2} \quad (3.4)$$

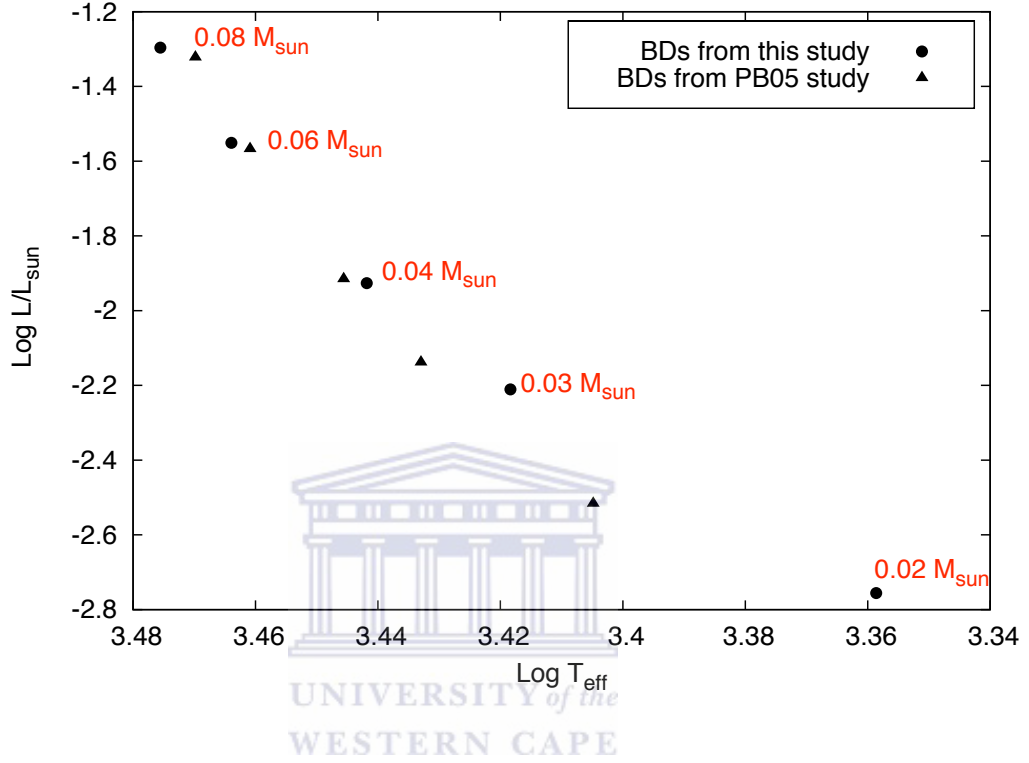


Figure 3.9: An H-R diagram showing the position of the BDs from our study. Data from the PB05 study is also plotted.

M (M_{\odot})	ω_R (rad h^{-1})	ω_I (rad h^{-1})	P_0	τ_{e0}
0.08	4.603E-10	1.491	4.214	2.4802E-01
0.07	4.069E-10	1.650	3.807	2.7266E-01
0.06	3.711E-10	1.850	3.397	3.0758E-01
0.05	3.189E-10	2.113	2.974	3.5796E-01
0.04	2.5911E-10	2.491	2.523	4.4057E-01

Table 3.4: The real and the imaginary parts of the pulsation frequencies for the fundamental mode.

$M(M_{\odot})$	ω_R (rad h^{-1})	ω_I (rad h^{-1})	P_1 (h)	τ_{e1} (Myr)
0.08	2.807E-09	3.109	2.0213	4.0667E-02
0.07	2.161E-09	3.450	1.8210	5.2824E-02
0.06	1.530E-09	3.870	1.6181	7.4601E-02
0.05	9.868E-10	4.460	1.4087	1.1568E-01
0.04	5.589E-10	5.283	1.1893	2.0423E-01

Table 3.5: A Summary of the results for the First Harmonic in the frozen-in case.

$M(M_{\odot})$	ω_R (rad h^{-1})	ω_I (rad h^{-1})	P_2 (h)	τ_{e2} (Myr)
0.08	4.769E-08	4.380	1.4347	2.3938E-03
0.07	6.195E-08	4.855	1.2943	3.2840E-03
0.06	2.233E-08	5.451	1.1528	5.1114E-03
0.05	1.242E-08	6.239	1.0070	9.1929E-03
0.04	5.658E-09	7.382	0.8512	2.0176E-02

Table 3.6: A summary of the results for the Second Harmonic mode in the frozen-in approximation case.

where Π is the pulsation period, M is the mass of the model, R is the radius, M_{\odot} and R_{\odot} are the mass and radius of the sun respectively. The significance of the pulsation constant Q can be understood from the following argument: since the pulsation period of a variable is often given reliably by both observations and theory (Stellingwerf, 1975), pulsation models can be used to predict periods using equation 3.4. Since Q is generally a variable of the ratio M/R^3 , the knowledge of any two periods for a star from theoretical models can be used in the fitting formulae (such as the Gaussian fitting formulae derived by Cox et al. (1972) for linear classical cepheids) to give M and R directly. However, for such a comparison to be possible, a highly accurate fit is needed.

In table 3.7 we present the pulsation constants for the fundamental mode and the first two harmonics from our study together with the period ratios. A plot of the pulsation constants for the three modes versus the ratio M/R was made following Stellingwerf (1984), where M and R are expressed in solar units and is shown in figure 3.10. Figure 3.11 also shows a plot of the pulsation constants as a function of mass. We find that Q remains nearly

$M(M_{\odot})$	$R(R_{\odot})$	Q_0 (d)	Q_1 (d)	Q_2 (d)	P_1/P_0	$\frac{P_2}{P_0}$
0.08	0.85	0.07295	0.03499	0.02484	0.4797	0.3405
0.07	0.76	0.07289	0.03487	0.02478	0.4783	0.3400
0.06	0.67	0.07303	0.03479	0.02478	0.4764	0.3394
0.05	0.58	0.07285	0.03450	0.02467	0.4737	0.3386
0.04	0.48	0.07281	0.03432	0.02456	0.4714	0.3374

Table 3.7: Pulsation constants for the fundamental mode and the first two harmonics from our study. The ratio of the first harmonic to the fundamental mode periods is also shown.

constant with the mass-radius ratio for both the fundamental, first overtone and second overtone in the case of higher masses.

Plots of the ratios of the fundamental mode periods to the first harmonic and second harmonic periods are shown in figure 3.12. The results show that both the ratios $\frac{P_0}{P_1}$ and $\frac{P_0}{P_2}$ decrease with an increase in mass in a more or less linear relation. These plots are interesting and if verified can be very useful in providing a direct way of measuring BD masses which are hard to determine. For instance, using observations, the period ratios can be measured to very high accuracy and then figure 3.12 used to estimate the mass directly. However, accurate theoretical input models are required for such direct comparisons in order to obtain meaningful constrains.

3.2.2.3 The radial eigen functions and the work integrals

In stellar pulsation theory, existence of unstable radial eigen-modes characterizes stellar pulsations about the hydrostatic equilibrium position. To study the predicted pulsations due to the epsilon mechanism (which occurs near the center), we plotted the size of the relative sizes of the radial eigen-functions as functions of the Lagrangian mass coordinate M_r in solar units. This together with a plot of the total integrated partial work integral (per cycle) as a function of M_r are shown in figure 3.13 for the $0.08M_{\odot}$ model and figure 3.14 for the $0.04M_{\odot}$ model.

Figures 3.13 and 3.14 show that the relative sizes of the radial-eigenfunctions near the centers of these BD models are relatively large as was found by PB05. Similarly, the total integrated work integrals indicate that most of the work is done within the inner $\sim 1/8$ th

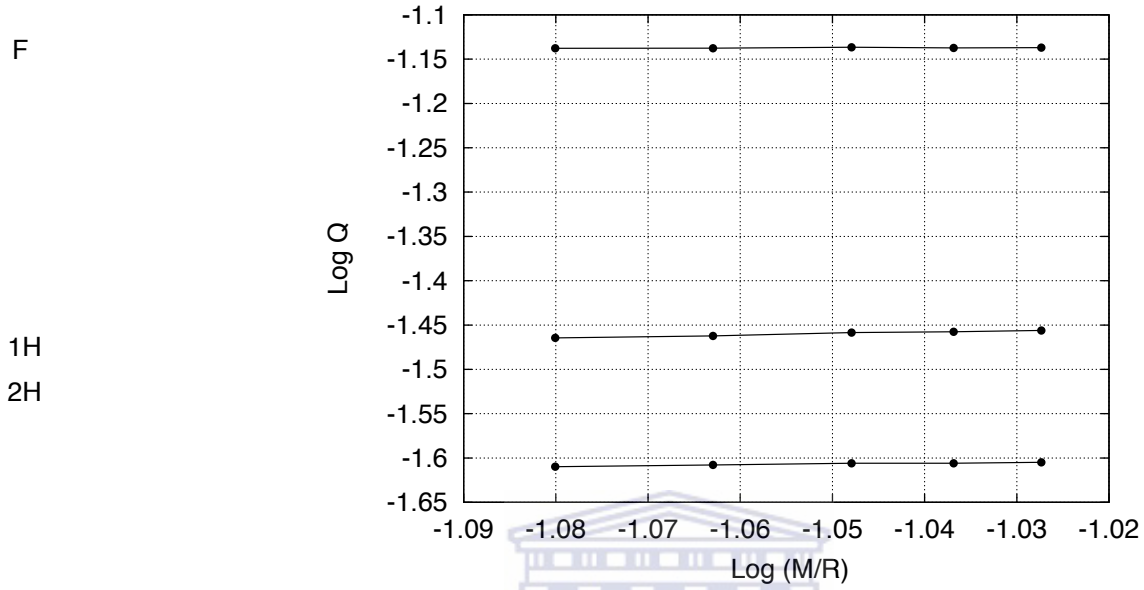


Figure 3.10: A plot of the pulsation constants for the first three modes as functions of the mass to radius ratio (in solar units).

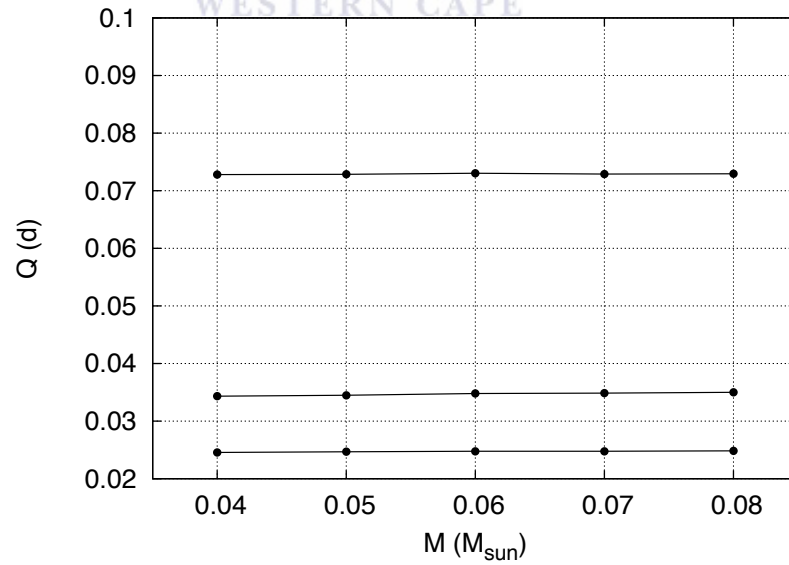


Figure 3.11: Plot of the theoretical pulsation constants of the fundamental mode and the first two overtones as a function of mass from our study.

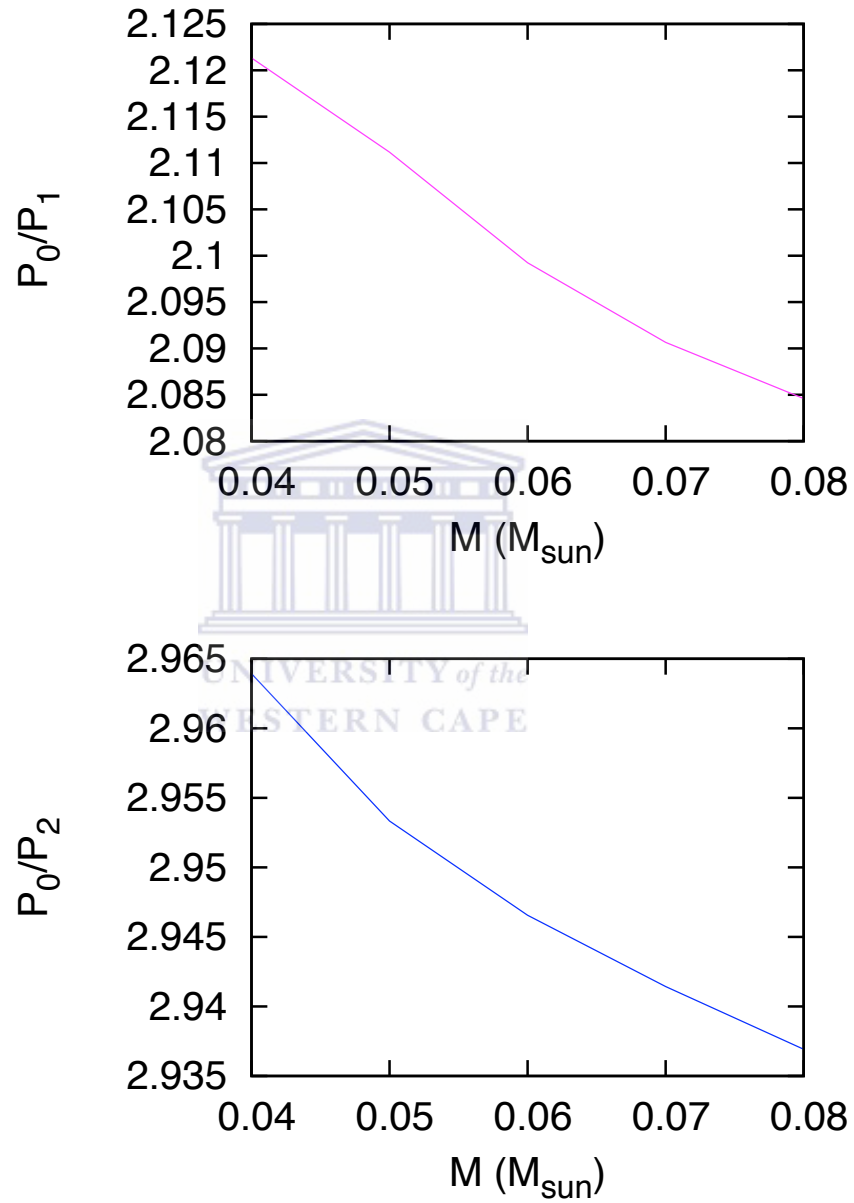


Figure 3.12: Plots of the ratio of the fundamental mode periods to the first harmonic periods (top plot) and the second harmonic periods (bottom plot) from our study.

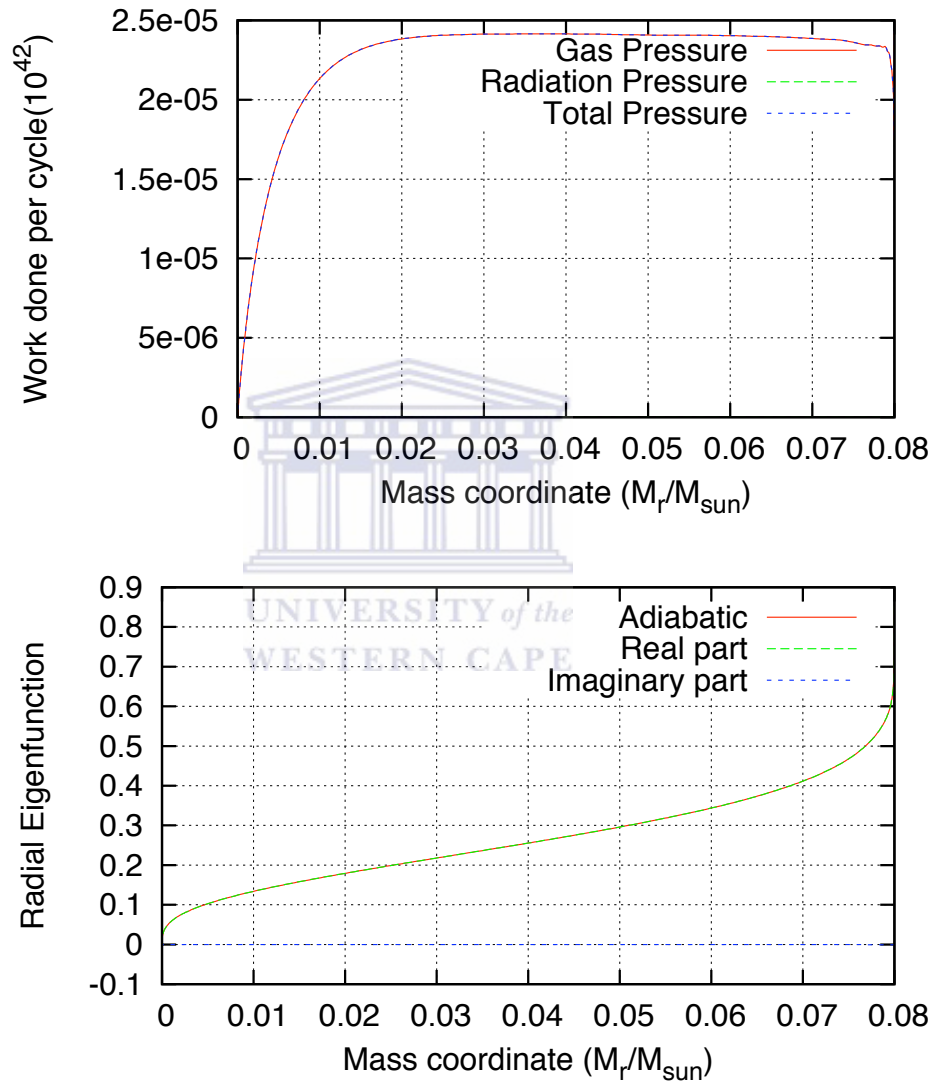


Figure 3.13: The radial eigen functions and the total integrated work integrals plotted as functions of the mass coordinate in the frozen-in approximation case for the $0.08M_{\odot}$ model.

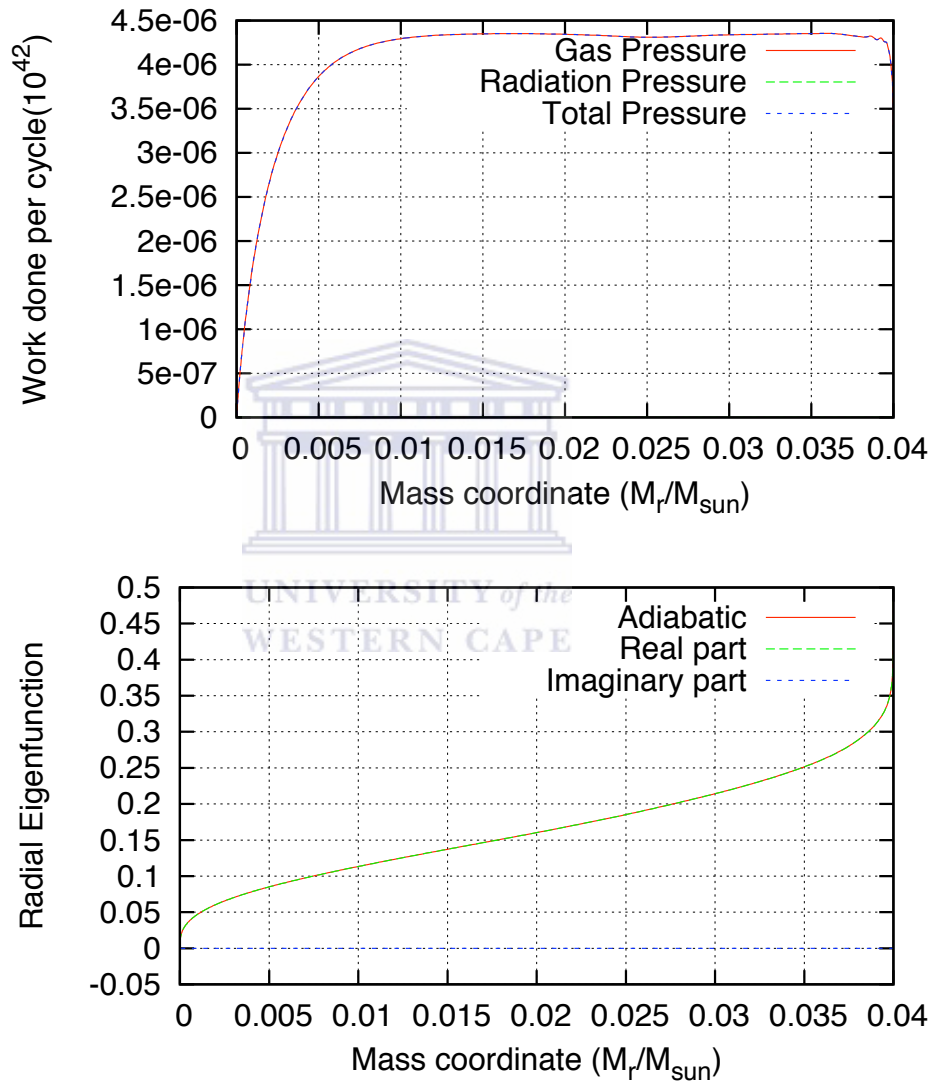


Figure 3.14: A similar plot as 3.13 for the $0.04M_{\odot}$ model.

of the models as expected for the epsilon mechanism. Plots of the work integrals and the radial eigen functions for the other masses used in our study are shown in figures (3.15), (3.16), (3.17), (3.18) and (3.19).

The maximum integrated work done per cycle decreases with decrease in mass. These results are in agreement with the prediction by PB05 with their ‘frozen-in’ convection approximation, and shows a very good agreement between the static model structures, the pulsation periods and the e-folding times for the higher masses. Due to this, in the next analysis we focus only on the higher mass models and exclude the $0.02M_{\odot}$ and $0.03M_{\odot}$ models.



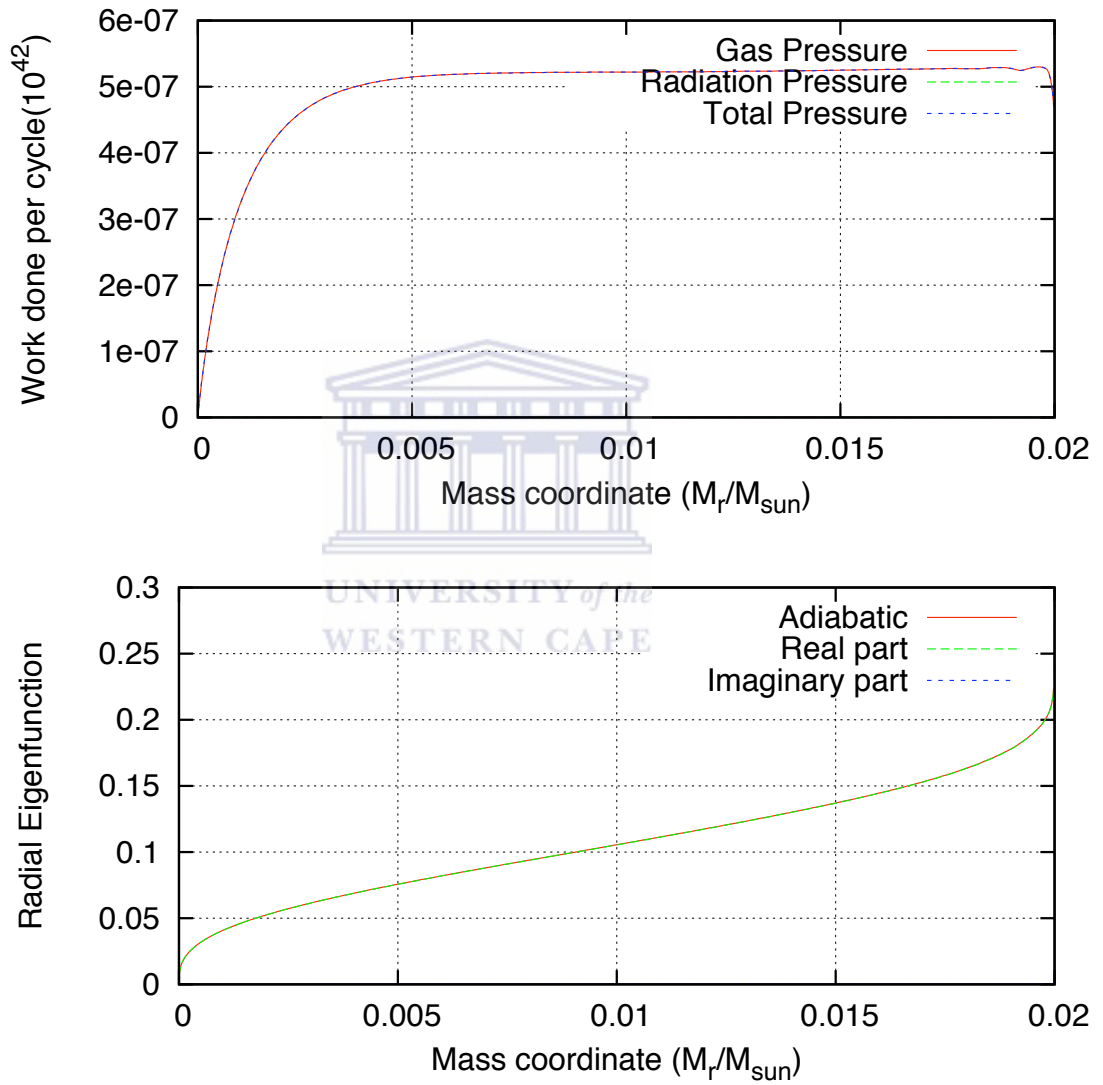


Figure 3.15: The total partial work integrals and the radial eigenfunction for the $0.02M_{\odot}$.

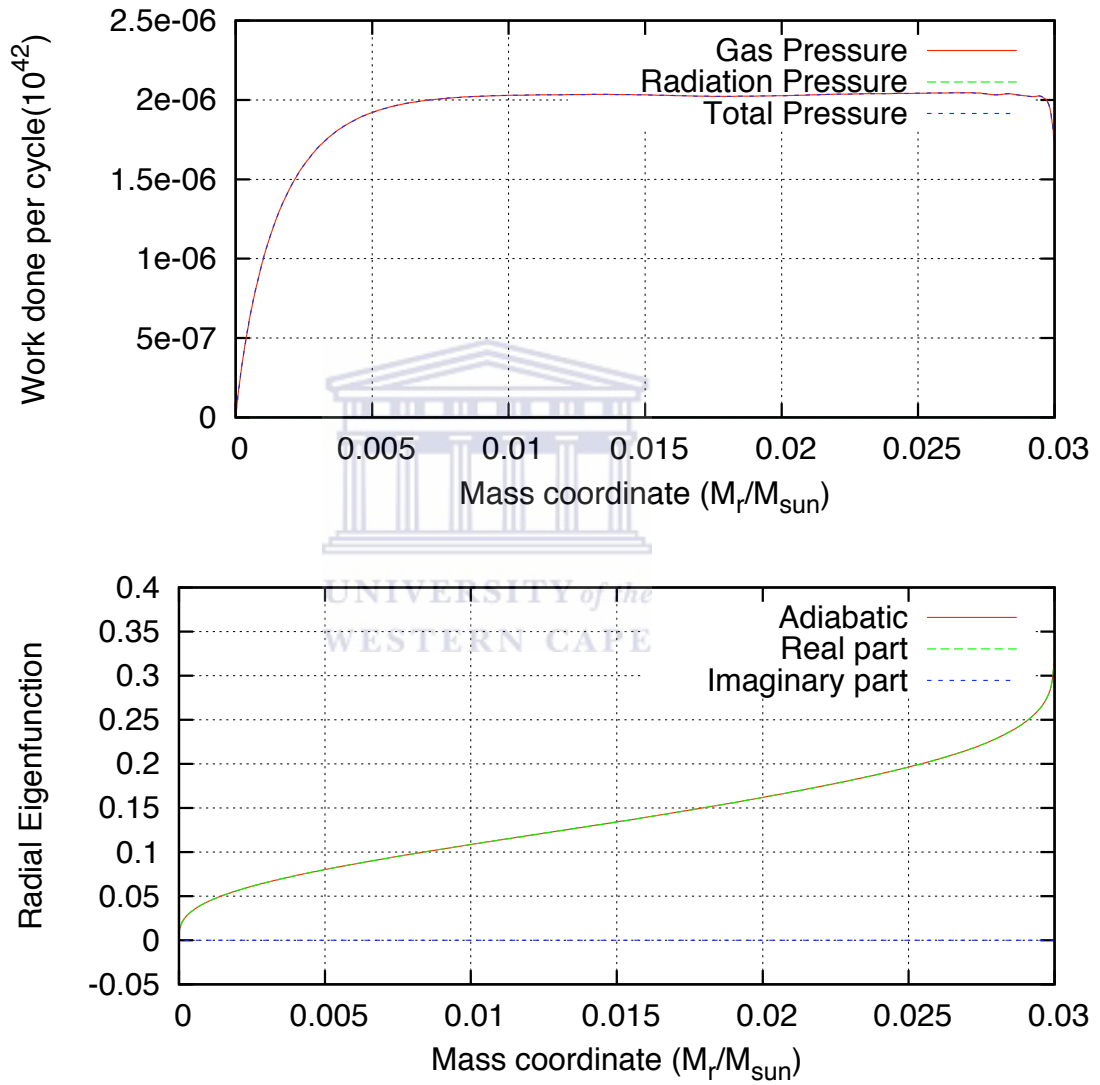


Figure 3.16: The total partial work integrals and the radial eigenfunction for the $0.03M_{\odot}$.

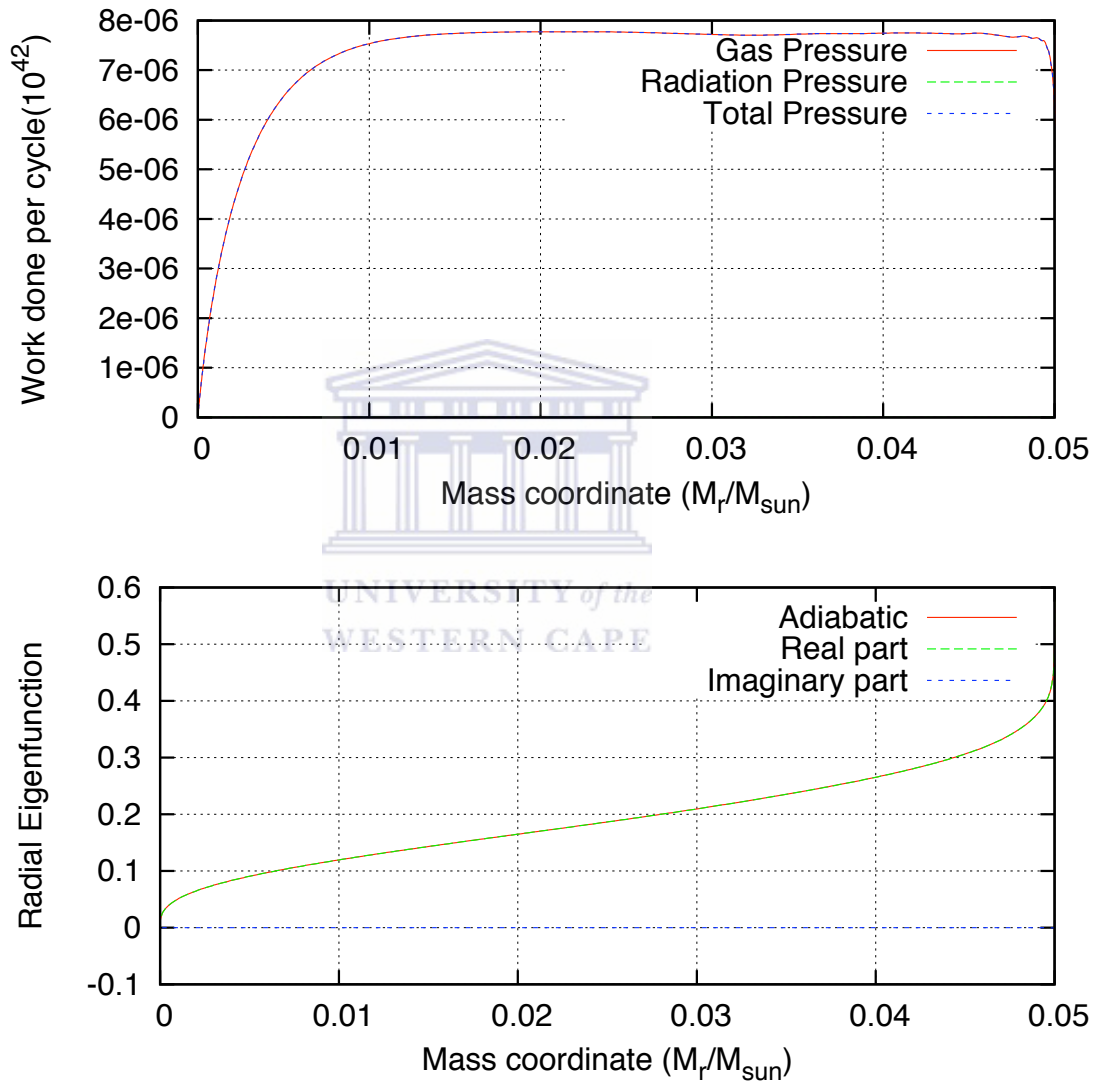


Figure 3.17: The total partial work integrals and the radial eigenfunction for the $0.05M_{\odot}$.

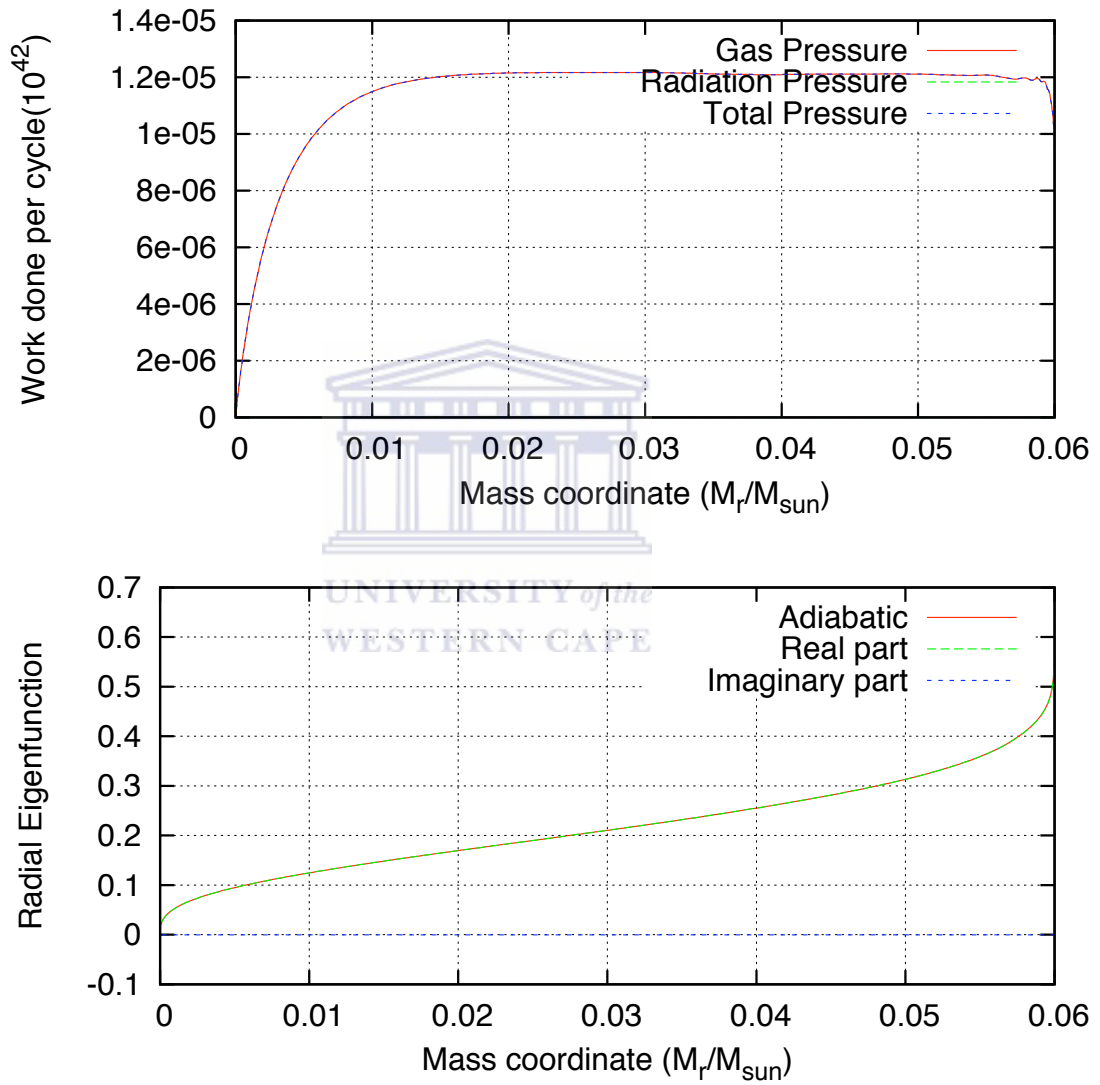


Figure 3.18: The total partial work integrals and the radial eigenfunction for the $0.06M_{\odot}$.

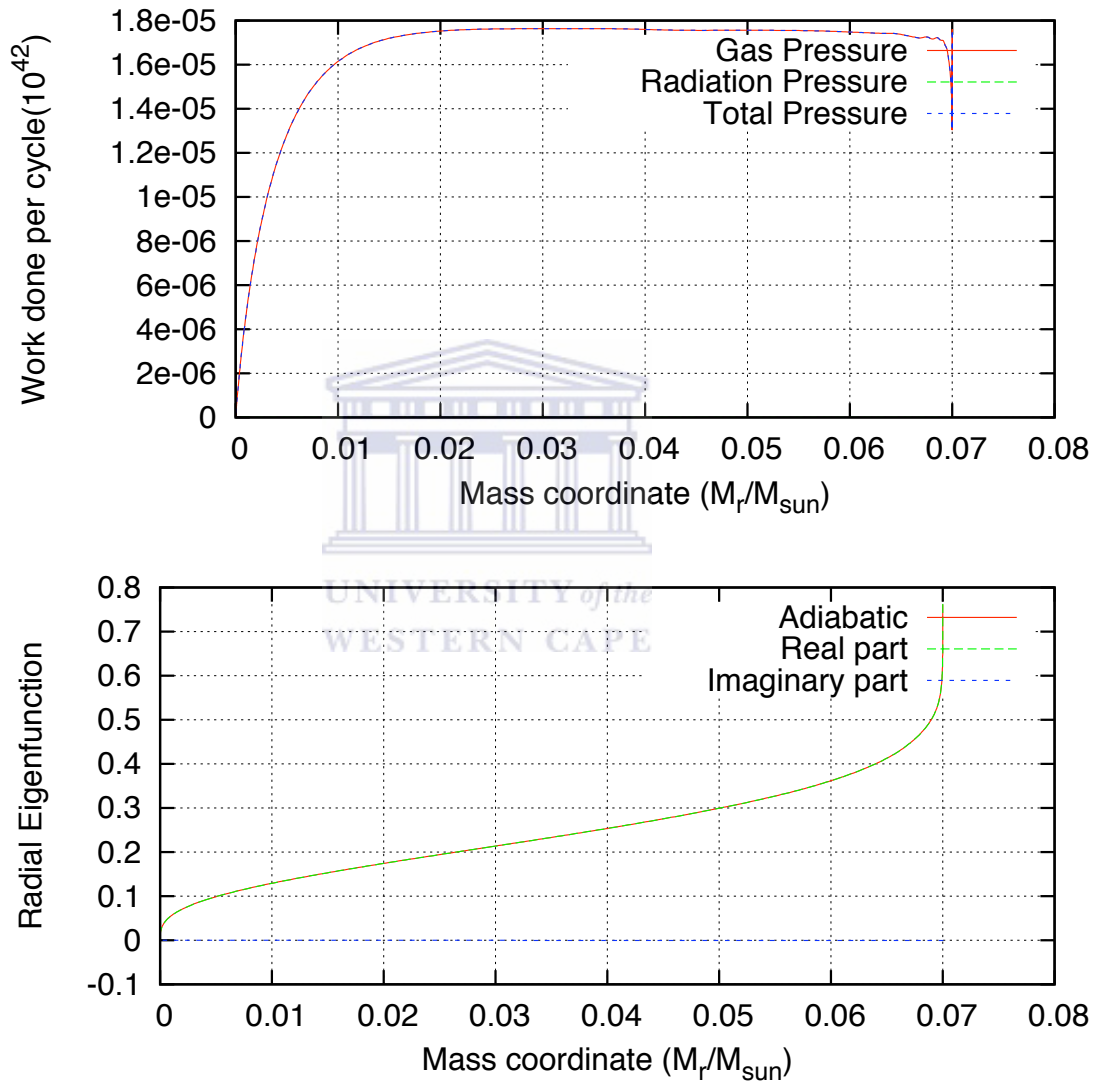
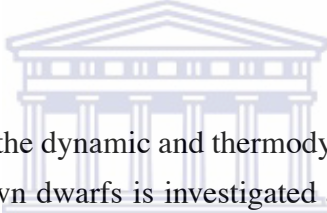


Figure 3.19: The total partial work integrals and the radial eigenfunction for the $0.07M_{\odot}$.

Chapter 4

Results II: A Time-Dependent Model of Convection



In this chapter, the effect of the dynamic and thermodynamic coupling between convection and pulsation in young brown dwarfs is investigated and discussed. An account of these effects, as pointed out by previous studies (see e.g. Gough, 1977; Xiong, 1977), requires a non-local time-dependent model of convection. Such a model, similar to Kuhfuß (1986) and Stellingwerf (1984), as stated earlier, is applied. The effect of perturbations in convective flux ignoring turbulence is presented in §4.1. Turbulent pressure is included and its effect discussed in §4.2. The effect of turbulent viscosity is investigated in §4.3. Finally the two major free parameters α_t and α_μ , (the turbulent diffusion and turbulent viscosity parameters respectively) in the convective model are varied and the effect of their variation on the stability properties investigated in §4.4. Similar values of the initial deuterium abundances, model parameters and scaling factors have been used unless stated otherwise.

4.1 Effect of perturbation in convective flux

4.1.1 The pulsation periods, growth rates and e-folding times

For fully convective objects such as brown dwarfs, the overall stability properties are dependent on the coupling between convection and pulsation. This occurs through the convective

M (M_{\odot})	ω_R (h^{-1})	ω_I (h^{-1})	P (h)	τ_e (Myr)
0.08	-3.2430E-05	1.4912	4.2136	-3.5200E-06
0.07	-3.3274E-05	1.6504	3.8071	-3.4307E-06
0.06	-3.4282E-05	1.8498	3.3968	-3.3299E-06
0.05	-3.5675E-05	2.1127	2.9740	-3.1999E-06
0.04	-3.7287E-05	2.4904	2.5229	-3.0615E-06

Table 4.1: Some properties of five BD models with the turbulent treatment of convection ignoring turbulent pressure and turbulent viscosity for the fundamental mode. The pulsation frequencies have been scaled by the factors, ω_{scale} , same as in chapter (3).

M (M_{\odot})	ω_R (rad h^{-1})	ω_I (rad h^{-1})	P_1 (h)	τ_e (Myr)
0.08	-7.5094E-05	3.1085	2.0213	-1.5202E-06
0.07	-7.8277E-05	3.4504	1.8210	-1.4553E-06
0.06	-8.2832E-05	3.8831	1.6181	-1.3782E-06
0.05	-8.8026E-05	4.4601	1.4087	-1.2968E-06
0.04	-9.2588E-05	5.2830	1.1893	-1.2329E-06

Table 4.2: Some properties of five BD models with the turbulent treatment of convection ignoring turbulent pressure and turbulent viscosity for the first harmonic.

energy transfer (thermodynamic coupling) and turbulent stresses (dynamic coupling). This section deals with the effects of the perturbation in the convective flux (thermodynamic coupling), ignoring turbulent pressure and turbulent viscosity. The main pulsation properties for five objects from our study in this case are shown in tables 4.1 (fundamental mode), 4.2 (first harmonic), and 4.3 (second harmonic). The pulsation periods are found to remain the same as the case when the convection was assumed to be frozen in the linear stability analysis presented in chapter 3. For any given mode, the pulsation periods are found to decrease with mass and lie in the range of $\sim 2 - 4$ hours. However, the time-dependent treatment of convection is found to make the models stable against pulsations. This can be seen from the pulsation amplitude decay rates (proportional to ω_R) and the resulting decay times for different objects shown in tables 4.1, 4.2 and 4.3 for the fundamental, first harmonic and second harmonic modes respectively. All the three modes identified here were found to be stable against oscillations for all masses shown.

$M (M_{\odot})$	$\omega_R (\text{rad } h^{-1})$	$\omega_I (\text{rad } h^{-1})$	$P (\text{h})$	$\tau_e (\text{Myr})$
0.08	-1.199E-04	4.3794	1.4347	-9.5211E-07
0.07	-1.239E-04	4.8546	1.2943	-9.2131E-07
0.06	-1.270E-04	5.4506	1.1528	-8.9854E-07
0.05	-1.324E-04	6.2401	1.0070	-8.6215E-07
0.04	-1.4081E-04	7.3807	0.8512	-8.1072E-07

Table 4.3: Some properties of five BD models with the turbulent treatment of convection ignoring turbulent pressure and turbulent viscosity for the second harmonic.

4.1.2 The Work integrals

The partial work integrals and the radial eigenfunctions for the masses in the range $0.04M_{\odot} - 0.08M_{\odot}$ from our study are displayed in figures 4.3, 4.4, 4.5, 4.6, 4.7, 4.8 and 4.9. These plots correspond to the case when a time-dependent treatment of convection was applied and turbulent pressure and turbulent viscosity ignored. The plots of the total integrated work display a decrease in the total work done as function of the mass coordinate throughout the radial structures of all models. This indicates that the time-dependent treatment of convective energy transfer leads in general to damping. Figure 4.1 shows plots of the real and imaginary parts of the convective luminosity eigenfunction δL_c plotted as a function of the radial mass coordinate M_r . Note that the real part of δL_c is much larger than the imaginary part. In the stellar interior, the amplitude δL_c decreases. This implies that in the interior, the stellar material is losing thermal energy through convective energy transfer during contraction, and gaining thermal energy during expansion. This result is exactly the reverse carnot cycle on the P-V diagram and is responsible for damping of the pulsations. On the other hand, in the upper stellar layers, the amplitude of the convective flux, δL_c , decrease towards the surface. This causes the fluid elements to gain thermal energy during contraction and lose thermal energy during expansion, in a pulsation cycle. Convective energy transfer, therefore, in these regions acts as an excitation mechanism of the pulsations. A similar mechanism was seen in operation in δ Scuti stellar models of Xiong and Deng (2001). This is clearly illustrated in figure (4.2) showing the contributions of the convective luminosity and the nuclear energy generation to the work integral as calculated from the expressions given in chapter 2.

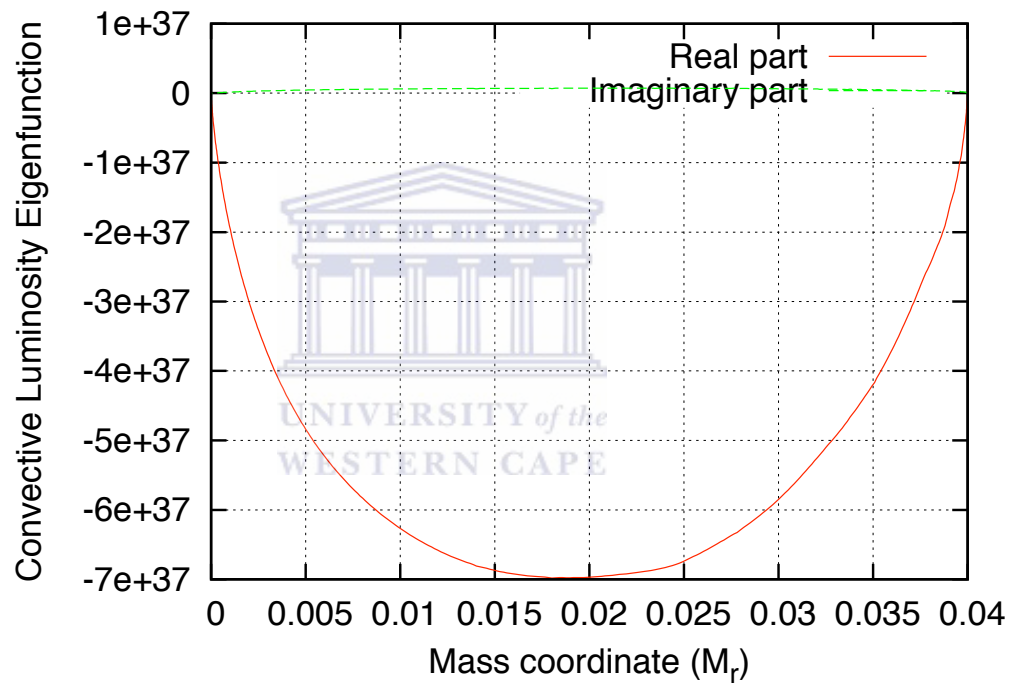


Figure 4.1: Plots of the real and imaginary parts of the convective luminosity eigenfunctions as a function of the radial mass coordinate M_r for the $0.04M_{\odot}$ model.

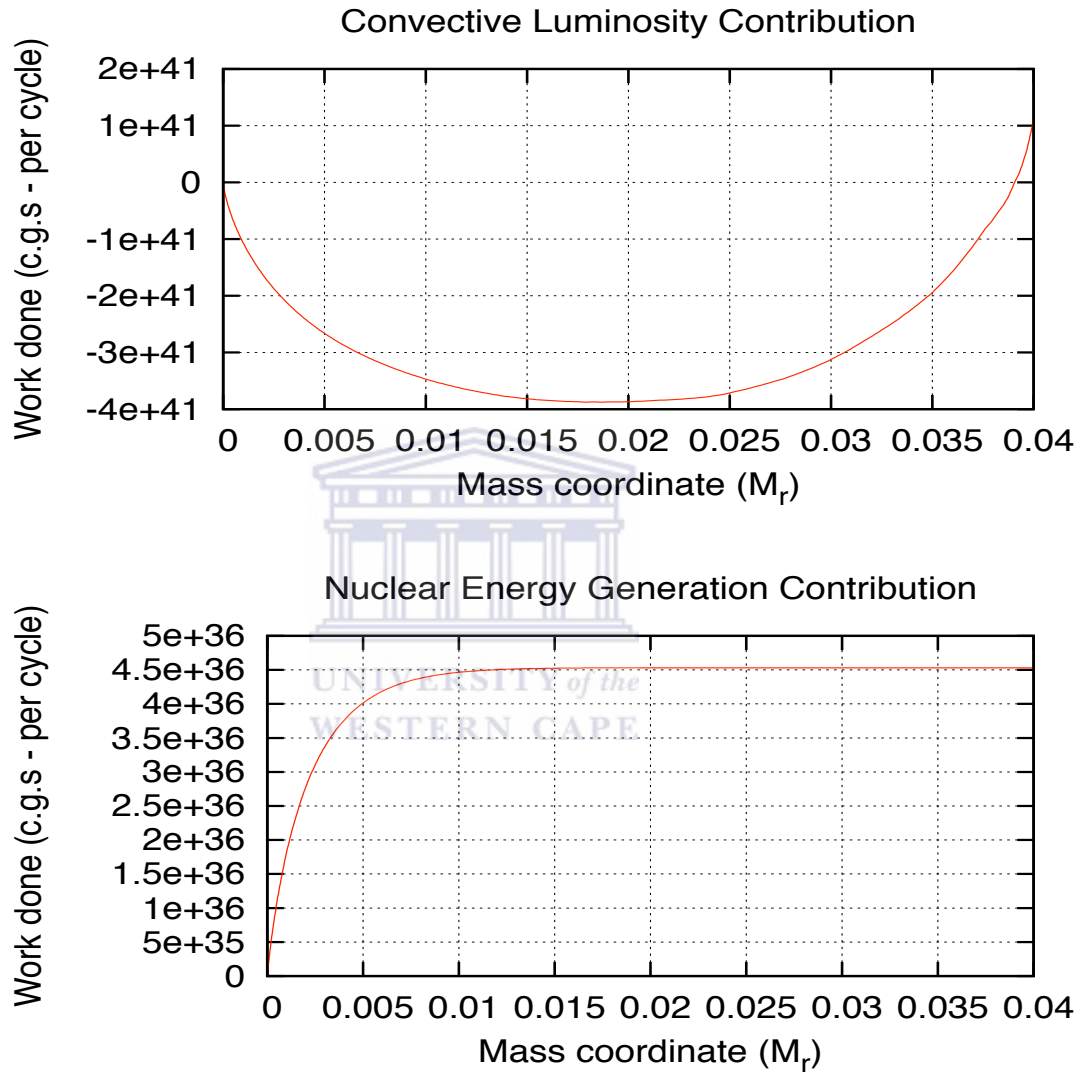


Figure 4.2: Plots of the analytical expressions for contributions from the perturbation in the convective flux (top plot) and the perturbation in nuclear energy generation rate (bottom plot), as functions of mass for the $0.04M_{\odot}$. Here, turbulent viscosity and turbulent pressure are ignored. Contribution from the convective flux can be seen to dominate that from the nuclear energy generation rate which is what leads to net overall damping displayed in work integral plots for this case.

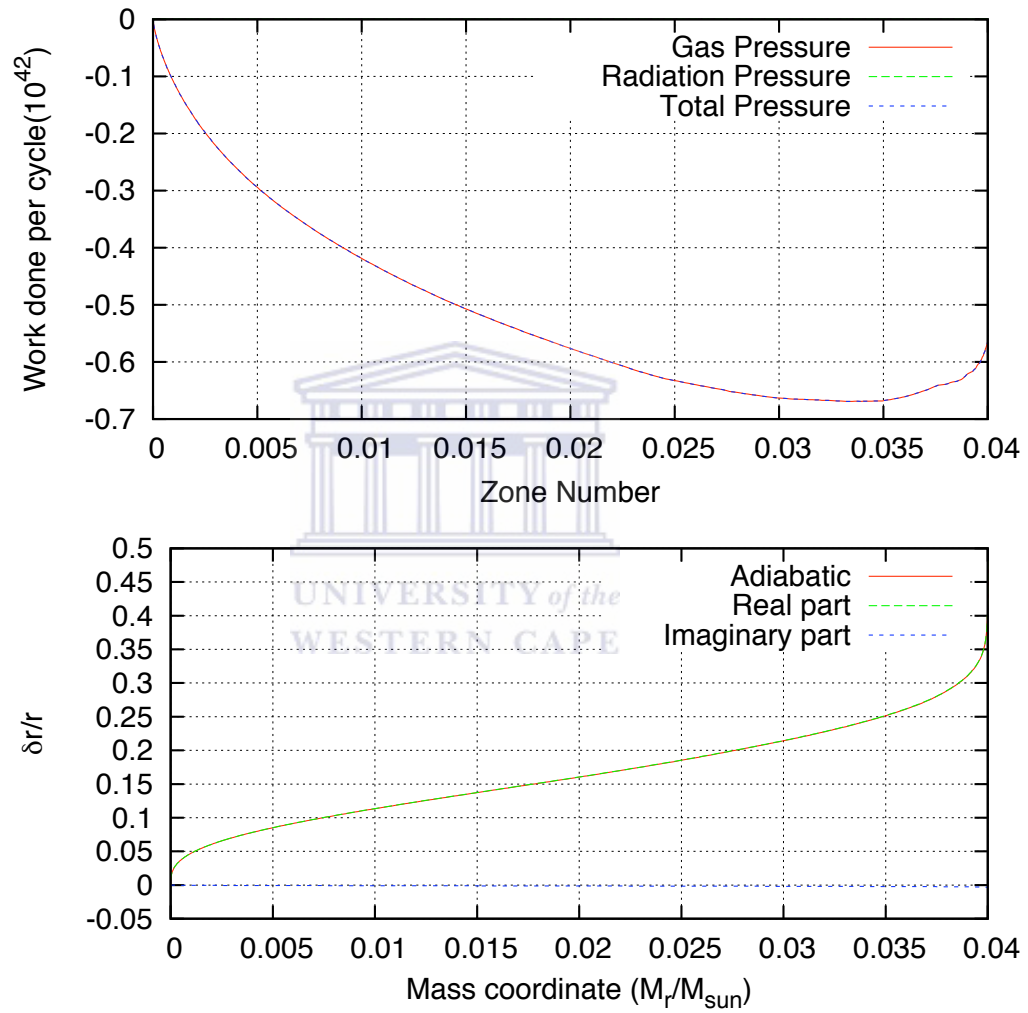


Figure 4.3: Plots of the total partial work integrals (top plot) and the radial eigenfunctions (bottom plot) when the perturbations in the convective flux are included and turbulent pressure and turbulent viscosity ignored for the $0.04M_{\odot}$ model.

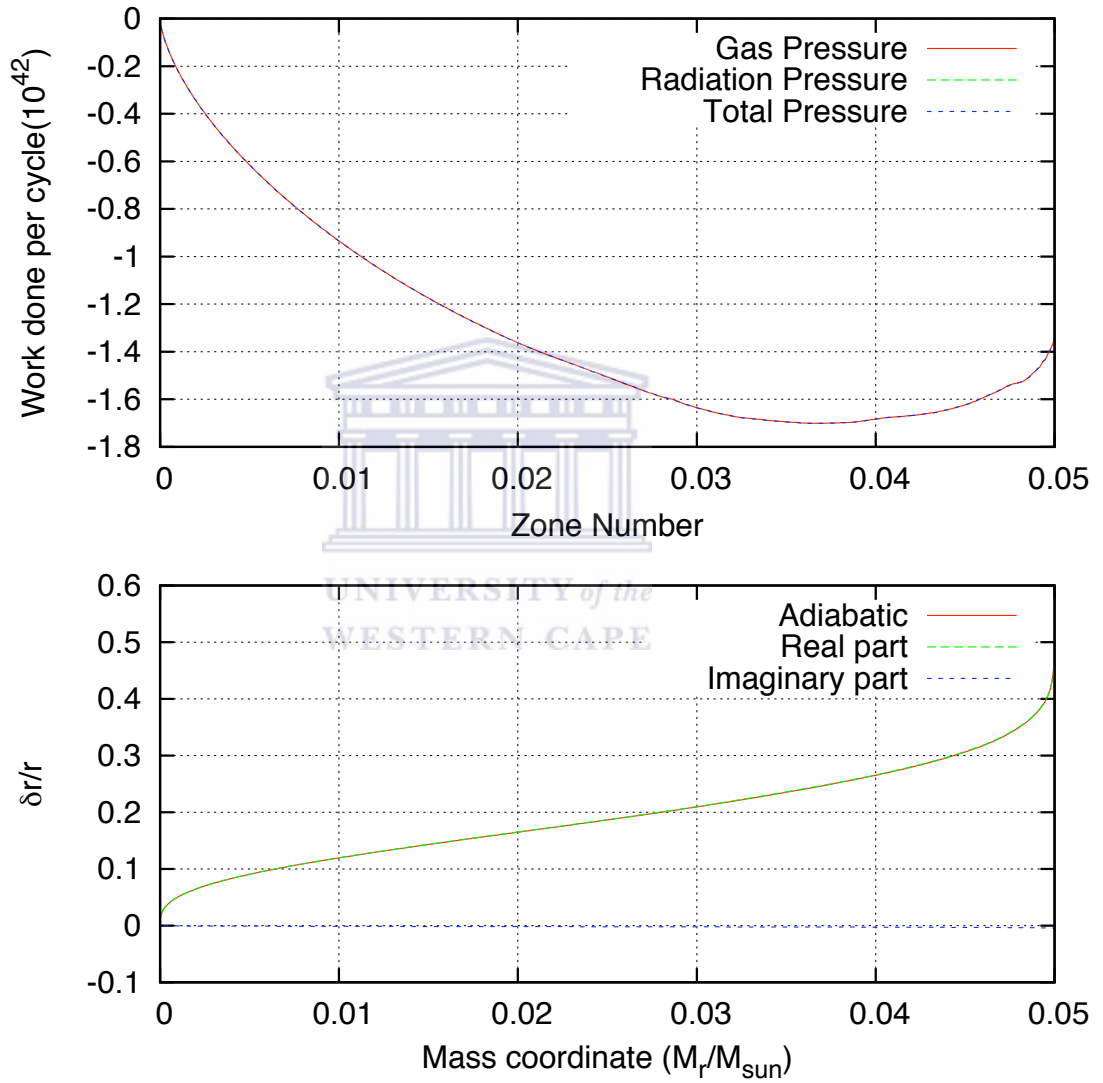


Figure 4.4: Plots same as figure 4.3 but for the $0.05M_{\odot}$ model.

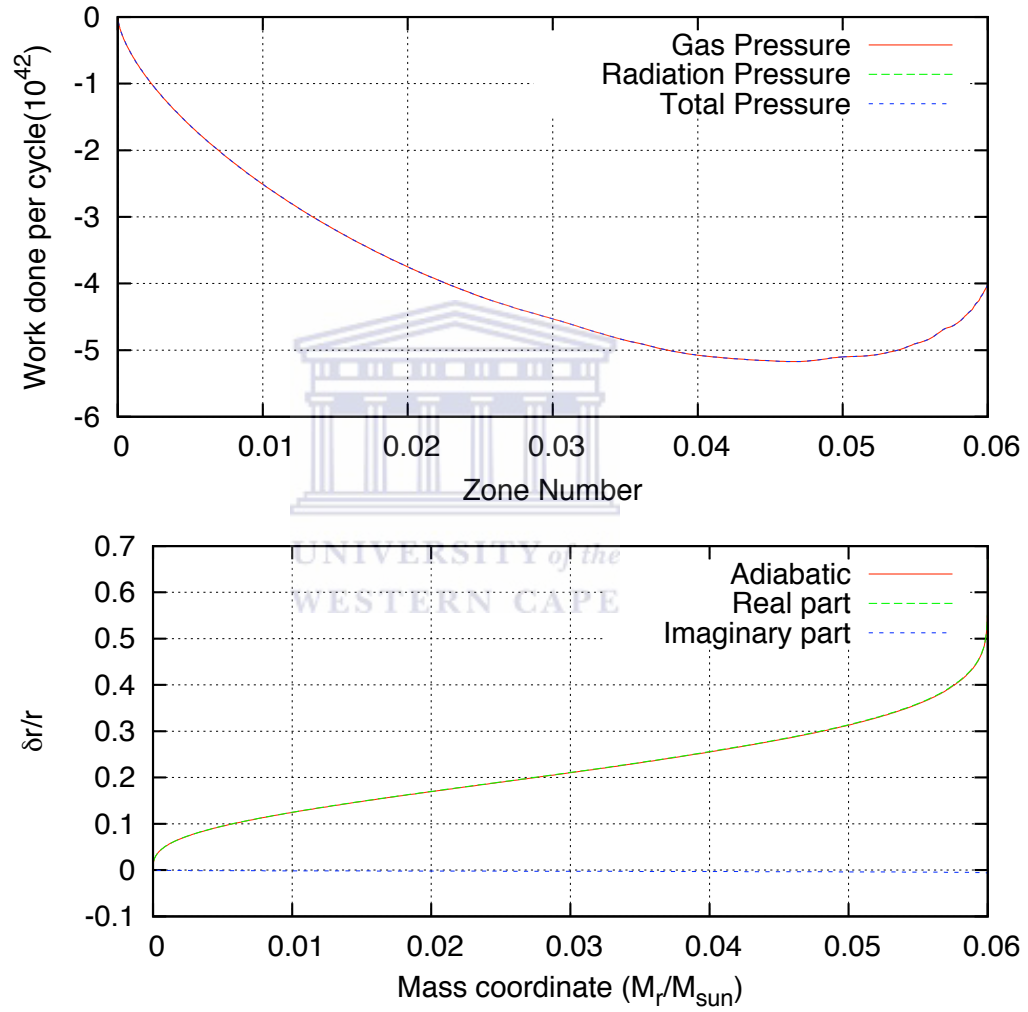


Figure 4.5: Plots for the $0.06M$ model. Same as figure 4.3.

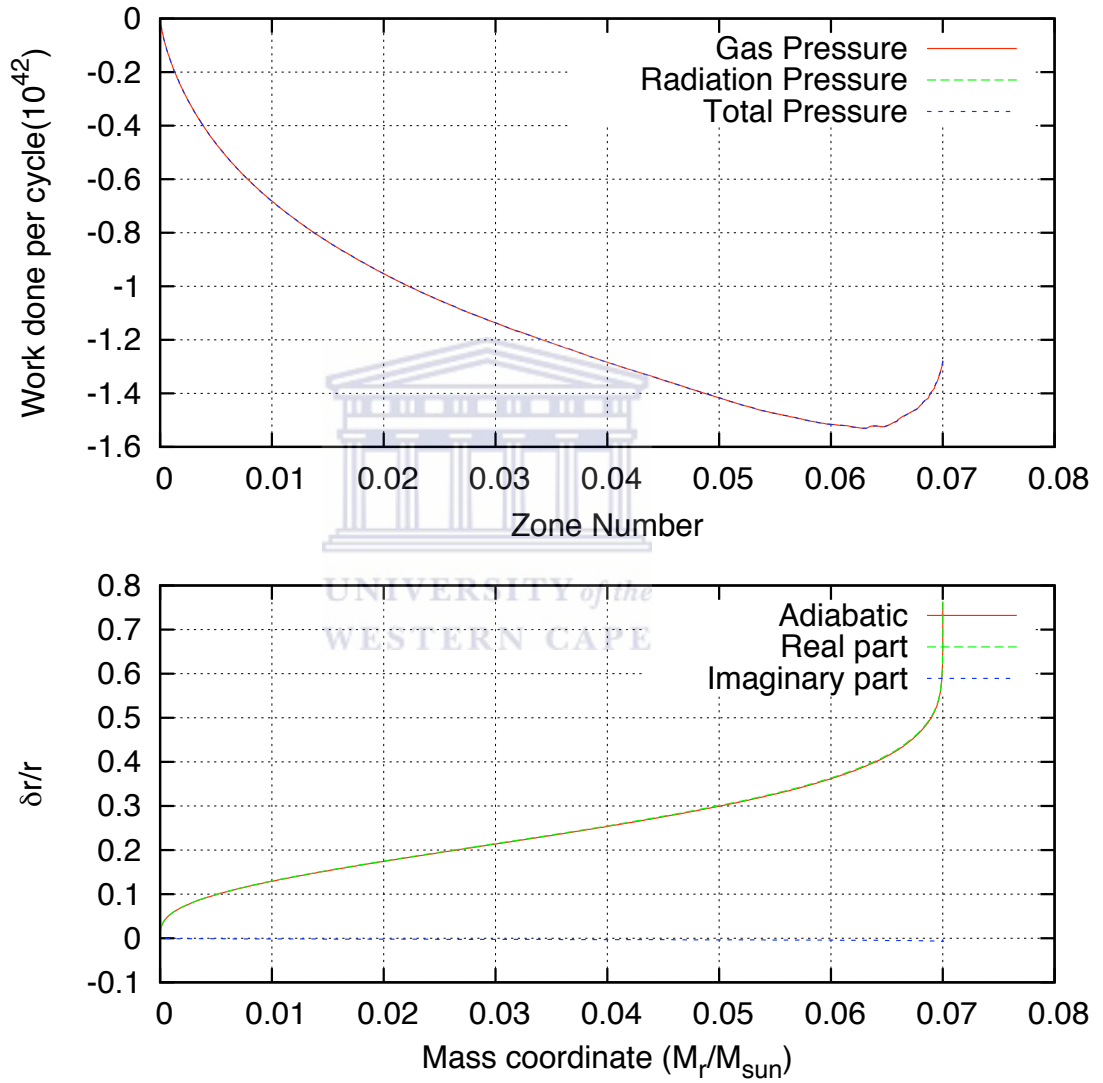


Figure 4.6: Plots for the $0.07M_{\odot}$ model. Same as figure 4.3.

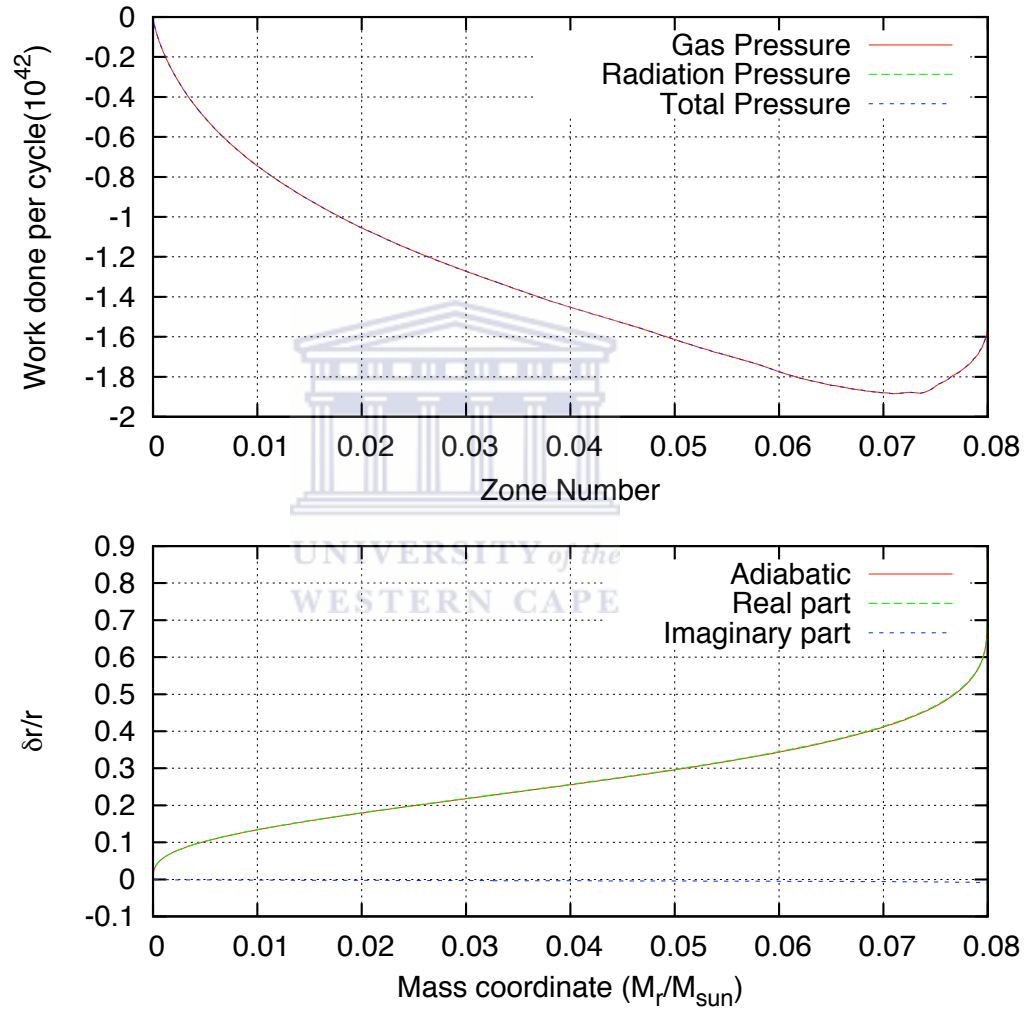


Figure 4.7: Plots for the $0.08M_{\odot}$ model. Same as figure 4.3.

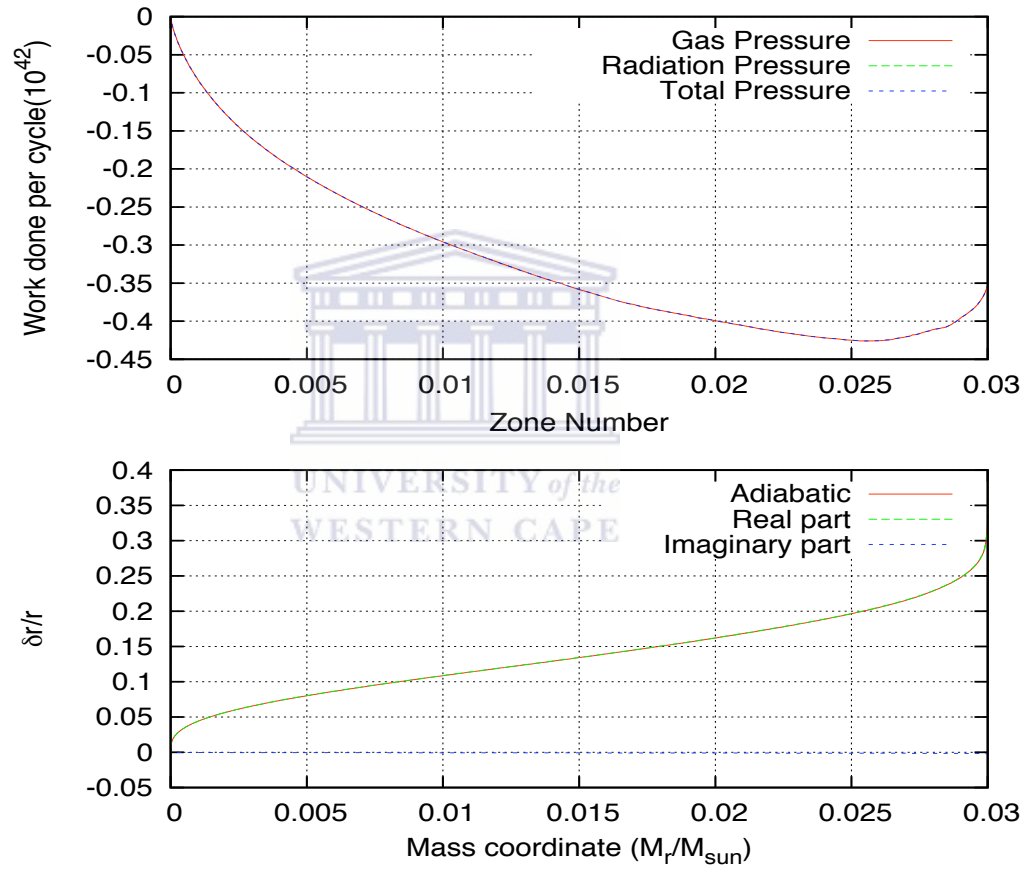


Figure 4.8: Plots for the $0.03M$ model. Same as figure 4.3.

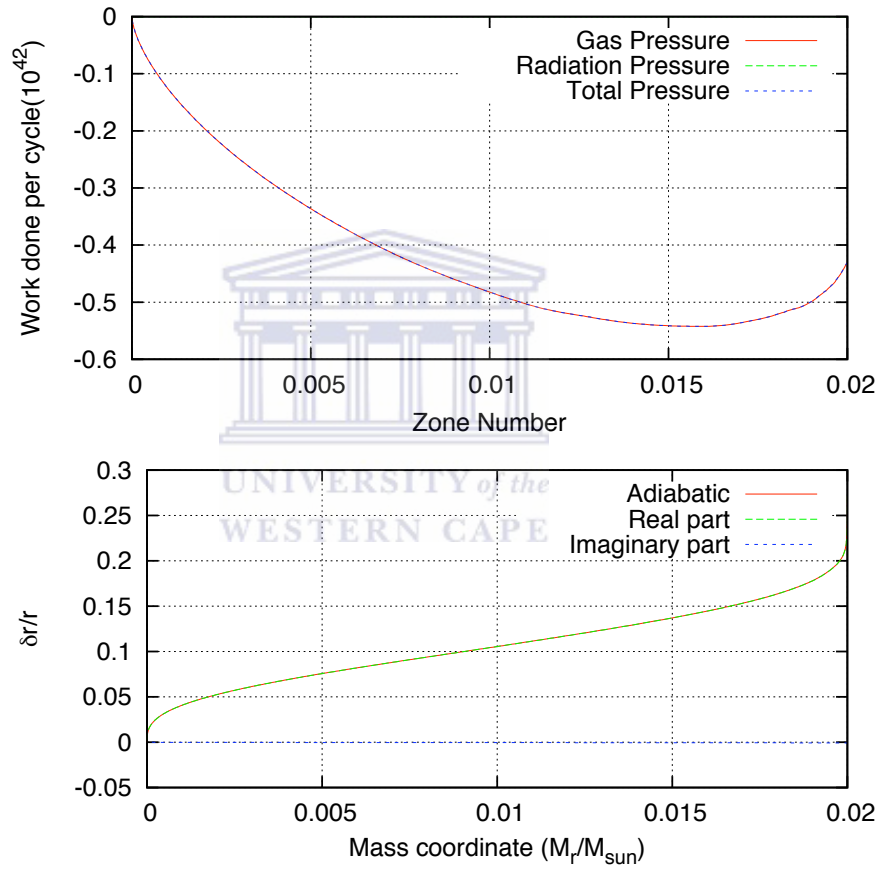


Figure 4.9: Plots for the $0.02M_{\odot}$ model. Same as figure 4.3.

4.2 Effect of turbulent pressure

Studies of solar p-mode oscillations have shown that turbulent pressure is an important excitation mechanism for stellar oscillations in regions where nonadiabatic effects are less pronounced (Xiong and Deng, 2001). However, other studies have found that inclusion of turbulent pressure leads to damping of the acoustic oscillations (see e.g. Stellingwerf, 1984, 1982, for RR Lyrae stars). Excitation of stellar oscillations occurs because turbulent pressure lags behind the density. This leads to a clockwise Carnot cycle effect on the P-V diagram which causes driving. In the results presented here, we included turbulent pressure in the time-dependent treatment of convection through the turbulent pressure parameter $\alpha_{pt} = \frac{2}{3}$. Plots of the partial work integrals from the different pressure components for the $0.04M_{\odot}$ and $0.08M_{\odot}$ objects are shown in figures 4.11 and 4.10 respectively.

Figures 4.11 and 4.10 show that the contribution of the turbulent pressure component is everywhere positive in all zones of these objects giving pulsation amplitude growth rates many orders of magnitude higher than the epsilon mechanism alone. To further probe this result, we plotted the phase difference between turbulent pressure and the density as shown in figure 4.12.

We find a phase difference of slightly larger than $\frac{\pi}{2}$ between the turbulent pressure and the density for all models presented. This is in agreement with the requirement for driving stated previously. Also, since turbulent pressure has two components: turbulent velocity and specific volume connected by the perturbation equation

$$\frac{\delta P_t}{P_t} = \frac{2\delta\varpi}{\varpi} - \frac{\delta V}{V} \quad (4.1)$$

where V is the specific volume and ϖ is the turbulent velocity, we made plots of two ratios; $\sigma = \frac{|\delta\varpi|}{|\delta P_t|}$ and $\beta = \frac{|\delta V|}{|\delta P_t|}$ where “|” denotes absolute values of the quantities, to establish the term which dominates in causing perturbations in turbulent pressure. Plots of these ratios are shown in figure 4.13. Perturbations in the turbulent velocity are found to dominate in the overall perturbations in turbulent pressure.

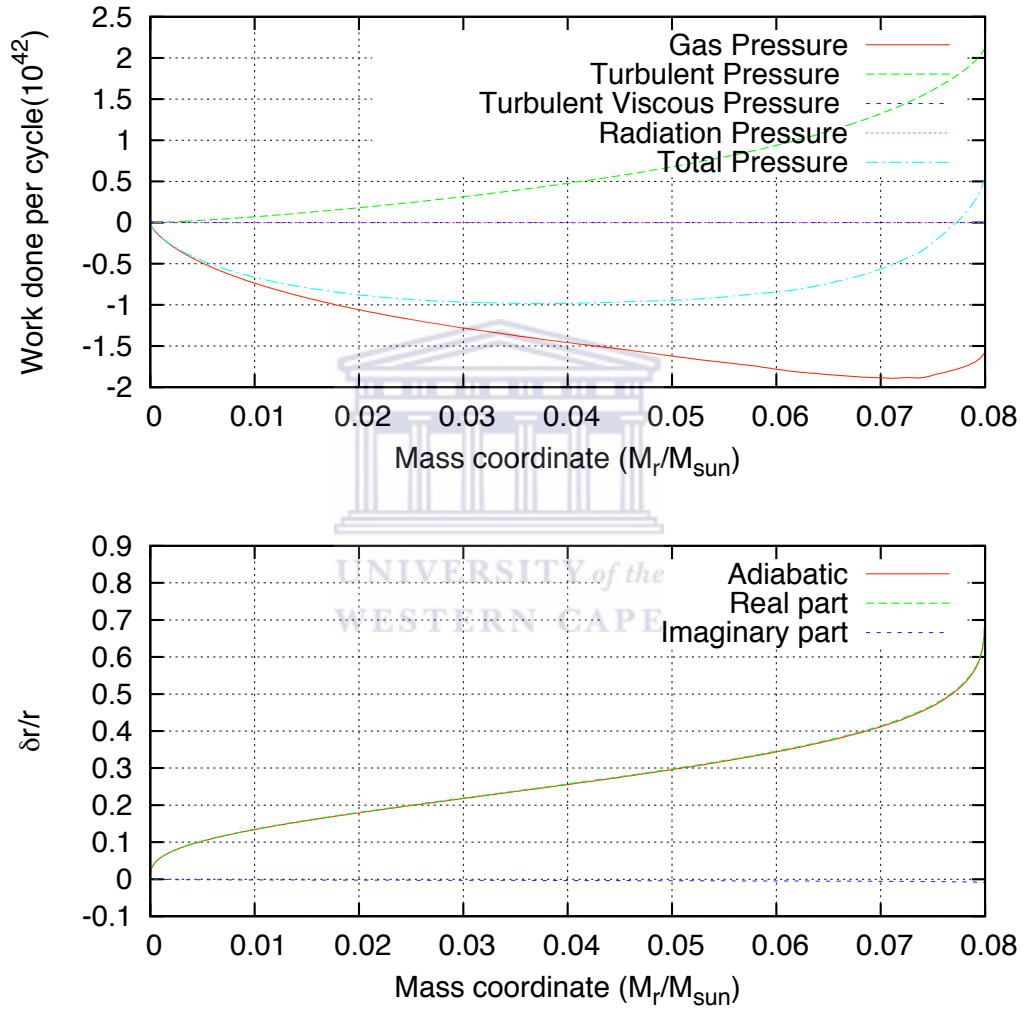


Figure 4.10: Plots of the work integrals and the radial eigenfunction vs mass coordinate for the $0.08M_{\odot}$ model.

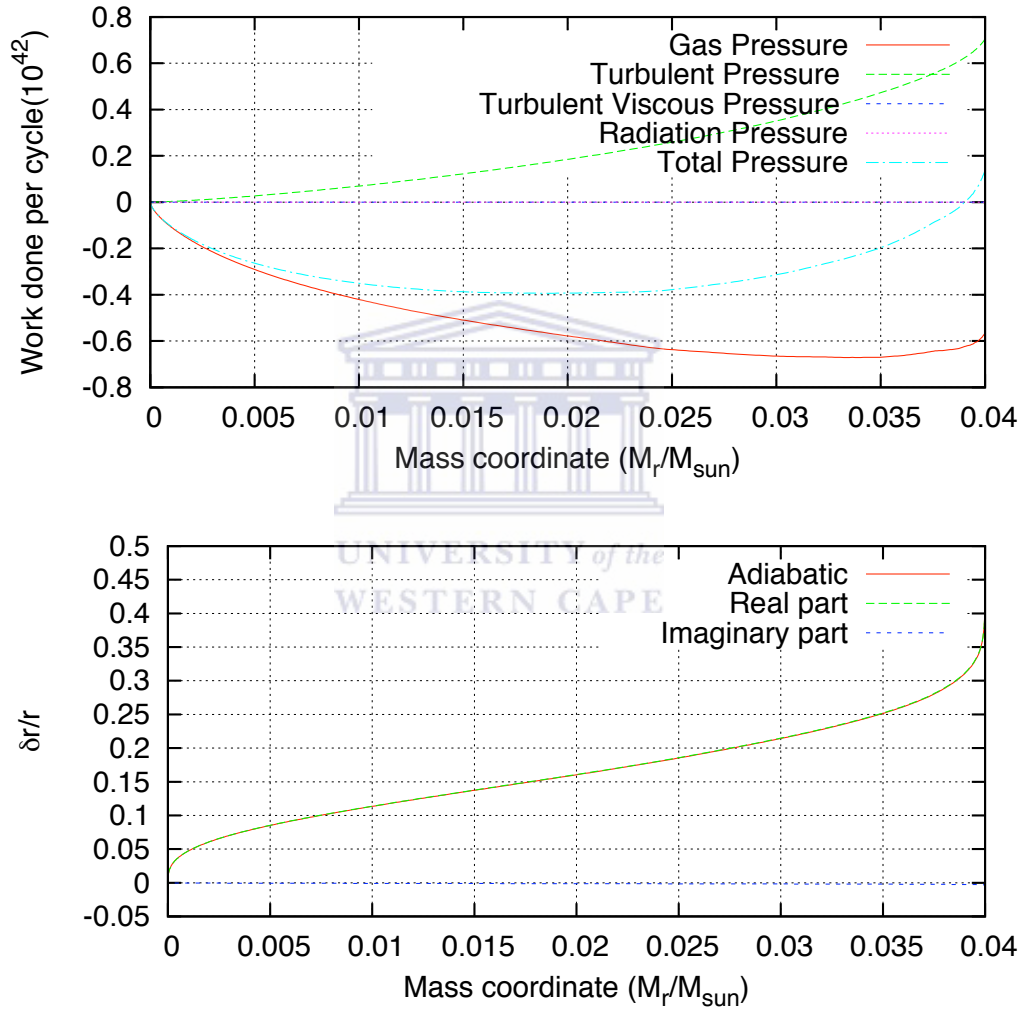


Figure 4.11: Same as figure 4.10 but for the $0.04M_{\odot}$ model.

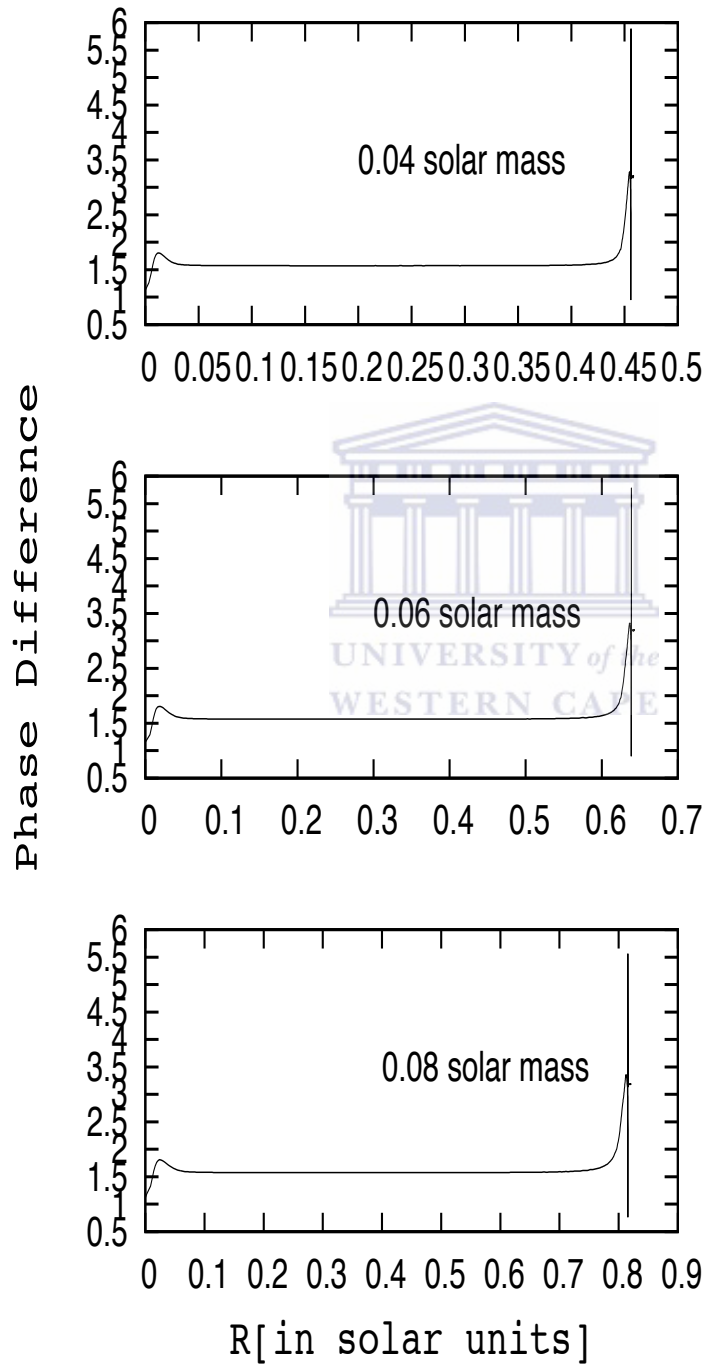


Figure 4.12: Plots of the phase difference between turbulent pressure and the density as a function of radius for three masses from our study.

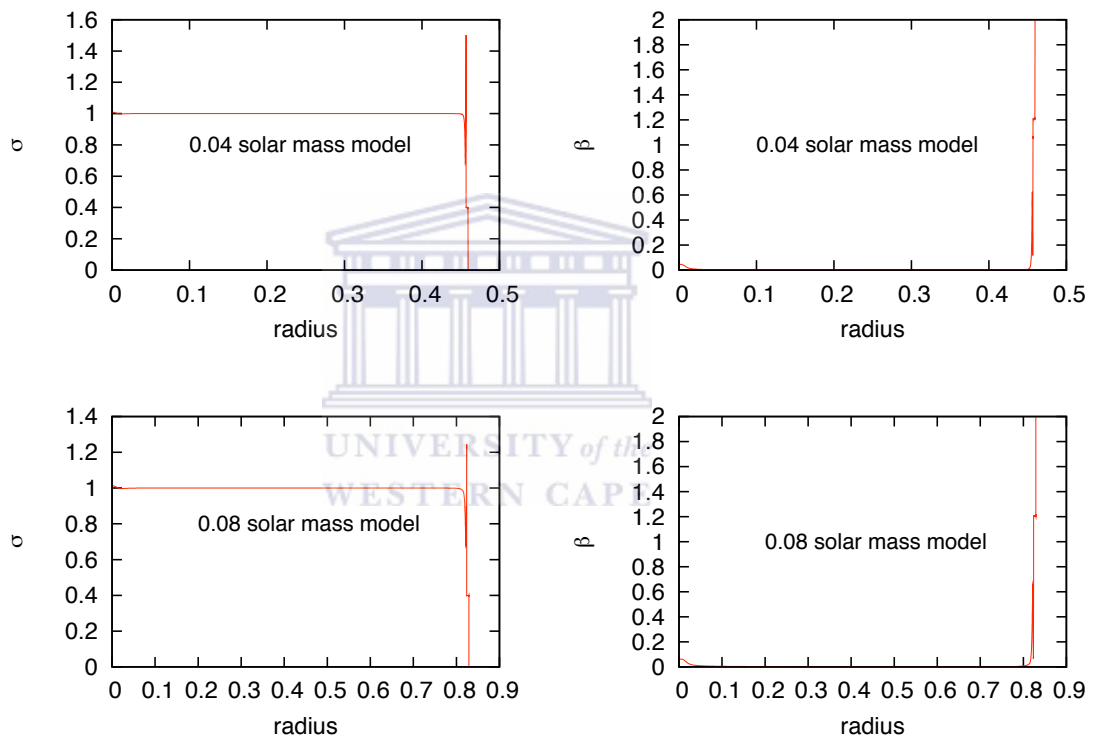


Figure 4.13: Plots of the absolute ratios of the perturbations in turbulent velocity to the perturbations in turbulent pressure, σ , for the $0.04 M_{\odot}$ model and $0.08 M_{\odot}$ and the ratio of the absolute value of perturbations in specific volume to the absolute value of perturbations in turbulent pressure, β .

4.3 Effect of turbulent viscosity

Here, results obtained when the turbulent viscosity parameter was made to vary between values of 0.0 and 2.0 are presented and discussed. Since, α_μ is considered a ‘free parameter’ in the theoretical model used in this study, evaluation of the effect of this parameter on the major pulsation properties is important. Figure 4.14 shows plots of the fundamental mode periods and the growth rate as functions of the parameter α_μ for three objects with masses $0.08M_\odot$, $0.06M_\odot$ and $0.04M_\odot$. As shown from our plots, this parameter has very little effect on the fundamental mode periods for the masses of interest and the above mentioned range of α_μ . Plots of the pulsation amplitude growth (or decay) rates as functions of the parameter α_μ are also shown in figure 4.14. The plot shows a decrease in the growth rate with increasing α_μ . According to Kuhfuß (1986), the value of α_μ should be one or two magnitudes less than the parameter α_ν introduced in chapter 2. We find that the models are unstable for $\alpha_\mu < 0.8$ and become stable for values of $\alpha_\mu > 0.8$.

4.4 Effect of the turbulent diffusion parameter

In this section, we discuss the effect of the turbulent diffusion free parameter, α_t . For this analysis, the following values of the other input parameters were used and kept constant: $\alpha'_\mu = 1$, $\alpha'_{tp} = 1.0$. Plots of the fundamental mode periods and the pulsation amplitude decay rates, η_0 , for the fundamental mode when α_t was made to vary between 0.0 and 2.0, are shown in figure 4.15. This parameter is found to make our objects stable as displayed from the decay rates. The results also show that the pulsation periods and the growth rates for the fundamental mode remain nearly constant for the whole range of values of α_t used in our study. However, the effect of this parameter for an extended range of values need to be investigated.

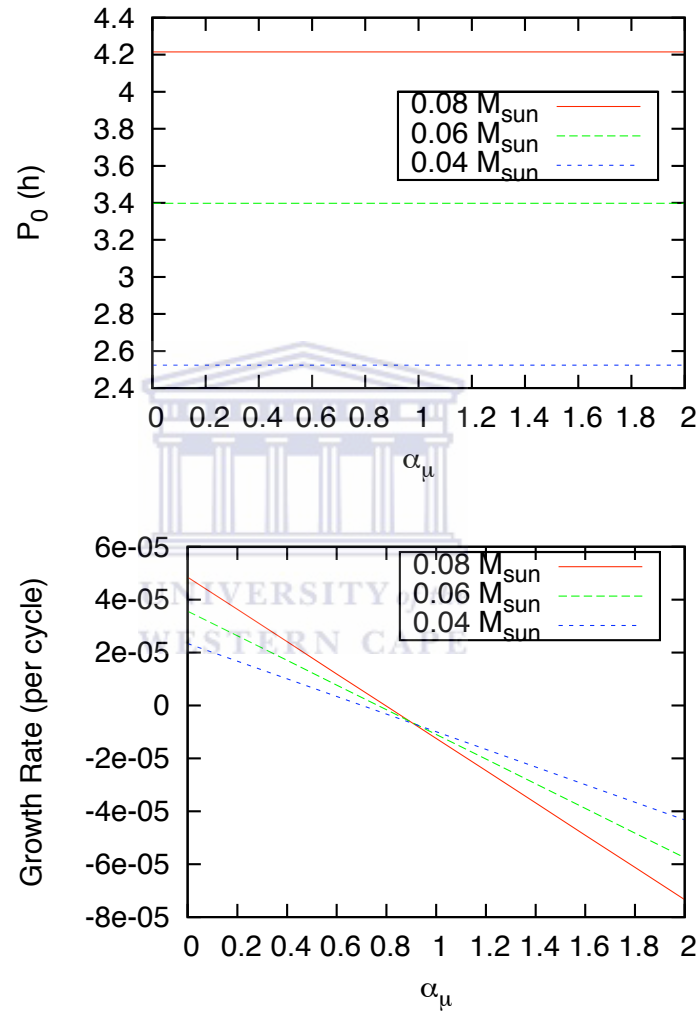


Figure 4.14: Plots of the fundamental mode periods vs the turbulent viscosity parameter α_μ for masses $0.08M_\odot$, $0.06M_\odot$ and $0.04M_\odot$ (top graph) and the growth rate, η , per cycle vs α_μ (bottom graph).

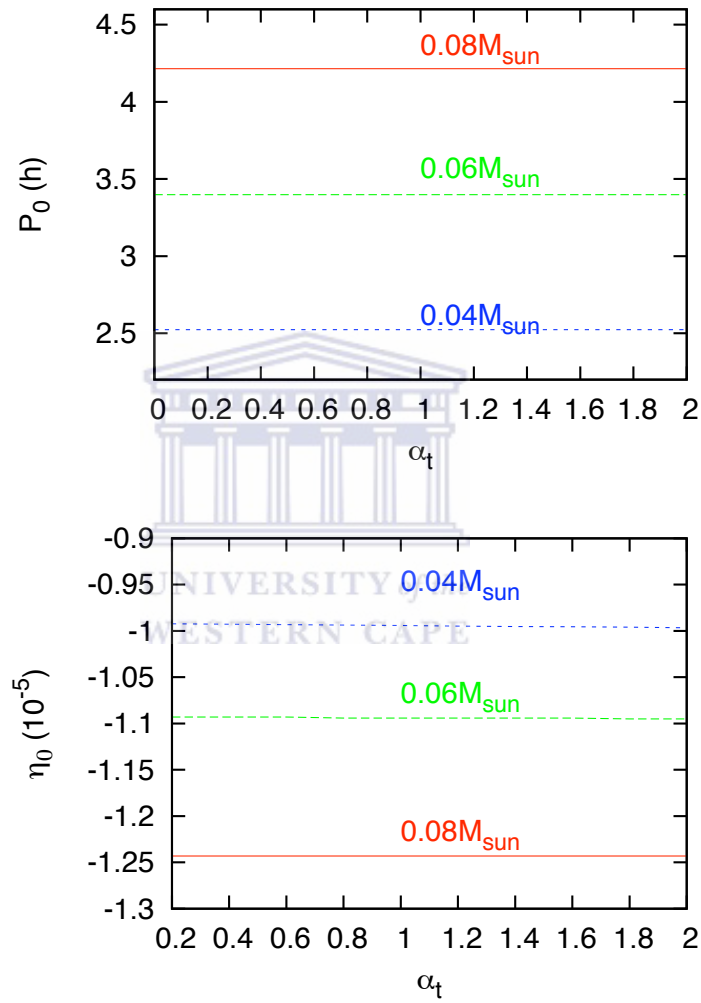
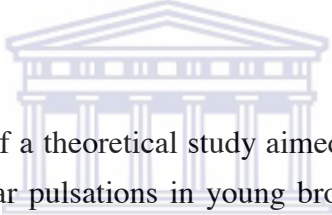


Figure 4.15: Plots of the fundamental mode periods vs the turbulent diffusion parameter, α_t , for three objects(top graph) and the pulsation amplitude decay rate (per cycle) for the fundamental mode, η_0 , for the same objects(bottom graph).

Chapter 5

Discussions, conclusions and call for further work



We have presented results of a theoretical study aimed at understanding the recently proposed phenomenon of stellar pulsations in young brown dwarfs. We have performed a non-adiabatic linear stability analysis using various brown dwarf models spanning the entire BDs mass regime. We have applied a time-dependent model of convection and performed pioneering calculations to establish the effect of such time-dependent process on the pulsation properties of the newly proposed class of young BDs pulsators, during the deuterium burning phase. No time-dependent theory of convection has been applied to date to study the proposed stellar pulsations. As a side lobe, we have presented a consistent derivation of the basic perturbation and pulsation equations and the relevant formulae for the pulsation work integrals.

Adopting the ‘frozen-in’ convection approximation assumed by PB05, we have comprehensively revisited the calculations presented in their seminal study by PB05, and determined the fundamental mode periods and the e-folding times for objects with masses in the range $0.02M_{\odot} - 0.08M_{\odot}$. Results from our calculations have been compared to the PB05 results, for the masses $0.02M_{\odot}$, $0.03M_{\odot}$, $0.04M_{\odot}$, $0.06M_{\odot}$ and $0.08M_{\odot}$. The comparison has been performed in two steps: first, the equilibrium structures of two objects with masses $0.04M_{\odot}$ and $0.08M_{\odot}$ from our study have been compared with similar objects from PB05, and, secondly the linear stability analysis results from the two studies have

been compared. For the former comparison, a very good agreement is established between the equilibrium structures of the two models to the PB05 models. The very slight differences in the temperature and density profiles for the $0.08M_{\odot}$ is understood to be due to differences in the outer boundary conditions. For the latter comparison, the fundamental mode periods, e-folding times and pulsation amplitude growth (or decay) rates from our calculations have been compared to those from PB05. The effective temperatures and the luminosities have also been compared. Only the fundamental mode was considered for comparison since the PB05 results are for the fundamental mode only. An agreement to within less than 0.1% and less than 8% is established in the fundamental periods and the e-folding times, for the higher mass objects. The effective temperatures are found to be in agreement to within 1% while the luminosities agree to within one decimal point in magnitude. The lowest mass objects: $0.02M_{\odot}$ and $0.03M_{\odot}$ show a fairly large disagreement in both the fundamental mode periods and e-folding times with the PB05 results. We attribute this to differences in the equilibrium structures of this particular models and ignore them in subsequent calculations.

In deviation from the PB05, we have determined fundamental mode pulsation constants Q , the fundamental mode to the first harmonic period ratios $\frac{P_0}{P_1}$, and the fundamental mode to the second harmonic period ratios $\frac{P_0}{P_2}$. Such calculations have not been reported by PB05 or any other study to date. We find values of pulsation constants that fall well within the range of the theoretical values calculated for variable stars. This is not a surprising result since the physical input underlying stellar pulsations should be fundamentally similar. The constant ‘ Q ’ is found to be ‘nearly a constant’ for the higher masses used in our study while the lowest masses show a varying value of ‘ Q ’. More analysis on the lowest mass models needs to be done in order to estimate the values of Q more accurately.

Using our time-dependent model of convection similar to that used in Olivier and Wood (2005) based on the models by Stellingwerf (1984) and Kuhfuß (1986), we have investigated the effects of the time-dependent model of convection (ignoring turbulent pressure, turbulent viscosity and turbulent diffusion), including turbulent pressure (α_{tp}), turbulent viscosity (α_{μ}) and turbulent diffusion (α_t) in the time-dependent treatment and also studied the effects of varying the turbulent viscosity and turbulent diffusion parameters, α_{μ} and α_t respectively. A time-dependent treatment of convection ignoring turbulent stresses is

found to make the objects stable against pulsations. In particular, it is the perturbation in the convective flux that causes the damping because the driving due to the epsilon mechanism becomes negligible with such a treatment. This is supported by plots of the analytic expression for the total work partial integral which shows exactly the same behavior as the actual work integrals. These results are in agreement with previous studies such as Xiong and Deng (2001, and references therein.) Perturbation in the specific volume is found to alter the behavior of the nuclear energy generation rate eigenfunction. The cause of this needs to be investigated.

Inclusion of turbulent viscosity in the time-dependent treatment is found to damp the modes while turbulent pressure causes driving of the pulsations. The latter result is displayed from the turbulent pressure work integrals throughout the structure of our objects which are found to be positive everywhere. Furthermore, the driving by turbulent pressure is found to yield growth rates that are many orders of magnitudes higher than the growth rates corresponding to driving due to the epsilon mechanism alone. This is an interesting result that requires further analysis. As a preliminary conclusion, we argue that inclusion of turbulent pressure may be important in future studies of the proposed pulsations in young BDs.

With regard to studying the effect of varying the major free parameters in the convective model, we find the following: the turbulent diffusion parameter α_t is found to have no effect on the pulsation periods, the growth rates and the e-folding times while the turbulent viscosity parameter α_μ has a very slight effect on pulsation periods. Turbulent viscosity being a purely dissipative term (as modeled in section 2.1), the turbulent viscosity parameter is found to damp the pulsation modes with the intensity of damping increasing with an increase in values of α_μ . For values of α_μ in the range: $0 < \alpha_\mu < 0.8$, the growth rate is positive but decreases with increasing values of α_μ . Driving is found to stop at $\alpha_\mu \sim 0.8$, beyond which the objects become stable against pulsations. The α_μ parameter therefore seems to define some ‘edge’ of the pulsation instability at $\alpha_\mu \sim 0.8$.

The major deliverables of this thesis work can therefore be summarized as follows:

- Using a different pulsation code and a different set of equilibrium models, we have independently verified the results by PB05 with their frozen-in convection approximation.

- Using a non-adiabatic linear stability analysis, we have performed preliminary calculations and determined theoretical pulsation constants Q and the period ratios $\frac{P_2}{P_0}$ and $\frac{P_1}{P_0}$ which can be used for comparison with future observations.
- We have carefully investigated the effects of:
 - (i) A time-dependent treatment of convection ignoring any turbulent stresses,
 - (ii) A time-dependent treatment including turbulent pressure and turbulent diffusion only and
 - (iii) A time-dependent treatment including turbulent pressure, turbulent diffusion and turbulent viscosity.
- We have studied the effects of varying the major free parameters; turbulent diffusion and turbulent viscosity on the stability properties of objects of different masses spanning the BD regime.

From these results, we call for further independent calculations to verify the driving due to turbulent pressure in young BDs. Also, more analysis is needed to study the effects of varying the mixing length parameter which was not done in our work, since variation in this parameter could alter the theoretical hydrostatic model structures.

Appendix A

Numerical modelling

This section describes the working of ‘StaRPuS’, the pulsation code used in this thesis. The equations and numerical techniques shown are based on Olivier & Wood (2005) and were kindly provided by Dr. E. Olivier.

A.1 The Difference Equations

Imagine one can divide the stellar envelope into N mass zones as depicted in Figure A.1. Zones are denoted by half-integer values and the interfaces between zones by whole integer values. In general a zone $j - \frac{1}{2}$ is bounded by the interfaces j and $j - 1$. The whole stellar envelope is bounded by the interfaces $j = N$ at the interior and $j = 0$ at the surface. It is convenient, for example, to define the variables ρ , T , ϖ in the zones and L_t , L , and r at the interfaces. Denote a variable in a zone or at an interface by a subscript such as in $T_{j-\frac{1}{2}}^n$ and r_j^n . The superscript n shall refer to the value of the variable at some time $t = t_n$. To calculate the value of some variables in a zone (or at an interface) which is not usually defined there, some average based on the values at (or in) the bounding interfaces (or zones) will be used. A geometric or arithmetic average is used, which ever seems the more appropriate. It is also necessary to define time-averages during the time-step $\Delta t_n = t_n - t_{n-1}$ denoted by $n - \frac{1}{2}$. These time-averages are usually calculated based on energy conservation considerations and numerical stability of the difference equations. As

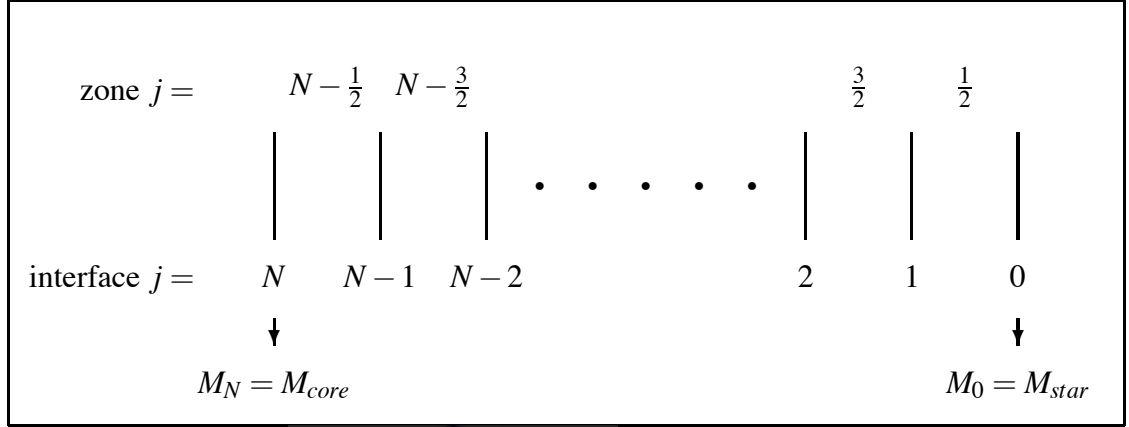


Figure A.1: Stellar envelope mesh.

an example, the time-average velocity is written as:

$$v_j^{n-\frac{1}{2}} = \theta_v v_j^n + (1 - \theta_v) v_j^{n-1} \quad (\text{A.1})$$

where $0 \leq \theta_v \leq 1$. Any other time-averages that appear in the difference equations are written in a similar form as the time-average velocity in equation A.1 with $\theta = \frac{1}{2}$ exactly. The time-averages for r^2 and its inverse however (see equation A.6) are chosen according to Fraley scheme (see Fraley 1968) to ensure conservation of total energy if $\theta_v = \frac{1}{2}$:

$$(r^2)_j^{n-\frac{1}{2}} = \frac{1}{3} (r_j^n r_j^n + r_j^n r_j^{n-1} + r_j^{n-1} r_j^{n-1}) \quad (\text{A.2})$$

$$\left(\frac{1}{r^2}\right)_j^{n-\frac{1}{2}} = \frac{1}{r_j^n r_j^{n-1}} \quad (\text{A.3})$$

The mass-steps across an interface $j - 1$ and zone $j - \frac{1}{2}$ are also defined by $\Delta M_{j-1} = \frac{1}{2}[M_j - M_{j-2}]$ and $\Delta M_{j-\frac{1}{2}} = [M_j - M_{j-1}]$ respectively. Note that in this notation ΔM_{j-1} and $\Delta M_{j-\frac{1}{2}}$ are negative. We then approximate the pulsation differential equations and the modified velocity-entropy correlation function, Π , on this mesh by the following system of

difference equations:

$$\frac{\left(r_j^n\right)^3 - \left(r_{j-1}^n\right)^3}{\Delta M_{j-\frac{1}{2}}} - \frac{3}{4\pi\rho_{j-\frac{1}{2}}^n} = 0 \quad (\text{A.4})$$

$$\frac{r_{j-1}^n - r_{j-1}^{n-1}}{\Delta t_n} - v_{j-1}^{n-\frac{1}{2}} = 0 \quad (\text{A.5})$$

$$\frac{v_{j-1}^n - v_{j-1}^{n-1}}{\Delta t_n} + 4\pi (r^2)_{j-1}^{n-\frac{1}{2}} \frac{(P_{tot})_{j-\frac{1}{2}}^{n-\frac{1}{2}} - (P_{tot})_{j-\frac{3}{2}}^{n-\frac{1}{2}}}{\Delta M_{j-1}} + GM_{j-1} \left(\frac{1}{r^2}\right)_{j-1}^{n-\frac{1}{2}} = 0 \quad (\text{A.6})$$

$$\frac{(e_{tot})_{j-\frac{1}{2}}^n - (e_{tot})_{j-\frac{1}{2}}^{n-1}}{\Delta t_n} + (P_{tot})_{j-\frac{1}{2}}^{n-\frac{1}{2}} \frac{1/\rho_{j-\frac{1}{2}}^n - 1/\rho_{j-\frac{1}{2}}^{n-1}}{\Delta t_n} + \frac{L_j^{n-\frac{1}{2}} - L_{j-1}^{n-\frac{1}{2}}}{\Delta M_{j-\frac{1}{2}}} - (\epsilon_{nuc})_{j-\frac{1}{2}}^{n-\frac{1}{2}} = 0 \quad (\text{A.7})$$

$$\frac{J_{j-\frac{1}{2}}^n/\rho_{j-\frac{1}{2}}^n - J_{j-\frac{1}{2}}^{n-1}/\rho_{j-\frac{1}{2}}^{n-1}}{\Delta t_n} + 4\pi (P_r)_{j-\frac{1}{2}}^n \frac{\left(r_j^n\right)^2 v_j^n - \left(r_{j-1}^n\right)^2 v_{j-1}^n}{\Delta M_{j-\frac{1}{2}}} + \frac{(L_r)_j^n - (L_r)_{j-1}^n}{\Delta M_{j-\frac{1}{2}}} - (C_r)_{j-\frac{1}{2}}^n = 0 \quad (\text{A.8})$$

$$\frac{\left(\varpi_{j-\frac{1}{2}}^n\right)^2 - \left(\varpi_{j-\frac{1}{2}}^{n-1}\right)^2}{\Delta t_n} + 4\pi (P_t + P_{tv})_{j-\frac{1}{2}}^n \frac{\left(r_j^n\right)^2 v_j^n + \left(r_{j-1}^n\right)^2 v_{j-1}^n}{\Delta M_{j-\frac{1}{2}}} + \frac{(L_t)_j^n - (L_t)_{j-1}^n}{\Delta M_{j-\frac{1}{2}}} - (C_\varpi)_{j-\frac{1}{2}}^n = 0 \quad (\text{A.9})$$

$$\Pi_{j-1}^n - \alpha_s \alpha_\Lambda \left[\frac{\varpi_{j-\frac{1}{2}}^n + \varpi_{j-\frac{3}{2}}^n}{2} \right] \left[(c_P)_{j-\frac{1}{2}}^n T_{j-\frac{1}{2}}^n (c_P)_{j-\frac{3}{2}}^n T_{j-\frac{3}{2}}^n \right]^{\frac{1}{2}} \left[\nabla_{j-1}^n - \left[(\nabla_{ad})_{j-\frac{1}{2}}^n (\nabla_{ad})_{j-\frac{3}{2}}^n \right]^{\frac{1}{2}} \right] = 0 \quad (\text{A.10})$$

The total internal energy is expressed as:

$$(e_{tot})_{j-\frac{1}{2}}^n = (e_g)_{j-\frac{1}{2}}^n + J_{j-\frac{1}{2}}^n/\rho_{j-\frac{1}{2}}^n + \left(\varpi_{j-\frac{1}{2}}^n\right)^2 \quad (\text{A.11})$$

while the total pressure is expressed as:

$$(P_{tot})_{j-\frac{1}{2}}^n = (P_g)_{j-\frac{1}{2}}^n + (P_r)_{j-\frac{1}{2}}^n + (P_t)_{j-\frac{1}{2}}^n + (P_{tv})_{j-\frac{1}{2}}^n + (P_{av})_{j-\frac{1}{2}}^n \quad (\text{A.12})$$

where:

$$(P_g)_{j-\frac{1}{2}}^n = P_g \left(\rho_{j-\frac{1}{2}}^n, T_{j-\frac{1}{2}}^n \right) \quad (\text{A.13})$$

$$(P_r)_{j-\frac{1}{2}}^n = \frac{1}{3} J_{j-\frac{1}{2}}^n \quad (\text{A.14})$$

$$(P_t)_{j-\frac{1}{2}}^n = \alpha_p \rho_{j-\frac{1}{2}}^n \left(\varpi_{j-\frac{1}{2}}^n \right)^2 \quad (\text{A.15})$$

$$(P_{tv})_{j-\frac{1}{2}}^n = -16\pi\alpha_\mu\alpha_\Lambda\rho_{j-\frac{1}{2}}^n (P_g)_{j-\frac{1}{2}}^n \frac{\left(r_j^n r_{j-1}^n\right)^{\frac{5}{2}} \left[\frac{v_j^n}{r_j^n} - \frac{v_{j-1}^n}{r_{j-1}^n}\right]}{G(M_j M_{j-1})^{\frac{1}{2}} \Delta M_{j-\frac{1}{2}}} \quad (\text{A.16})$$

$$(P_{av})_{j-\frac{1}{2}}^n = a_1^2 \rho_{j-\frac{1}{2}}^n \left[v_j^n - v_{j-1}^n - a_2 (c_s)_{j-\frac{1}{2}}^n \right]^2 \quad (\text{A.17})$$

for $v_j^n - v_{j-1}^n > a_2 (c_s)_{j-\frac{1}{2}}^n$, else zero if otherwise. Here c_s is the local adiabatic sound speed and a_1 and a_2 are free parameters (usually set to $a_1 = 4$ and $a_2 = 0.1$). See Stellingwerf (1975) for more details. The luminosity terms are expressed as:

$$(L_r)_{j-1}^n = -\frac{16}{3} \pi^2 c (r_{j-1}^n)^4 \left(\frac{J}{\kappa} \right)_{j-1}^n \frac{\ln J_{j-\frac{1}{2}}^n - \ln J_{j-\frac{3}{2}}^n}{\Delta M_{j-1}} \quad (\text{A.18})$$

(where

$$\left(\frac{J}{\kappa} \right)_{j-1}^n = \frac{J_{j-\frac{1}{2}}^n / \kappa_{j-\frac{1}{2}}^n - J_{j-\frac{3}{2}}^n / \kappa_{j-\frac{3}{2}}^n}{\ln \left(J_{j-\frac{1}{2}}^n / \kappa_{j-\frac{1}{2}}^n \right) - \ln \left(J_{j-\frac{3}{2}}^n / \kappa_{j-\frac{3}{2}}^n \right)} \quad (\text{A.19})$$

similarly to Stellingwerf 1975.)

$$(L_c)_{j-1}^n = 4\pi (r_{j-1}^n)^2 \left(\rho_{j-\frac{1}{2}}^n \rho_{j-\frac{3}{2}}^n \right)^{\frac{1}{2}} \Pi_{j-1}^n \quad (\text{A.20})$$

$$(L_t)_{j-1}^n = -\frac{32}{3} \pi^2 \frac{\alpha_t \alpha_\Lambda (r_{j-1}^n)^6 \left(\rho_{j-\frac{1}{2}}^n P_{j-\frac{1}{2}}^n \rho_{j-\frac{3}{2}}^n P_{j-\frac{3}{2}}^n \right)^{\frac{1}{2}} \left(\varpi_{j-\frac{1}{2}}^n \right)^3 - \left(\varpi_{j-\frac{3}{2}}^n \right)^3}{GM_{j-1} \Delta M_{j-1}} \quad (\text{A.21})$$

The temperature gradient is expressed as:

$$\nabla_{j-1}^n = -\frac{4\pi (r_{j-1}^n)^4 \left(P_{j-\frac{1}{2}}^n P_{j-\frac{3}{2}}^n \right)^{\frac{1}{2}} \ln T_{j-\frac{1}{2}}^n - \ln T_{j-\frac{3}{2}}^n}{GM_{j-1} \Delta M_{j-1}} \quad (\text{A.22})$$

The remaining terms in the equations A.9 and A.8 are expressed as:

$$(C_r)^n_{j-\frac{1}{2}} = c\kappa^n_{j-\frac{1}{2}} \left(a \left(T^n_{j-\frac{1}{2}} \right)^4 - J^n_{j-\frac{1}{2}} \right) \quad (\text{A.23})$$

$$(C_{\varpi})^n_{j-\frac{1}{2}} = \alpha_\Lambda \frac{GM_{j-1}\rho^n_{j-\frac{1}{2}}}{\left(r^n_{j-1} \right)^2 \left(P_g \right)^n_{j-\frac{1}{2}}} \left[\alpha_\Lambda \left(\nabla_{ad} \right)^n_{j-\frac{1}{2}} \left(\frac{\Pi_j^n + \Pi_{j-1}^n}{2} \right) - \alpha_d \left(\left(\varpi^n_{j-\frac{1}{2}} \right)^3 - \varpi_F^3 \right) \right] \quad (\text{A.24})$$

where ϖ_F is a small positive velocity (see Olivier & Wood 2005 for details). Finally it is assumed all the remaining thermodynamic variables, the nuclear energy generation rate and the opacity are functions of the density and temperature, and is thus expressed as

$$(e_g)^n_{j-\frac{1}{2}} = e_g \left(\rho^n_{j-\frac{1}{2}}, T^n_{j-\frac{1}{2}} \right) \quad (\text{A.25})$$

$$\left(\nabla_{ad} \right)^n_{j-\frac{1}{2}} = \nabla_{ad} \left(\rho^n_{j-\frac{1}{2}}, T^n_{j-\frac{1}{2}} \right) \quad (\text{A.26})$$

$$(c_s)^n_{j-\frac{1}{2}} = c_s \left(\rho^n_{j-\frac{1}{2}}, T^n_{j-\frac{1}{2}} \right) \quad (\text{A.27})$$

$$\left(\varepsilon_{nuc} \right)^n_{j-\frac{1}{2}} = \varepsilon_{nuc} \left(\rho^n_{j-\frac{1}{2}}, T^n_{j-\frac{1}{2}} \right) \quad (\text{A.28})$$

$$\left(\kappa \right)^n_{j-\frac{1}{2}} = \kappa \left(\rho^n_{j-\frac{1}{2}}, T^n_{j-\frac{1}{2}} \right) \quad (\text{A.29})$$

We have a total of $7N$ unknowns (r_j^n , v_j^n , $\rho^n_{j-\frac{1}{2}}$, $T^n_{j-\frac{1}{2}}$, $\varpi^n_{j-\frac{1}{2}}$, $J^n_{j-\frac{1}{2}}$ and Π_j^n). The equations A.4 to A.10, each couple some or all the variables associated across different mass zones. In total there are $7(N-1)$ equations of this form. An additional 7 equations are obtained from the imposed boundary conditions.

A.2 The boundary conditions

We assume a rigid core at the interior ($j = N$, $M_N = M_{core}$):

$$r_N^n - r_{core} = 0 \quad (\text{A.30})$$

$$v_N^n = 0 \quad (\text{A.31})$$

and

$$\Pi_{N-1}^n - \Pi_N^n = 0 \quad (\text{A.32})$$

At the interior we also set $(L_t)_N^n = 0$ and $L_N^n = L_{core}$. At the outer point ($j = 0, M_0 = M_{star}$) we have:

$$\frac{v_0^n - v_0^{n-1}}{\Delta t_n} + 4\pi (R_s^2)^{n-\frac{1}{2}} \frac{(P_{tot})_{\frac{1}{2}}^{n-\frac{1}{2}} - P_0^{n-\frac{1}{2}}}{\frac{1}{2}\Delta M_{\frac{1}{2}}} + GM_{star} \left(\frac{1}{R_s^2}\right)^{n-\frac{1}{2}} = 0 \quad (\text{A.33})$$

$$\frac{(e_{tot})_{\frac{1}{2}}^n - (e_{tot})_{\frac{1}{2}}^{n-1}}{\Delta t_n} + (P_{tot})_{\frac{1}{2}}^{n-\frac{1}{2}} \frac{1/\rho_{\frac{1}{2}}^n - 1/\rho_{\frac{1}{2}}^{n-1}}{\Delta t_n} + \frac{L_1^{n-\frac{1}{2}} - L_s^{n-\frac{1}{2}}}{\Delta M_{j-\frac{1}{2}}} - (\epsilon_{nuc})_{\frac{1}{2}}^{n-\frac{1}{2}} = 0 \quad (\text{A.34})$$

$$\frac{J_{\frac{1}{2}}^n/\rho_{\frac{1}{2}}^n - J_{\frac{1}{2}}^{n-1}/\rho_{\frac{1}{2}}^{n-1}}{\Delta t_n} + 4\pi (P_r)_{\frac{1}{2}}^n \frac{(r_1^n)^2 v_1^n - (R_s^n)^2 v_0^n}{\Delta M_{\frac{1}{2}}} + \frac{(L_r)_1^n - (L_r)_0^n}{\Delta M_{\frac{1}{2}}} - (C_r)_{\frac{1}{2}}^n = 0 \quad (\text{A.35})$$

$$\varpi_{\frac{1}{2}}^n = 0 \quad (\text{A.36})$$

with the following definitions:

$$(R_s^n)^3 = (r_1^n)^3 - \frac{3}{4\pi\rho_{\frac{1}{2}}^n\Delta M_{\frac{1}{2}}} \quad (\text{A.37})$$

$$(L_r)_0^n = 2\pi c (R_s^n)^2 J_{\frac{1}{2}}^n \quad (\text{A.38})$$

$$P_0^n = P_{ext} + \frac{1}{3}J_{\frac{1}{2}}^n \quad (\text{A.39})$$

$$v_0^n = \frac{1}{\theta_v} \left[\frac{R_s^n - R_s^{n-1}}{\Delta t_n} - (1 - \theta_v) v_0^{n-1} \right] \quad (\text{A.40})$$

At the surface it is also assumed that $(L_t)_0^n = 0$ and $(L_c)_0^n = 0$, so that $L_s^n = (L_r)_0^n$. With the above 7 boundary conditions (equations A.30 to A.35) we now have a closed system of $7N$ difference equations and $7N$ unknowns

A.3 Solution of the difference equations

The time-dependent equations

In principle the set of $M = 7N$ difference equations and $M = 7N$ unknowns can be solved at time t_n given a model at time t_{n-1} and a time-step Δt_n . The pulsation is thus treated as an initial value problem. The set of nonlinear difference equations are solved with the well-known Henyey method which uses a generalized Newton-Raphson iteration procedure. This iteration procedure can be understood as follows. Given a set of M nonlinear equations ($f_j = 0 \ j = 1, M$), and an approximate solution (x_1, \dots, x_M) , one would like to find a set of M corrections, $(\delta x_1, \dots, \delta x_M)$ such that:

$$f_j(x_1 + \delta x_1, \dots, x_M + \delta x_M) = 0 \quad j = 1, \dots, M \quad (\text{A.41})$$

Linearization (i.e truncating the Taylor series expansion at first order) of the left-hand sides of the above set of equations one have:

$$f_j(x_1, \dots, x_M) + \sum_{i=1}^M \frac{\partial f_j}{\partial x_i} \delta x_i = 0 \quad j = 1, \dots, M \quad (\text{A.42})$$

or

$$\mathbf{J} \delta \tilde{\mathbf{x}} = -\tilde{\mathbf{f}} \quad (\text{A.43})$$

where \mathbf{J} is the Jacobian matrix (size $M \times M$) with components $\left(J_{ij} = \frac{\partial f_j}{\partial x_i}, i, j = 1, M \right)$, $\delta \tilde{\mathbf{x}}$ is the one dimensional vector of corrections with components $(\delta x_i, i = 1, M)$ and $\tilde{\mathbf{f}}$ is the one dimensional vector of function values with components $(f_j(x_1, \dots, x_M), j = 1, M)$. In general the set of corrections obtained by solving this linear system will not take us exactly to the true solution from an initial approximate solution, since we have ignored higher order terms in the linearization process. This is particularly true if the approximate solution is far from the true solution. So in general the process has to be repeated, updating the Jacobian matrix \mathbf{J} and the vectors $\delta \tilde{\mathbf{x}}$ and $\tilde{\mathbf{f}}$ each time. In summary, given an approximate solution $\tilde{\mathbf{x}}^{k-1}$ with components $(x_1^{k-1}, \dots, x_M^{k-1})$, calculate the Jacobian matrix \mathbf{J}^{k-1} and the vector

$\tilde{\mathbf{x}}^{k-1}$, solve for the corrections $\delta\tilde{\mathbf{x}}^k$ and calculate a new approximation to the solution:

$$\tilde{\mathbf{x}}^k = \tilde{\mathbf{x}}^{k-1} + \beta \delta\tilde{\mathbf{x}}^k \quad (\text{A.44})$$

where $\beta = 1$ normally. Repeat the process several times until the solution has been reached to desired precision, e.g. when $|\delta x_i^k/x_i^k|_{\max} < \varepsilon_1$ where ε_1 is some small tolerance value. Here $|\delta x_i^k/x_i^k|_{\max}$ denotes the maximum fractional correction of all the variables. During the initial iteration steps, when still far from true solution, the full corrections $\tilde{\delta\mathbf{x}}^k$ are not used but are rather scaled by a factor $\beta = \varepsilon_2/|\delta x_i^k/x_i^k|_{\max}$ first. Here ε_2 is some user estimated tolerance. Once the corrections become sufficiently small, i.e. when close enough to the true solution (taken when $|\delta x_i^k/x_i^k|_{\max} < \varepsilon_2$), during the iteration process, the full corrections ($\beta = 1$) are applied. In the current implementation of the code the solution at the current time ($t = t_n$) is found by such a Newton-Raphson iteration scheme using the solution at the previous time-step ($t = t_{n-1}$) (or an extrapolation in time from two previous time steps, $t = t_{n-1}$ and $t = t_{n-2}$) as a starting point. In general the matrix \mathbf{J} is a sparse matrix, since the individual difference equations depend only on variables defined in a small number of neighbouring zones, as opposed to the full set of $M = 7N$ variables. Careful inspection current system here will show only a maximum of 4 zones are coupled by any given difference equation. Proper ordering (as opposed random ordering) of the variables and equations will lead to a so-called block diagonal form of the matrix \mathbf{J} . In the current implementation of the code, the following ordering of the $7N$ variables and $7N$ equations is implemented:

$$\tilde{\mathbf{x}} = \left(\ln \varpi_{\frac{1}{2}}^n, \ln V_{\frac{1}{2}}^n, \ln T_{\frac{1}{2}}^n, \ln J_{\frac{1}{2}}^n, \ln r_1^n, v_1^n, \Pi_1^n, \dots, \ln \varpi_{N-\frac{1}{2}}^n, \ln V_{N-\frac{1}{2}}^n, \ln T_{N-\frac{1}{2}}^n, \ln J_{N-\frac{1}{2}}^n, \ln r_N^n, v_N^n, \Pi_N^n \right)$$

$$\vec{f} = (f_1^\varpi, f_1^V, f_1^T, f_1^J, f_1^r, f_1^v, f_1^\Pi, \dots, f_N^\varpi, f_N^V, f_N^T, f_N^J, f_N^r, f_N^v, f_N^\Pi)$$

The set of functions, f_j^x , are given by the left hand sides of the following difference equations (denoted F^K where K is the relevant equation number) As mentioned above, at most 4 zones are coupled by any given difference equation, this means that any given row in the Jacobian matrix \mathbf{J} will have at most $4 \times 7 = 28$ non-zero entries. Taking as an example a

stellar model divided up into 6 zones, inspection of the relevant equations, given the ordering above, will show that \mathbf{J} will have the structure shown in figure A.2. For a given number of zones N the ratio of possible non-zero matrix elements ($4 \times 7^2 N$) to total number of entries ($7N \times 7N$) is $\frac{4}{N}$. For large $N = 400$, as an example, this ratio is just 1%. The matrix can be efficiently stored (by storing only the x's in figure A.2) and solution of this system can also be very efficiently done, using standard gaussian elimination techniques only on the stored non-zero matrix elements. Since an implicit hydrodynamical scheme is used (i.e. variables at $t = t_n$ depend on variables at $t = t_{n-1}$ AND $t = t_n$), there is no restriction on the time-step size based on stability considerations such as the Courant-Friedrichs-Lewy condition. However, one usually restricts the time step by not letting some of the variables at any given mesh point (usually the pressure, temperature and specific turbulent energy) change by more than a specified upper limit. Also the time-step is not allowed to increase by more than a given fraction of the previous time-step (usually ~ 35 percent) and is forced to remain smaller than a specified upper limit, usually a tenth or less of the pulsation period. To start the pulsation of the stellar model, a static model ($\frac{1}{\Delta t} = 0$ and $\theta = 1$) is constructed by the same Newton-Raphson procedure from an initial approximate static solution, and then given a small velocity perturbation. This perturbed model is then used as the model at time t_0 . Construction of the needed approximate static solution is discussed below.

Construction of approximate static model

An initial approximate static ($\frac{1}{\Delta t} = 0$ and $\theta = 1$) solution is obtained by ignoring L_t , P_t and P_r . We also ignore equation A.8, and assume that the radiation energy density is given by $J = aT^4$. With these approximations following system of difference equations results:

$$\frac{r_j^3 - r_{j-1}^3}{\Delta M_{j-\frac{1}{2}}} - \frac{3}{4\pi} V_{j-\frac{1}{2}} = 0 \quad (\text{A.45})$$

$$\frac{P_{j-\frac{1}{2}} - P_{j-\frac{3}{2}}}{\Delta M_{j-1}} + \frac{GM_{j-1}}{4\pi r_{j-1}^4} = 0 \quad (\text{A.46})$$

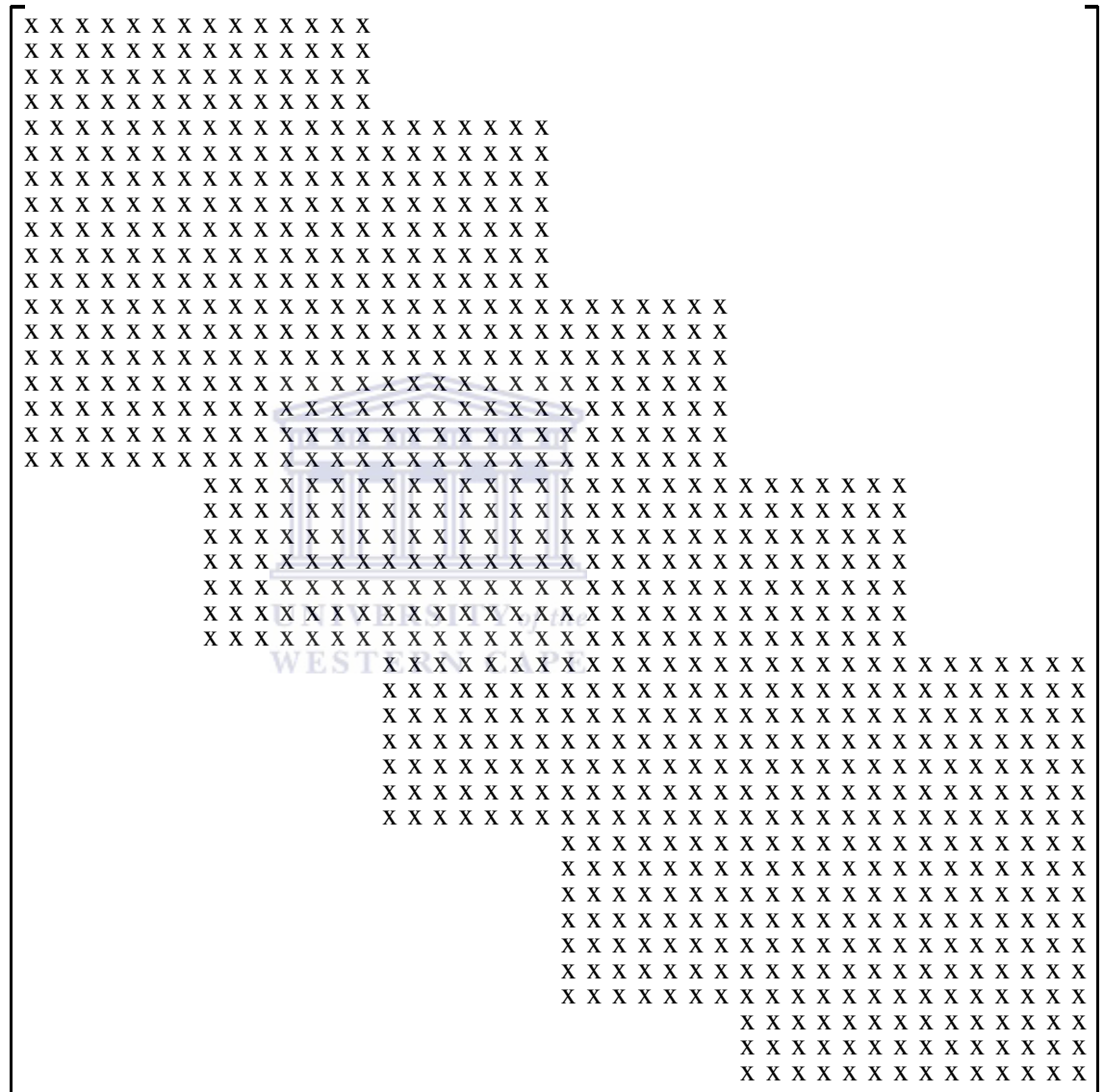


Figure A.2: Structure of the Jacobian matrix J for a 6 zone stellar model. Here x denotes a possible non-zero matrix element and a blank entry denotes a zero value matrix element.

$$\frac{\ln T_{j-\frac{1}{2}} - \ln T_{j-\frac{3}{2}}}{\Delta M_{j-1}} + \frac{GM_{j-1} \nabla_{j-1}^n}{4\pi (r_{j-1})^4 \left(P_{j-\frac{1}{2}} P_{j-\frac{3}{2}}\right)^{\frac{1}{2}}} = 0 \quad (\text{A.47})$$

$$\frac{L_j - L_{j-1}}{\Delta M_{j-\frac{1}{2}}} - (\varepsilon_{nuc})_{j-\frac{1}{2}} = 0 \quad (\text{A.48})$$

with

$$P_{j-\frac{1}{2}} = (P_g)_{j-\frac{1}{2}} = P_g \left(V_{j-\frac{1}{2}}, T_{j-\frac{1}{2}}\right) \quad (\text{A.49})$$

$$(\varepsilon_{nuc})_{j-\frac{1}{2}} = \varepsilon_{nuc} \left(V_{j-\frac{1}{2}}, T_{j-\frac{1}{2}}\right) \quad (\text{A.50})$$

$$L_{j-1} = (L_r)_{j-1} + (L_c)_{j-1} \quad (\text{A.51})$$

The luminosity terms are:

$$(L_r)_{j-1} = \frac{16}{3} \pi a c \frac{GM_{j-1}}{\left(P_{j-\frac{1}{2}} P_{j-\frac{3}{2}}\right)^{\frac{1}{2}}} \left(\frac{T^4}{\kappa}\right)_{j-1} \nabla_{j-1} \quad (\text{A.52})$$

$$(L_c)_{j-1} = 4\pi (r_{j-1})^2 \left(V_{j-\frac{1}{2}} V_{j-\frac{3}{2}}\right)^{-\frac{1}{2}} \Pi_{j-1} \quad (\text{A.53})$$

where

$$\left(\frac{T^4}{\kappa}\right)_{j-1} = \frac{T_{j-\frac{1}{2}}^4 / \kappa_{j-\frac{1}{2}} - T_{j-\frac{3}{2}}^4 / \kappa_{j-\frac{3}{2}}}{\ln \left(T_{j-\frac{1}{2}}^4 / \kappa_{j-\frac{1}{2}}\right) - \ln \left(T_{j-\frac{3}{2}}^4 / \kappa_{j-\frac{3}{2}}\right)} \quad (\text{A.54})$$

$$\Pi_{j-1} = \alpha_s \alpha_\Lambda \varpi_{j-1} \left[(cP)_{j-\frac{1}{2}} T_{j-\frac{1}{2}} (cP)_{j-\frac{3}{2}} T_{j-\frac{3}{2}}\right]^{\frac{1}{2}} \left[\nabla_{j-1} - \left[(\nabla_{ad})_{j-\frac{1}{2}} (\nabla_{ad})_{j-\frac{3}{2}}\right]^{\frac{1}{2}}\right] \quad (\text{A.55})$$

$$\kappa_{j-\frac{1}{2}} = \kappa \left(V_{j-\frac{1}{2}}, T_{j-\frac{1}{2}}\right) \quad (\text{A.56})$$

$$(\nabla_{ad})_{j-\frac{1}{2}} = \nabla_{ad} \left(V_{j-\frac{1}{2}}, T_{j-\frac{1}{2}}\right) \quad (\text{A.57})$$

Using equation A.51, A.52, A.53 and treating ϖ as an interface quantity one can rewrite equation A.55 as:

$$A_{j-1} \left[(\nabla_{rad})_{j-1} - \nabla_{j-1} \right] - \alpha_s \alpha_\Lambda \varpi_{j-1} \left[(cP)_{j-\frac{1}{2}} T_{j-\frac{1}{2}} (cP)_{j-\frac{3}{2}} T_{j-\frac{3}{2}} \right]^{\frac{1}{2}} \left[\nabla_{j-1} - \left[(\nabla_{ad})_{j-\frac{1}{2}} (\nabla_{ad})_{j-\frac{3}{2}} \right]^{\frac{1}{2}} \right] = 0 \quad (\text{A.58})$$

where

$$(\nabla_{rad})_{j-1} = \frac{3}{16} \frac{\left(P_{j-\frac{1}{2}} P_{j-\frac{3}{2}} \right)^{\frac{1}{2}}}{\pi a c G M_{j-1}} \left(\frac{T^4}{\kappa} \right)_{j-1}^{-1} L_{j-1} \quad (\text{A.59})$$

$$A_{j-1} = \frac{4 a c G M_{j-1}}{3 (r_{j-1})^2} \left(\frac{V_{j-\frac{1}{2}} V_{j-\frac{3}{2}}}{P_{j-\frac{1}{2}} P_{j-\frac{3}{2}}} \right)^{\frac{1}{2}} \left(\frac{T^4}{\kappa} \right)_{j-1} \quad (\text{A.60})$$

Setting $(C_\varpi)_{j-1} = 0$, fully consistent with the above approximations, and ignoring ϖ_F leads to the following equation for ϖ_{j-1} :

$$\alpha_\Lambda \left[(\nabla_{ad})_{j-\frac{1}{2}} (\nabla_{ad})_{j-\frac{3}{2}} \right]^{\frac{1}{2}} A_{j-1} \left[(\nabla_{rad})_{j-1} - \nabla_{j-1} \right] - \alpha_d (\varpi_{j-1})^3 = 0 \quad (\text{A.61})$$

Given the values, $V_{j-\frac{3}{2}}, T_{j-\frac{3}{2}}, r_{j-1}, L_{j-1}$ as well as $V_{j-\frac{1}{2}}, T_{j-\frac{1}{2}}$ and ΔM_{j-1} one can simultaneously solve for ∇_{j-1} and ϖ_{j-1} using equations A.58 and A.61. If $(\nabla_{rad})_{j-1} < \left[(\nabla_{ad})_{j-\frac{1}{2}} (\nabla_{ad})_{j-\frac{3}{2}} \right]^{\frac{1}{2}}$ we set $\nabla_{j-1} = (\nabla_{rad})_{j-1}$ and $\varpi_{j-1} = 0$. This leads to the following numerical algorithm to calculate the dependent variables related to current zone $(V_{j-\frac{1}{2}}, T_{j-\frac{1}{2}}, r_j, L_j)$ from those in the previous zone $(V_{j-\frac{3}{2}}, T_{j-\frac{3}{2}}, r_{j-1}, L_{j-1})$ given the mass steps $\Delta M_{j-\frac{3}{2}}$ and $\Delta M_{j-\frac{1}{2}}$:

- Obtain $\Delta M_{j-\frac{1}{2}}, \Delta M_{j-\frac{3}{2}}, V_{j-\frac{3}{2}}, T_{j-\frac{3}{2}}, r_{j-1}$ and L_{j-1} as input, (as well as $P_{j-\frac{3}{2}}, (\nabla_{ad})_{j-\frac{3}{2}}, (cP)_{j-\frac{3}{2}}$ and $\kappa_{j-\frac{3}{2}}$)
- Calculate $\Delta M_{j-1} = \frac{1}{2} \left(\Delta M_{j-\frac{1}{2}} + \Delta M_{j-\frac{3}{2}} \right)$
- Calculate $P_{j-\frac{1}{2}}$ from equation A.46
- Find $V_{j-\frac{1}{2}}$ and $T_{j-\frac{1}{2}}$ by simultaneously solving equations A.49 and A.47.
- Save calculated values for $P_{j-\frac{1}{2}}, (\nabla_{ad})_{j-\frac{1}{2}}, (cP)_{j-\frac{1}{2}}$ and $\kappa_{j-\frac{1}{2}}$

- Calculate r_j from equation A.45
- Calculate L_j from equation A.48
- Save $\Delta M_{j-\frac{1}{2}}, V_{j-\frac{1}{2}}, T_{j-\frac{1}{2}}, r_j$ and L_j

Using the procedure above one can integrate the stellar structure equations inwards towards the stellar centre, given the conditions in the surface of the star. During such an integration the mass-step is usually not allowed to change by more than about 25 to 30 percent from the previous step. Also, the change in temperature and pressure from one zone to the next is forced to remain below a certain upper limit. Given a surface radius R_s , a surface luminosity L_s and $\Delta M_{\frac{1}{2}}$ the conditions in the surface zone is determined by solving the following set of equations:

$$\frac{r_1^3 - R_s^3}{\Delta M_{\frac{1}{2}}} - \frac{3}{4\pi} V_{\frac{1}{2}} = 0 \quad (\text{A.62})$$

$$\frac{P_{\frac{1}{2}} - P_0}{\frac{1}{2}\Delta M_{\frac{1}{2}}} + \frac{GM_{j-1}}{4\pi R_s^4} = 0 \quad (\text{A.63})$$

$$L_s = 2\pi a c R_s^2 T_{\frac{1}{2}}^4 \quad (\text{A.64})$$

$$L_1 - L_s = 0 \quad (\text{A.65})$$

where

$$P_0 = P_{ext} \quad (\text{A.66})$$

$\Delta M_{\frac{1}{2}}$ is usually chosen such that the optical depth across the zone is less than a small upper limit, typically 0.01 or less. Once the values in the surface zone has been determined, one can integrate inwards and until either the radius, mass coordinate or luminosity reach their desired interior values (whichever happens to occur first during the integration process). One can then define the following two functions:

$$f_N^r = \frac{4\pi}{3} (r_{N-1}^3 - r_{core}^3) / V_{N-\frac{1}{2}} - (M_{N-1} - M_{core}) \quad (\text{A.67})$$

$$f_N^L = (L_{N-1} - L_{core}) - (\varepsilon_{nuc})_{N-\frac{1}{2}} (M_{N-1} - M_{core}) \quad (\text{A.68})$$

where N denotes the zone number of the inner most zone. If $f_N^r = 0$ and $f_N^L = 0$ then all three interior boundary conditions will be satisfied. For arbitrary values of R_s and L_s this will usually not be the case. An iteration scheme is used to find the correct values of R_s and L_s that yields $f_N^r = 0$ and $f_N^L = 0$ simultaneously.

A.4 Linear stability Analysis

Consider the difference equations A.4 to A.10 and the associated boundary conditions A.30 to A.36. Letting $\Delta t_n \rightarrow 0$ analytically, one will have $x^n \rightarrow x^{n-1}$ and the equations will become (dropping the time index n):

$$\frac{r_j^3 - r_{j-1}^3}{\Delta M_{j-\frac{1}{2}}} - \frac{3}{4\pi} V_{j-\frac{1}{2}} = 0 \quad (\text{A.69})$$

$$\frac{d}{dt} r_{j-1} - v_{j-1} = 0 \quad (\text{A.70})$$

$$\frac{d}{dt} v_{j-1} + 4\pi r_{j-1}^2 \frac{(P_{tot})_{j-\frac{1}{2}} - (P_{tot})_{j-\frac{3}{2}}}{\Delta M_{j-1}} + \frac{GM_{j-1}}{r_{j-1}^2} = 0 \quad (\text{A.71})$$

$$\frac{d}{dt} (e_{tot})_{j-\frac{1}{2}} + (P_{tot})_{j-\frac{1}{2}} \frac{d}{dt} V_{j-\frac{1}{2}} + \frac{L_j - L_{j-1}}{\Delta M_{j-\frac{1}{2}}} - (\epsilon_{nuc})_{j-\frac{1}{2}} = 0 \quad (\text{A.72})$$

$$\frac{d}{dt} (V_{j-\frac{1}{2}} J_{j-\frac{1}{2}}) + (P_r)_{j-\frac{1}{2}} \frac{d}{dt} V_{j-\frac{1}{2}} + \frac{(L_r)_j - (L_r)_{j-1}}{\Delta M_{j-\frac{1}{2}}} - (C_r)_{j-\frac{1}{2}} = 0 \quad (\text{A.73})$$

$$\frac{d}{dt} \varpi_{j-\frac{1}{2}}^2 + (P_t + P_{tv})_{j-\frac{1}{2}} \frac{d}{dt} V_{j-\frac{1}{2}} + \frac{(L_t)_j - (L_t)_{j-1}}{\Delta M_{j-\frac{1}{2}}} - (C_\varpi)_{j-\frac{1}{2}} = 0 \quad (\text{A.74})$$

$$\Pi_{j-1} - \alpha_s \alpha_\Lambda \varpi_{j-1} (c_P)_{j-1} T_{j-1} \left[\nabla_{j-1} - (\nabla_{ad})_{j-1} \right] = 0 \quad (\text{A.75})$$

with the following boundary conditions

$$r_N - r_{core} = 0 \quad (\text{A.76})$$

$$v_N = 0 \quad (\text{A.77})$$

$$\Pi_{N-1} - \Pi_N = 0 \quad (\text{A.78})$$

$$\frac{d}{dt}v_0 + 4\pi R_s^2 \frac{(P_{tot})_{\frac{1}{2}} - P_0}{\frac{1}{2}\Delta M_{\frac{1}{2}}} + \frac{GM_{star}}{R_s^2} = 0 \quad (\text{A.79})$$

$$\frac{d}{dt}(e_{tot})_{\frac{1}{2}} + (P_{tot})_{\frac{1}{2}} \frac{d}{dt}V_{\frac{1}{2}} + \frac{L_1 - L_s}{\Delta M_{j-\frac{1}{2}}} - (\epsilon_{nuc})_{\frac{1}{2}} = 0 \quad (\text{A.80})$$

$$\frac{d}{dt}(V_{\frac{1}{2}}J_{\frac{1}{2}}) + (P_r)_{\frac{1}{2}} \frac{d}{dt}V_{\frac{1}{2}} + \frac{(L_r)_1 - (L_r)_0}{\Delta M_{\frac{1}{2}}} - (C_r)_{\frac{1}{2}} = 0 \quad (\text{A.81})$$

$$\varpi_{\frac{1}{2}} = 0 \quad (\text{A.82})$$

where:

$$R_s^3 = r_1^3 - \frac{3}{4\pi}V_{\frac{1}{2}}\Delta M_{\frac{1}{2}} \quad (\text{A.83})$$

$$L_s = (L_r)_0 = 2\pi c (R_s)^2 J_{\frac{1}{2}} \quad (\text{A.84})$$

$$P_0 = P_{ext} \quad (\text{A.85})$$

$$v_0 = \frac{dR_s}{dt} \quad (\text{A.86})$$

The equations above represent a discretization in space only of the original partial differential equations. It is on this set of equations that a linear stability analysis is performed. First we write each time-dependent variable the time-dependent solution to the above set of equations as $x(t) = x_0 + \delta x(t)$, where x_0 is value of the variable in the hydrostatic solution. We then assume that $\frac{\delta x}{x} \ll 1$ and truncate the Taylor expansions of the above set $7N$ of nonlinear time-dependent difference equations around the static solution to first order. This results in the following set of linearized difference equations

$$\frac{r_j^2 \delta r_j - r_{j-1}^2 \delta r_{j-1}}{\Delta M_{j-\frac{1}{2}}} - \frac{1}{4\pi} \delta V_{j-\frac{1}{2}} = 0 \quad (\text{A.87})$$

$$\frac{d}{dt} \delta r_{j-1} - \delta v_{j-1} = 0 \quad (\text{A.88})$$

$$\frac{d}{dt} \delta v_{j-1} + 4\pi r_{j-1}^2 \frac{(\delta P_{tot})_{j-\frac{1}{2}} - (\delta P_{tot})_{j-\frac{3}{2}}}{\Delta M_{j-1}} - 4 \frac{GM_{j-1}}{r_{j-1}^3} \delta r_{j-1} = 0 \quad (\text{A.89})$$

$$\frac{d}{dt}(\delta e_{tot})_{j-\frac{1}{2}} + (P_{tot})_{j-\frac{1}{2}} \frac{d}{dt} \delta V_{j-\frac{1}{2}} + \frac{\delta L_j - \delta L_{j-1}}{\Delta M_{j-\frac{1}{2}}} - (\delta \varepsilon_{nuc})_{j-\frac{1}{2}} = 0 \quad (\text{A.90})$$

$$\frac{d}{dt}(\delta J_{j-\frac{1}{2}}) + 4(P_r)_{j-\frac{1}{2}} \frac{d}{dt} \delta V_{j-\frac{1}{2}} + \frac{(\delta L_r)_j - (\delta L_r)_{j-1}}{\Delta M_{j-\frac{1}{2}}} - (\delta C_r)_{j-\frac{1}{2}} = 0 \quad (\text{A.91})$$

$$2\varpi \frac{d}{dt} \delta \varpi_{j-\frac{1}{2}} + (P_t)_{j-\frac{1}{2}} \frac{d}{dt} \delta V_{j-\frac{1}{2}} + \frac{(\delta L_t)_j - (\delta L_t)_{j-1}}{\Delta M_{j-\frac{1}{2}}} - (\delta C_\varpi)_{j-\frac{1}{2}} = 0 \quad (\text{A.92})$$

$$\delta \Pi_{j-1} - \left(\frac{\delta \varpi_{j-1}}{\varpi_{j-1}} + \frac{(\delta c_P)_{j-1}}{(c_P)_{j-1}} + \frac{\delta T_{j-1}}{T_{j-1}} + \frac{\delta \nabla_{j-1} - (\delta \nabla_{ad})_{j-1}}{\nabla_{j-1} - (\nabla_{ad})_{j-1}} \right) \Pi_{j-1} = 0 \quad (\text{A.93})$$

with the following linearized boundary conditions

$$\delta r_N = 0 \quad (\text{A.94})$$

$$\delta v_N = 0 \quad (\text{A.95})$$

$$\delta \Pi_{N-1} - \delta \Pi_N = 0 \quad (\text{A.96})$$

$$\frac{d}{dt} \delta v_0 + 4\pi R_s^2 \frac{(\delta P_{tot})_{\frac{1}{2}} - \delta P_0}{\frac{1}{2} \Delta M_{\frac{1}{2}}} - 4 \frac{GM_{star}}{R_s^3} \delta R_s = 0 \quad (\text{A.97})$$

$$\frac{d}{dt}(\delta e_{tot})_{\frac{1}{2}} + (P_{tot})_{\frac{1}{2}} \frac{d}{dt} \delta V_{\frac{1}{2}} + \frac{\delta L_1 - \delta L_0}{\Delta M_{j-\frac{1}{2}}} - (\delta \varepsilon_{nuc})_{\frac{1}{2}} = 0 \quad (\text{A.98})$$

$$\frac{d}{dt}(\delta J_{\frac{1}{2}}) + 4(P_r)_{\frac{1}{2}} \frac{d}{dt} \delta V_{\frac{1}{2}} + \frac{(\delta L_r)_1 - (\delta L_r)_0}{\Delta M_{\frac{1}{2}}} - (\delta C_r)_{\frac{1}{2}} = 0 \quad (\text{A.99})$$

$$\delta \varpi_{\frac{1}{2}} = 0 \quad (\text{A.100})$$

where:

$$R_s^2 \delta R_s = r_1^2 \delta r_1 - \frac{1}{4\pi} \delta V_{\frac{1}{2}} \Delta M_{\frac{1}{2}} \quad (\text{A.101})$$

$$\delta L_0 = (\delta L_r)_0 = \left(2 \frac{\delta R_s}{R_s} + \frac{\delta J_{\frac{1}{2}}}{J_{\frac{1}{2}}} \right) (L_r)_0 \quad (\text{A.102})$$

$$\delta P_0 = 0 \quad (\text{A.103})$$

$$\delta v_0 = \frac{d \delta R_s}{dt} \quad (\text{A.104})$$

Linearizing the perturbations of the nuclear energy generation term, the pressure terms, energy flux terms and the thermodynamic variables in terms of the perturbations of the basic set of $7N$ variables:

$$\varpi_{\frac{1}{2}}^n, V_{\frac{1}{2}}^n, T_{\frac{1}{2}}^n, J_{\frac{1}{2}}^n, r_1^n, v_1^n, \Pi_1^n, \dots, \varpi_{N-\frac{1}{2}}^n, V_{N-\frac{1}{2}}^n, T_{N-\frac{1}{2}}^n, J_{N-\frac{1}{2}}^n, r_N^n, v_N^n, \Pi_N^n$$

the above set of linearized equations can be represented as:

$$\mathbf{J}_0 \delta \tilde{\mathbf{x}} + \mathbf{J}_1 \frac{d}{dt} \delta \tilde{\mathbf{x}} + \mathbf{J}_2 \frac{d^2}{dt^2} \delta \tilde{\mathbf{x}} = 0 \quad (\text{A.105})$$

where the one-dimensional vector $\delta \tilde{\mathbf{x}}$ is:

$$\left(\frac{\delta \varpi_{\frac{1}{2}}^n}{\varpi_{\frac{1}{2}}^n}, \frac{\delta V_{\frac{1}{2}}^n}{V_{\frac{1}{2}}^n}, \frac{\delta T_{\frac{1}{2}}^n}{T_{\frac{1}{2}}^n}, \frac{\delta J_{\frac{1}{2}}^n}{J_{\frac{1}{2}}^n}, \frac{\delta r_1^n}{r_1^n}, \delta v_1^n, \delta \Pi_1^n, \dots, \frac{\delta \varpi_{N-\frac{1}{2}}^n}{\varpi_{N-\frac{1}{2}}^n}, \frac{\delta V_{N-\frac{1}{2}}^n}{V_{N-\frac{1}{2}}^n}, \frac{\delta T_{N-\frac{1}{2}}^n}{T_{N-\frac{1}{2}}^n}, \frac{\delta J_{N-\frac{1}{2}}^n}{J_{N-\frac{1}{2}}^n}, \frac{\delta r_N^n}{r_N^n}, \delta v_N^n, \delta \Pi_N^n \right)$$

and \mathbf{J}_0 is the jacobian matrix in the static case defined earlier. \mathbf{J}_1 and \mathbf{J}_2 are sparse matrices of the same dimensions as \mathbf{J}_0 (i.e. $7N \times 7N$). The above system of coupled linear differential equations can be solved using the usual method of letting $\delta \tilde{\mathbf{x}}(t) = \delta \tilde{\mathbf{x}}_{\text{sp}} \exp \omega t$, where ω and the components of $\delta \tilde{\mathbf{x}}_{\text{sp}}$ can be complex. Substituting the above form for $\delta \tilde{\mathbf{x}}(t)$ in equation A.105 gives:

$$(\mathbf{J}_0 + \omega \mathbf{J}_1 + \omega^2 \mathbf{J}_2) \delta \tilde{\mathbf{x}}_{\text{sp}} = 0 \quad (\text{A.106})$$

The system of equations A.106 is an eigenvalue problem, with ω representing the eigenvalues and $\delta \tilde{\mathbf{x}}_{\text{sp}}$ the eigenvectors. The eigenvalues and eigenvectors are in general complex, and each pair of eigenvalue and eigenvector describes one mode of vibration. Note that any linear combination of eigensolutions (or modes) is also a solution to linear stability problem A.105. The complex part of eigenvalue represents the frequency of the oscillatory motion, and the real part of the eigenvalue determines whether the amplitude of the oscillatory motion will grow or decay with time. The real part of the eigenvector components gives the amplitude (i.e. the amount of deviation from the hydrostatic solution) for that component at $t = 0$. The difference in the arguments of any two components of the eigenvector gives the phase difference between those components. Note that for a given

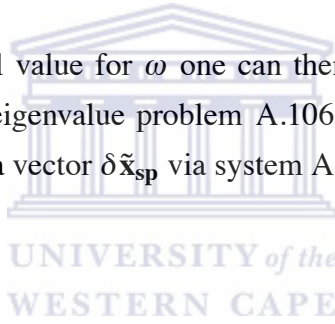
mode of vibration the components of the eigenvector can be scaled by an arbitrary constant, and it will still be a solution to the eigensystem A.106. We exploit this fact to solve the eigensystem as follows. First we remove equation A.94 from the original set of linearized equations and replace it with the surface boundary (or normalization) condition:

$$\frac{\delta R_s}{R_s} = 1 \quad (\text{A.107})$$

and update the matrices \mathbf{J}_0 , \mathbf{J}_1 and \mathbf{J}_2 appropriately. This then leads to the following set of non-homogenous linear equations:

$$(\mathbf{J}_0 + \omega \mathbf{J}_1 + \omega^2 \mathbf{J}_2) \delta \tilde{\mathbf{x}}_{\text{sp}} = \tilde{\mathbf{b}} \quad (\text{A.108})$$

where $\tilde{\mathbf{b}} \neq 0$. Given a trial value for ω one can then solve the system A.108 for $\delta \tilde{\mathbf{x}}_{\text{sp}}$. A solution to the original eigenvalue problem A.106 is then found by searching for the value(s) of ω which yields a vector $\delta \tilde{\mathbf{x}}_{\text{sp}}$ via system A.108 that satisfy condition A.94.



Bibliography

- D. R. Alexander and J. W. Ferguson. *Astrophysical Journal*, 437:879, 1994.
- C. A. L. Bailer-Jones and R. Mundt. *Journal of Astronomy and Astrophysics*, 348:800, 1999.
- I. Baraffe, G. Chabriel, F. Allard, and P. Hauschildt. *Journal of Astronomy and Astrophysics*, 337:403–412, 1998.
- I. Baraffe, G. Chabriel, F. Allard, and P. H. Hauschildt. *Journal of Astronomy and Astrophysics*, 382:563–572, 2002.
- D. Barrado, N. Huélamo, and M. Morales. *Astron. Nachr*, AN 326(10):981–984, 2005.
- G. Basri. *Annu. Rev. Astron. Astrophys.*, 38:485, 2000.
- B. W. Carrol and D. A. Ostlie. Addison-Wesley Publishing Company, Inc., 1996.
- J. I. Castor. *Astrophysical Journal*, 178:779, 1972.
- G. R. Caughlin and W. A. Fowler. *Atomic Data and Nuclear Data Tables*, 40:288, 1988.
- G. Chabriel and I. Baraffe. *Annu. Rev. Astron. Astrophys.*, 38:337–377, 2000.
- G. Chabriel, I. Baraffe, F. Allard, and P. H. Hauschildt. *ASP Conference Series*, TBA, 2005.
- A. M. Cody. Number CP948 in 978-0-7354-0462. American Institute of Physics, 2007.
- A. M. Cody. *arXiv:0908.0774v1 [astro-ph.SR]*, 2009.

- F. Comerón, R. Neuhäuser, and A. A. Kaas. *Journal of Astronomy and Astrophysics*, 359: 269–288, 2000.
- J. P. Cox. *Annu. Rev. Astron. Astrophys.*, 14:247C, 1976.
- J. P. Cox. Princeton Series in Astrophysics. Princeton Univ. Press, Princeton, New Jersey, 1980.
- J. P. Cox, D. S. King, and R. F. Stellingwerf. *Astrophysical Journal*, 171:93–102, 1972.
- A. Gabriel. *Ann. Astrophys.*, 27:141, 1964.
- B. Goldman, M. C. Cushing, M. S. Marley, É. Artigau, K. S. Baliyan, V. J. S. Bejar, J. A. Caballero, N. Chanover, M. Conelley, R. Doyon, T. Forveille, S. Ganesh, C. R. Gelino, H. B. Hammel, J. Holtzman, S. Joshi, U. C. Joshi, S. K. Leggett, E. L. Martín, V. Mohan, D. Nadeau, R. Sagar, and D. Stephens. *Journal of Astronomy and Astrophysics*, 487:277–292, 2008.
- D. A. Gough. *Astrophysical Journal*, 214:196, 1977.
- N. Grevesse and A. Noels. Cambridge Univ. Press, Cambridge, NY, 1993.
- R. Kuhfuß. *Journal of Astronomy and Astrophysics*, 160:116–120, 1986.
- S. Kumar. *Astrophysical Journal*, 137:1121, 1963.
- G. Lenain, R. Scuflaire, M. A. Dupret, and A. Noels. *Comm. in Asteroseismology*, 147: 39L, 2006.
- Linsky and L. Jeffrey. *Space Science Reviews*, 84:285, 1998.
- M. Marconi, V. Ripepi, M. Oliviero, L. Errico, M. Magrì, A. Vittone, F. Palla, and S. Bernabei. *Comm. in Asteroseismology*, 150:377M, 2007.
- M. Morales, D. B. y Navascués, J. A. Caballero, and E. L. Martín. *Astron. Nachr*, AN 326 (10):1065–1067, 2005.

- J. Muzerolle, L. Hillenbrand, N. Calvet, C. Briceno, and L. Hartmann. *Astrophysical Journal*, 592:266, 2003.
- T. Nakajima, B. R. Oppenheimer, B. R. Kulkarni, and S. R. et al. *Nature*, 378:463, 1995.
- E. A. Olivier and P. R. Wood. *Mon. Not. R. Astron. Soc.*, 362:1396–1412, 2005.
- B. R. Oppenheimer, S. R. Kulkarni, K. Mathews, and T. Nakajima. *Science*, 270(5241): 1478–1479, 1995.
- F. Palla and I. Baraffe. *Journal of Astronomy and Astrophysics*, 432:L57–L60, 2005.
- R. Rebolo, M. R. Zapatero, and E. L. Martin. *Nature*, 377:129, 1995.
- E. L. Rice, T. Barman, I. S. Mclean, L. Prato, and J. D. Kickpartric. *Astrophysical Journal-Supplement Series*, 186:63–84, 2010.
- H. Saio. *Astrophysics and Space Science*, 210:61–72, 1993.
- D. Saumon and G. Chabriel. *Phys. Rev.A*, 44:5122, 1991.
- D. Saumon and G. Chabriel. *Phys. Rev.A*, 46:2084, 1992.
- D. Saumon, G. Chabriel, and H. M. VanHom. *ApJS*, 99:713, 1995.
- A. Scholz and J. Eislöffel. *Journal of Astronomy and Astrophysics*, 419:249, 2004a.
- A. Scholz and J. Eislöffel. *Journal of Astronomy and Astrophysics*, 421:259, 2004b.
- A. Scholz, X. Xu, R. Jawardhana, K. Wood, J. Eislöffel, and C. Quinn. *Mon. Not. R. Astron. Soc.*, 398:873–886, 2009.
- R. F. Stellingwerf. *Astrophysical Journal*, 195:441–466, 1975.
- R. F. Stellingwerf. *Astrophysical Journal*, 262:330–338, 1982.
- R. F. Stellingwerf. *Astrophysical Journal*, 277:322–326, 1984.
- E. Toma. *Journal of Astronomy and Astrophysics*, 19:76, 1972.

W. Unno and E. A. Spiegel. *Publications of the Astronomical Society of Japan*, 18(2), 1966.

D. R. Xiong. *Acta Astron. Sin.*, 18:86, 1977.

D. R. Xiong and L. Deng. *Mon. Not. R. Astron. Soc.*, 324:243–248, 2001.

D. B. y Navascués and D. Martín. *AJ*, 126:2997, 2003.

M. R. Zapatero-Osorio, J. Cabellero, V. Bejar, and R. Rebolo. *Journal of Astronomy and Astrophysics*, 408:663–673, 2003.

